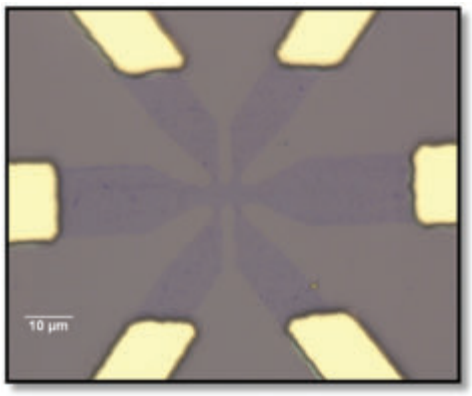

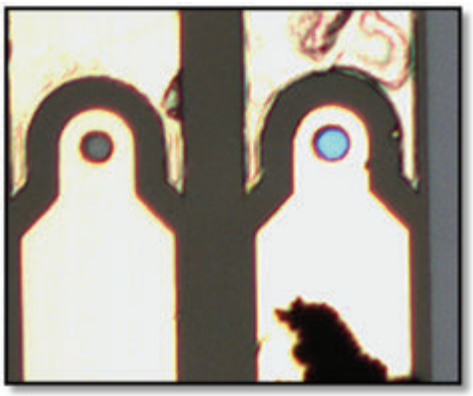

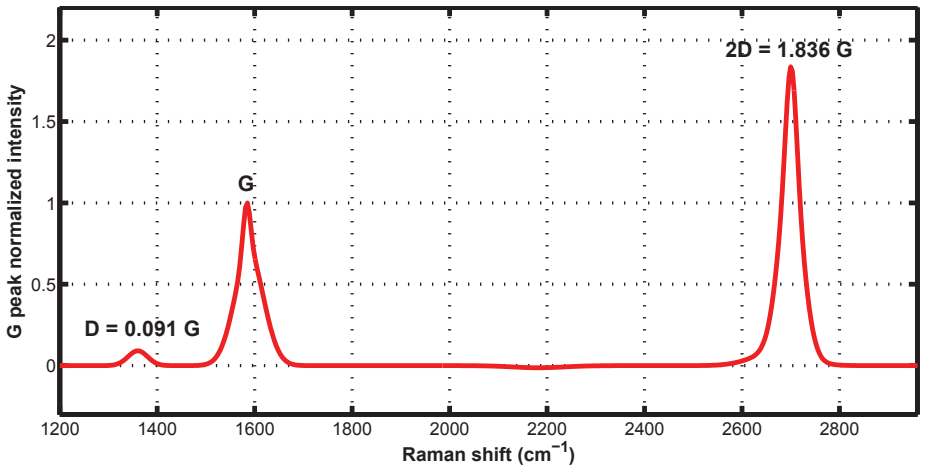

Graphene as Transparent Conductive Film for GaN-Based Vertical Cavity Surface Emitting Lasers

Erasmus Mundus Master of Nanoscience and Nanotechnology

César Javier Lockhart de la Rosa

Photonics Laboratory &
Quantum Device Physics Laboratory,
Department of Microtechnology and Nanoscience – MC2
Chalmers University of Technology
Gothenburg, Sweden, 2012

Graphene as Transparent Conductive Film for GaN-Based Vertical Cavity Surface Emitting Lasers

ERASMUS MUNDUS

César Javier Lockhart de la Rosa

Department of Microtechnology and Nanoscience – MC2

Chalmers Tekniska Högskola

A thesis submitted for the degree of

Master of Nanoscience and Nanotechnology Major Nano-Electronics

Göteborg, Sweden, 2012

Graphene as Transparent Conductive Film for GaN-Based Vertical Cavity Surface Emitting Lasers

César Javier Lockhart de la Rosa

Göteborg, June, 2012

Coordinators:

Åsa Haglund, Assistant Professor
Jie Sun, Assistant Professor
Marc Heyns, Professor

Department of Microtechnology and Nanoscience
Photonics Laboratory &
Quantum Device Physics Laboratory
Chalmers Tekniska Högskola
SE-412 96, Göteborg, Sweden
Phone: +46 (0) 31 772 1000

Front cover illustrations:
Top left, graphene device for electrical characterization.
Top right, LED device with graphene current spreader.
Bottom, Raman spectrum of graphene film on *p*-GaN.

Printed by Bibliotekets Reproservice,
Chalmers Tekniska Högskola
Göteborg, Sweden, June, 2012

Abstract

There is a need for lasers in the 370nm - 470nm spectrum (near ultraviolet - blue) for applications such as high storage, high resolution printers and biomedical applications. GaN-based vertical cavity surface emitting laser (VCSEL) is one interesting option due to the wide bandgap of the GaN and the 2D array capability and cost-effective production of VCSELs. Because of the high resistivity of p-GaN, these devices require the use of a transparent conductive film (TCF) to effectively laterally spread the current across the active region. The actual material used so far is ITO wish has problems related to the deposition technique and the constantly increasing price of the material. Graphene, a one atom layer thick (0.35 nm) graphite derivative 2D material, stands as a very good option due to its outstanding properties (high mobilities, high transmittance, etc.). In order to demonstrate the feasibility of replacing ITO with a graphene TCF the production, transfer, sheet resistance and contact resistivity to p-GaN have to be investigated and further developed. In this work a low-pressure cold-wall CVD reactor was used for reproducible production of large domains graphene films on 99.995% Cu foils of 50 μm. Different transfer techniques were assessed and reproducible graphene transfer was achieved by improving a recently developed method. The method is based on the separation of the graphene from the Cu foil by H_2 bubbles formation on the surface of the Cu foil that was used as a cathode in an electrolytic cell with aqueous 0.25 M NaOH solution. Different methods to improve the sheet resistance of the graphene were evaluated (artificially deposited dual layer films, doping with $FeCl_3$, S1813 and PVA). Devices were created to characterize the mobility, sheet resistance, carrier concentration, maximum current densities and contact resistivity to p-GaN. A GaN-based LED using a graphene TCF was fabricated and showed efficient current spreading by the graphene based TCF. The results show that graphene is an interesting option for TCF however, more effort is needed to further improve the contact resistivity.

Keywords: Laser, VCSEL, GaN, conductive film, graphene, CVD, transfer, doping.

A Karen, Judith, Chantal y mis padres, Julio y Rosario...

Acknowledgements

Before anything, I would like to thank God, and his ever virgin mother, Maria, for being to my side when I needed it and never leaving me alone. I have no word to express my gratefulness to my family; for all the support that they always give me, all the corrections and all the prays I asked them to do while I was writing these thesis or taking exams. I would also like to thank to Ass. Prof. Åsa Haglund and Ass. Prof. Jie Sun for the incalculable effort they put into me and all the late hours spent in the laboratory or discussing results, thank you for all the corrections and for pushing me always to do my best. I would also like to express my gratitude to Lic. Martin Stattin, and Lic. Niclas Lindvall for assisting me with the project and helping me when I get stuck with something about GaN-based devices or graphene. My thanks to Dr. Cole for his help with the transmittance analysis and the Raman mapping. I am also grateful to Msc. Luis Aguilera and Prof. Matic for training me and assisting me with the Raman measurements. I also would like to thank Prof. Marc Heyns from KU Leuven, I am really sorry that, due to the spatial constrains, it was not possible to share discussions more frequently. Thanks to the people from the Photonics and QDP labs. Thanks also to the staff and coordinators of the Erasmus Munsdus Master of Nanoscience and Nanothechnology: Prof. Guido Groeseneken, Prof. Göran Johanson, Elke Delfose, Anouck Brouwers; they really care about us and help us in giving the best of us. I also would like to thank Pavel, Bert, Abhitosh, Tatiana, Guntars, Aiva, Quing Pan and the rest of the Nano-Gang for making these last two years so wonderful. Finally, I would like to give special thanks to Dr. Larrondo Petrie. Without her guidance it would have been impossible for me to have this opportunity.

César J. Lockhart de la Rosa

Göteborg, 2012

Contents

List of Figures

LIST OF FIGURES

List of Tables

LIST OF TABLES

Chapter 1

Introduction

In the technology race there will be always a need for "more". More storage , more speed, more precision and, even if it looks contradictory, there is a need for more quantity with better quality at lower prices. This trend is dragging all the fields of technology including lasers. Nowadays lasers are everywhere, from digital storage to bio-medical applications and, in order to continue giving "more" in these fields with laser technologies, there is a need for shorter wavelengths; there is a need to go "blue".

Why is that regime so interesting? In optical storage media these blue lasers allow the storage of higher data densities due to the reduced spot size of the blue laser (405 nm) with respect to the previously used red lasers (650 - 780 nm) (fig. 1.1).

There are more applications like laser printers, 3D scanners, etc. where the small spot size of the blue laser will improve the overall performance. Other applications, like identification of cancerous tissue, also take advantage of the blue light emission of the laser to excite molecules or particles [1].

Basically, one of the most feasible ways of achieving the "near ultraviolet - blue" regime in semiconductor lasers is by using gallium nitride (GaN) based materials. Now, in order to tackle the part of having more quantity at lower price, the emerging technology is the Vertical Cavity Surface Emitting Laser (VCSEL). This laser structure allows the fabrication of, not only 1D arrays but also 2D arrays of lasers. This technology also allows for on-wafer testing of the lasers before packaging, greatly reducing production costs.

So far blue VCSELs are not commercially available, in fact only two research groups in the world had demonstrated lasing from such structures under electrical pumping

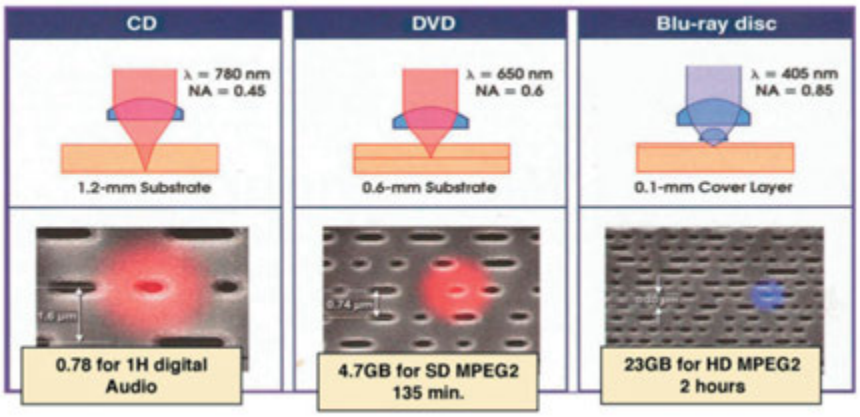

Figure 1.1: Comparison of different optical formats. [1]

[2, 3]. One of the key challenges is to achieve a uniform current injection despite the low electrical conductivity of the *p*-GaN. Thus, there is a need for a transparent current spreading layer and in this work the possibility of using the novel material graphene for this purpose is explored.

In the *second chapter*, the VCSEL is introduced together with the challenges to achieve blue emission and different options for current spreaders.

In the *third chapter*, the basic properties of graphene, the material that will be investigated as a transparent current spreading layer, is discussed together with an introduction to practical issues related to the production and transfer of this material.

The *fourth chapter* present the development and main outcomes of this work including not only the growth, transfer and doping of the graphene but also the device fabrication and characterization.

The conclusions are presented in *Chapter Five* and are followed by the future outlook proposal in *Chapter Six*.

The *Appendix A* present the recipes for the processes. Supplementary information obtained from the analysis of scanning electron microscope images of the graphene film is presented in *Appendix B* and some general description of Raman spectroscopy, the model used for mobility measurement, and the fabrication techniques will be left for *Appendix C*.

As a result of the experiments carried on in this work a journal manuscript was prepared to be submitted to *Applied Physics Letters*. The manuscript and the supplementary material can be found in *Appendix D*.

Chapter 2

Vertical Cavity Surface Emitting Lasers (VCSELs)

THERE are two main semiconductor-based laser structures. The *Edge Emitting Laser* and the *VCSEL*.

In a edge emitting lasers the cavity is formed horizontally along the active region. The waveguide is thin, especially in the vertical direction, which results in an elliptically-shaped output beam (large divergence in the vertical direction) as can be seen in fig. 2.1.

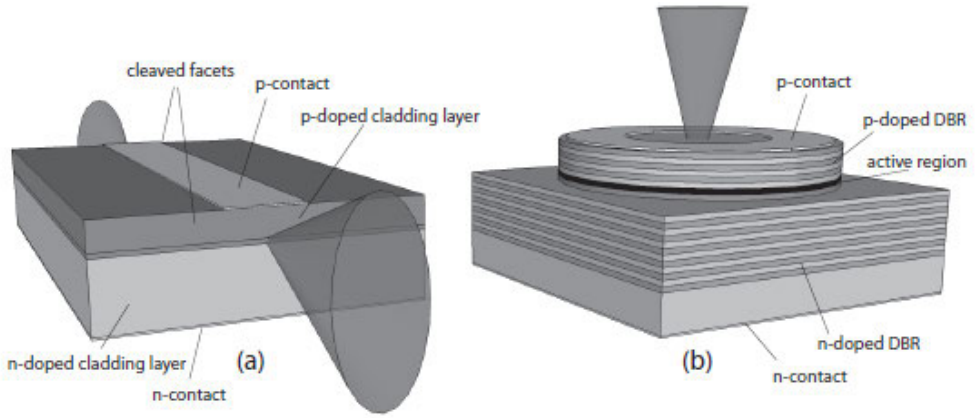

Figure 2.1: Different laser structures. (a) Fabry-Perot cavity laser (edge emitter) structure. (b) VCSEL structure.[4]

In a VCSEL, on the other hand, the cavity is in the vertical direction. This give some advantages and disadvantages at the same time. One disadvantage is that, due to the

fact that the cavity is normal to the active region, the overlap between the optical field and the gain region is poor and less gain is achieved per round-trip in the cavity. This introduce the need for high reflectivity mirrors which are achieved by using distributed brag reflectors (DBR).

Among the advantages is worth mentioning that, due to the normally large and symmetric waveguide of the VCSEL in comparison to edge emitting lasers, the resulting beam will have a lower divergence and will be more circular-shaped, which make easier to couple the light beam to optical fibres. Also, due to the surface emission, two dimensional arrays can be fabricated easily. It also allows for on-wafer testing before packaging, making the VCSEL a low-cost component. Other advantage of this structure is that due to the short resonator ($\sim 1\,\mu$m) the VCSEL is inherently a single longitudinal mode device. For these advantages, this work will focus on the VCSEL structure.

2.1 Gallium nitride VCSELs (GaN-VCSELs)

To achieve an emission wavelength in the near ultraviolet and blue regime (370 nm - 470 nm) semiconductor materials with direct energy band gaps between 3.35 eV and 2.64 eV should be used. Considering the requirements, gallium nitride (GaN) based materials stand as a very good solution. GaN has an energy band gap of about 3.28 eV at 300 °K and can be combined with aluminium nitride (AlN) or indium nitride (InN) to tune the band gap from 6.2 eV to 0.65 eV (see fig. 2.2).

However, the key problems challenging the realization of GaN-based VCSELs are the following:

1. Poor material quality, partly due to the lack of high quality substrates that are lattice matched to GaN. The most common substrate used for GaN growth is sapphire, shich has a lattice constant of 4.765 Å, much larger than that of GaN, 3.189 Å. This lattice mismatch introduce a considerable amount of defects in the GaN.
2. It is difficult to grow distributed brag reflector (DBR) mirror due to the difficulty in finding material combinations which have a high refractive index contrast and are lattice matched to each other.
3. Due to the low electrical conductivity of the p-GaN there is a need for an intra-cavity transparent conductive film to achieve homogeneous current injection into

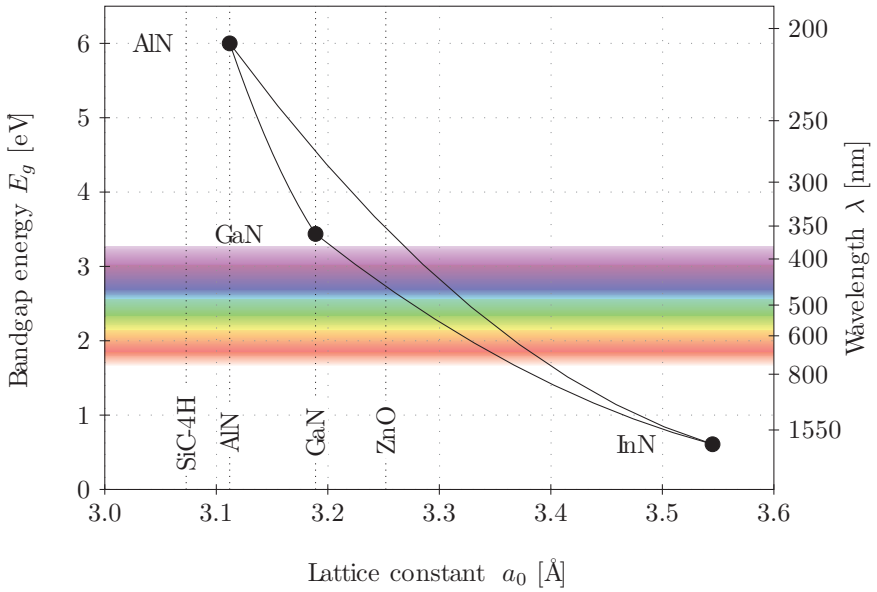

Figure 2.2: Bandgap and lattice constant for the III-nitrides at room temperature. The effective band gap can be tuned from 6.2eV (AlN) to 0.65eV(InN) while keeping direct transition between the valence and conduction band [5].

the active region. This layer should be as thin and transparent as possible to effectively reduce the optical absorption loss in the cavity.

How does GaN-VCSELs work?

The GaN-VCSEL, as in all laser structures, consist of an active region and a resonator (the region between the dielectric DBR and the epitaxial DBR). A schematic can be seen in fig. 2.3. The DBRs are high reflectivity mirrors formed by alternating high and low refractive index materials.

The active region is pumped by injecting current through the metal contacts. The transparent conductive film will spread the current laterally to achieve a homogeneous current injection through the active region. Photons are emitted in the active region. The photons will be bouncing back and forth in between the DBR mirrors. The top DBR mirror has a slightly lower reflectivity so that a small amount of the photons can escape the cavity.

The light is amplified in the active region and, to be able to reach lasing, the gain provided by the active region must equal the losses (inculidng the light lost through

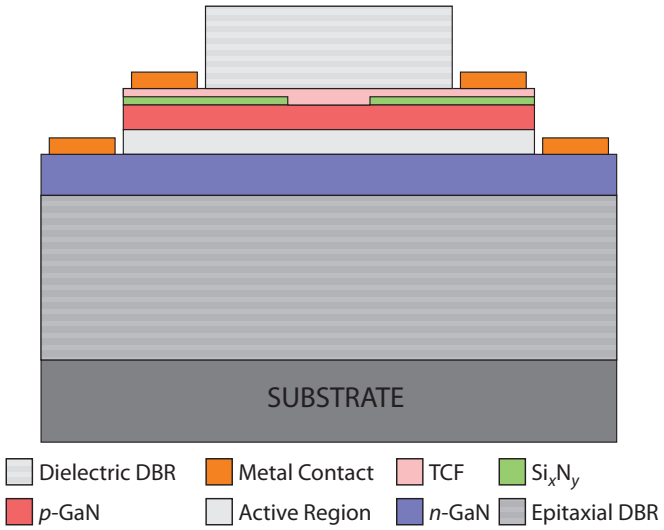

Figure 2.3: Schematic diagram of a VCSEL structure based on GaN.

out-coupling from the mirrors).

To the date of publication of this report two groups have achieved continuous wave operation of electrically pumped GaN-VCSELs at room temperature with threshold current densities of , 12.4 kA/cm^2 [3] and 3 kA/cm^2 [6]. All of them have used indium tin oxide as a transparent conductive film.

2.2 Transparent conductive film (TCF)

The most important properties of a TCF are:

- Low optical absorption of light in the 370 nm - 470 nm regime.
- Low sheet resistance.
- Low contact resistivity to p-GaN.
- Withstand current densities suitable for lasing.

There are different options that can be used to tackle these requirements and they will be described in the next subsections.

2.2.1 Metallic TCF

One of the first possible solutions is to use metallic thin films. The advantages of using metallic films is the low sheet resistance, high current density capabilities and the relatively good ohmic contact with p-GaN after thermal annealing. This good ohmic contact is due to the diffusion of the metal into the GaN forming Ga-metal inter-metallic phases.

The most studied metallic TCF has been the Ni/Au film. By depositing 2 nm of Ni on p-GaN followed by 6 nm of Au a specific contact resistivity of $2.43\times10^{-2}\,\Omega\,\mathrm{cm}^2$ and 88% transmittance have been achieved after annealing [7]. These properties are good for bright LEDs applications, but the high absorption of light make them unsuitable for the VCSELs intra-cavity current spreader in VCSELs.

Also some groups were trying to use Pd/Au films of about 5 nm placed in a null of the standing wave in the resonator. This way, even if the film has a considerable absorption, due to its thickness, the single pass loss could theoretically be under 0.05% [8]. The problem is that as the metal film has a significantly high absorption, if the film is positioned slightly out of the null of the standing wave (few nanometres shift) the overall loss will dramatically increase making it difficult to achieve lasing.

2.2.2 Conductive oxide semiconductors TCF

Other possible candidates are the doped oxide semiconductor-based TCF like indium oxide (In_2O_3), zinc oxide (ZnO) or tin oxide (SnO_2) or any ternary combination of these[9]. The most explored of these is the ternary compound $In_4Sn_3O_{12}$ (ITO). It has been demonstrated [10] that by depositing 30 nm ITO films sheet resistance values of $283.8\,\Omega/\square$ can be achieved with specific contact resistivity in the order of $0.0541\,\Omega\,\mathrm{cm}^2$ to p-GaN. The transmittance for ITO can also be very high showing absorption smaller than 0.5% for films with thickness of 50 nm [2]. ITO has also shown to withstand current densities in the order of $10^3\times\mathrm{A/cm}^2$ [2, 3, 6].

One of the main problems with ITO films is the contact resistivity to p-GaN. In order to reduce the contact resistivity, thermal annealing can be done[10]. Also, the introduction of a p^+-InGaN layer of about 2 nm between the p-GaN and the ITO can further reduce the contact resistivity with a minor decrease of the transmittance [3].

Parameter	Value
Sheet Resistance	$283.8\,\Omega/\square$ [10]
Contact Resistance	$0.0541\,\Omega\,\mathrm{cm}^2$ [10]
Absorption	$< 0.5\%$ [2]
Current Density	$\sim 10^3 \times \mathrm{A/cm}^2$ [2, 3, 6]

Table 2.1: Characteristic of ITO transparent conductive films.

Other problem with the ITO is related to the hegemony of the Chinese market in the indium refinery production [11]. As a result, the annual average price has increased 25% from 2010 - 2011.

Because of these problems, industry is looking for a material that could replace ITO as a TCF. It will be shown in the next chapter that grapehene, a novel 2D material, could stand as a possible option for the replacement of ITO.

2.3 Summary

The wavelengths of interest are 370 nm - 470 nm. In this regime the material of choice with the right band gap is GaN. The bandgap can be tuned by combining GaN with AlN and InN to achieve values from 0.65 eV to 6.2 eV.

Of the different laser diodes structures VCSELs are becoming more and more popular due to the circular shaped beam, higher modulation speed at low currents, single longitudinal mode, small angle of divergence, 1D and 2D array capability and the low cost production due to on-wafer testing. Nevertheless, GaN-based VCSELs needs a Transparent Conductive Film (TCF) inside the resonant cavity on top of the active region in order to homogeneously spread the current. This TCF should have low sheet resistance, low contact resistivity to p-GaN, high transmittance and should withstand relatively high current densities.

So far the TCF of choice has been ITO but due to different problems (specially cost related and thin film deposition problems) a new solution is needed. According to the actual performance of ITO in GaN-Based VCSELs the characteristics of the TCF that will replace ITO should be similar or better to the one described in table 2.1 for ITO films. Graphene could be a possible option for the ITO replacement.

Chapter 3

Graphene

In 2004 a group from the University of Manchester reported the isolation of one of the first naturally occurring 2D materials, *Graphene*[12]. Since then, this material has attracted the attention of several groups all around the world due to the extraordinary properties that it has demonstrated.

But, what is graphene? Graphene is the material that complete the carbon family. Graphite, the 3D version of carbon materials had been well known for long, then comes the buckyballs (0D version) and the carbon nano-tubes (the 1D version). Graphene is the 2D version of carbon materials, a one atom thick honeycomb lattice of carbon atoms in sp^2 hybridization. As 2D crystals were not supposed to exist according to the Mermin-Wagner theorem, the fact that this two-dimensional atomic crystal exist and is stable is by itself an amazing statement. It was later demonstrated that graphene owes its stability to a phenomena called 3D warping. This stabilize the 2D material by creating small wrinkles in the third dimension that allows the system to minimize its energy [13].

Figure 3.1: From left to right: Diamond and graphite (3D), graphene (2D), carbon nano-tubes (1D), buckyball(0D). [13]

Graphene has a complete set of interesting properties that make it a promising material for nano-applications and More-than-Moore technologies. The most important

of these properties will be introduced in the next sections. Also, basic consideration related to the production, transfer to different substrates and application of this material as a TCF will be addressed in the rest of this chapter.

3.1 Properties of graphene

3.1.1 Electronic properties

Graphene has demonstrated to have a very well suited kit of spectacular properties due to its irregular energy dispersion[1]. In this section the focus will be on those that are most relevant and interesting for the use of graphene as a TCF. For more detailed explanation and a complete overview of the electronic properties see reference [14].

Energy dispersion

The energy dispersion of graphene was formulated in 1947 [15] and is graphically shown in fig. 3.2. In order to obtain the energy dispersion graphene is analysed as a lattice with rhombohedral symmetry and a two basis unit cell. By using the tight-binding approach, the energy dispersion can fairly well be approximated and described by the following equation[16]:

$$E^{\pm}_{(k_x,k_y)} = \pm\gamma\sqrt{1 + 4\cos\left(\frac{\sqrt{3}k_x a}{2}\right)\cos\left(\frac{k_y a}{2}\right) + 4\cos^2\left(\frac{k_y a}{2}\right)} \tag{3.1}$$

Where γ is the nearest-neighbour hopping energy (2.7 eV) and a is the lattice constant (2.46).

This energy dispersion will have six points (Dirac points) where the conduction and the valence band touch each other. This makes graphene a semi-metal. Further more, in the vicinity of the Dirac points equation 3.1 can be expanded to yield a linear equation with respect to k instead of being parabolic as in normal metals. The linear dispersion near the Dirac points will then be:

$$E^{\pm}_{(\mathbf{k})} = \pm\hbar v_f |\mathbf{k}| \tag{3.2}$$

Here $\hbar$ is the reduced Planck constant and v_f is the Fermi velocity ($\sim 10^6$ m/s).

[1] Berry face, irregular quantum Hall effect, Klein tunnelling, Aharonov-Bohm effect, among others.

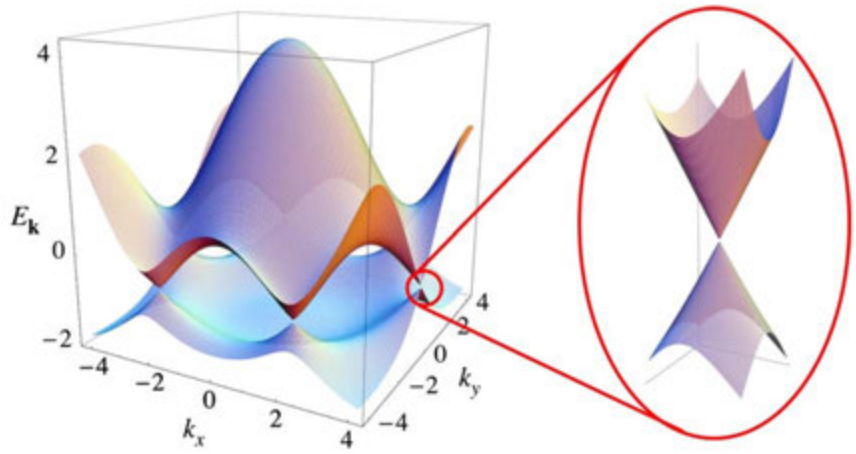

Figure 3.2: Energy dispersion of graphene (left). Zoom of the energy dispersion near Dirac points (right). [14]

This linear energy dispersion is similar to that of massless particles (Dirac-Weyl equation) the only difference being the fact that for massless particles the proportionality factor is the speed of light instead of the Fermi velocity.

Mobility and conductivity

Mobilities between 2,000 $cm^2/(Vs)$ and 20,000 $cm^2/(Vs)$ had been reported for graphene samples on different substrates [12, 17, 18] at low temperatures and for carrier concentrations in the order of $10^{12}\,cm^{-2}$. For suspended graphene mobilities in excess of 200,000 $cm^2/(Vs)$ have been reported for temperatures about 100 °K and carrier concentrations in the order of $10^{11}\,cm^{-2}$ [19]. These values of mobility applies the same for any carrier inside graphene no matter if it is electron or hole (graphene is ambipolar).

If the Drude model of conductivity is assumed it can be seen that the expected value for the graphene conductivity will range from 0.0032 S to 0.00032 S in unsuspended graphene and in the order of 0.0032 S for suspended graphene. Thus, to improve the conductivity, further doping is needed to increase the carrier concentration while maintaining the mobility.

Other interesting phenomena in graphene is the fact that even with zero carrier concentration there will always be a minimal conductivity. This minimal conductivity

is attributed to the suppression of localization in carriers transport due to disorders. Thus, the charge carriers can not be confined by smooth potential barriers.

This minimal conductivity has a theoretical value of $e^2/h\pi$. Nevertheless, in practice the minimal conductivity achieved is π times bigger than this value (e^2/h)[20]. Several groups had tried to explain why the disagreement between theory and practice but the picture is not completely understood yet [21].

3.1.2 Optical properties

The light transmittance of a single layer graphene is 97.7%. The transmittance remain almost invariant in the whole visible spectra regime. It can be shown that the absorption of the graphene will only depend on the fine-structure constant ($\alpha = 2\pi e^2/hc$) and that this absorption will increase linearly with the number of layers of graphene stacked together (experimentally demonstrated up to 5 layers)[22].

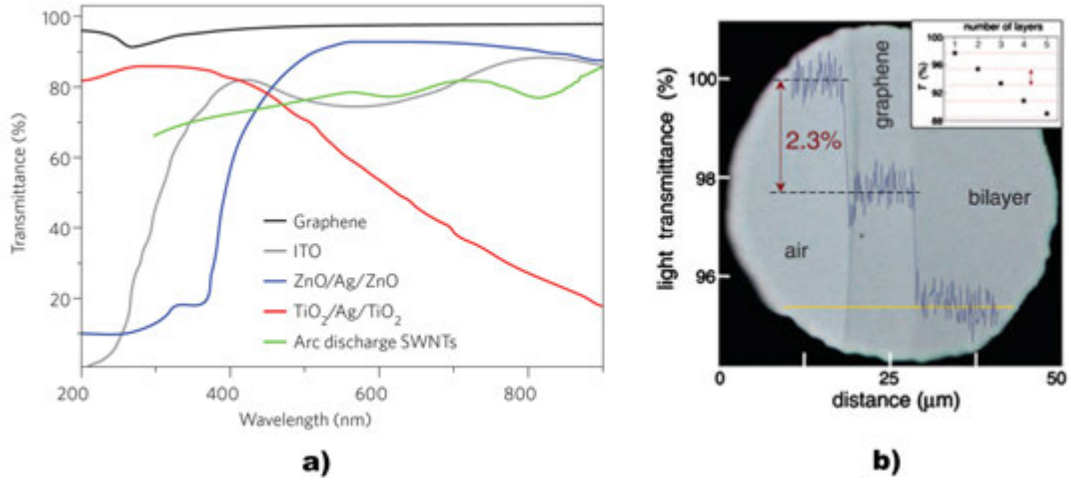

Figure 3.3: (a) Transmittance of graphene compared to that of other materials. [23]. (b) Optical transmittance for air, single-layer graphene and bi-layer graphene. In the upper right corner demonstration of the linear decrease of transmittance with the number of layers.[22]

Even more interesting is the fact that graphene, being just one atom thick, can still be seen with the bare eyes due to contrast difference induced by variations in the refractive index of different substrate at different thickness. It can be shown by Fresnel diffraction theory that this contrast can be maximize for certain thicknesses of the substrate [24].

3.1.3 Mechanical and thermal properties

Mechanically speaking graphene has been identified as the strongest material ever measured. It has a non-linear elastic stress-strain response, and yields second-order elastic stiffness of 340 $\mathrm{N\,m^{-1}}$ and third-order elastic stiffness of -690 $\mathrm{N\,m^{-1}}$. The Young's modulus is 1.0 TPa and the intrinsic strength 130 GPa [25].

From the thermal point of view suspended single-layer graphene has a thermal conductivity in the range of $\sim (4.84 \pm 0.44) \times 10^3$ to $(5.30 \pm 0.48) \times 10^3$ W/mK [26]. These values are remarkably good and suggest that graphene can establish itself as a very good material for thermal management.

3.2 Production of graphene

3.2.1 Mechanical exfoliation

Mechanical exfoliation was the first technique used to isolate graphene [12, 27]. The technique consists in the exfoliation of a graphene layer from a graphitic bulk material by use of an adhesive tape and then deposit it onto the target substrate. After the graphene has been deposited on the substrate the single layer flakes need to be identified and isolated from the sea of bulk graphite by using a phase-contrast microscope. Normally, due to its thickness, graphene is not visible, but on top of 300 nm or 90 nm SiO_2 it is possible due to the feeble interference-like contrast.

The graphene form such procedure is never exposed to active agents that could deteriorate the quality of the graphene. Also, the graphene sheets that are exfoliated from the graphitic materials are in its pure natural form, thus not needing to be synthesised. For these reasons the best quality graphene flakes produced at this moment come from mechanical exfoliation (mobility is in the order of $\sim 10^5\,\mathrm{cm^2/(Vs)}$). However, patience and perseverance are key point for the production of single layer graphene by this method, making it only suitable for laboratory fundamental research applications and not large scale industrial production.

3.2.2 Wet chemicals and graphite oxide routes

In the mechanical exfoliation the separation of the graphene layer was due to the balance between the inter-layer cohesion and the interaction with the adhesive tape. On

the other hand, in chemical exfoliation the main objective is the weakening of the $\pi - \pi$ stacking between the graphene layers in graphite by the intercalation of reactants in the space between the layers. After this weakening, the graphene sheet is separated by decomposing the intercalant and producing a high vapour pressure or by inducing some agitation (ultrasonication) that separate the previously loosened layer. As a consequence of the intercalant the sp^2 sheet will be partially degraded to a $sp^2 - sp^3$ sheet deteriorating the quality of the graphene.

One of the most well known ways to achieve this layer loosening is using the Hummers method or similar improved versions [28, 29] to oxidise the graphitic material and increase the interlayer spacing of the graphene layers in the bulk graphite from 0.34 nm to 0.65-0.75 nm depending on the water content of the solution. By doing a rapid thermal annealing CO_2 over pressure can be produced splitting the graphite oxide into individual sheets. Ultrasonication can help to further separate the resultant graphite oxide into single graphene oxide sheets.

The problem with this technique is that once the graphene oxide sheets are produced they need to be reduced in order to restore the sp^2 sheet. This reduction is not efficient enough to restore the properties of the graphene, and even if the characteristics are improved, at the end there is still a partially oxidized graphene sheet. Thus the quality of the graphene is not good enough even if the technique is inexpensive and scalable.

3.2.3 Silicon carbide decomposition

Graphene can also be obtained by decomposition of SiC substrate (4H or 6H normally). The SiC substrate is heated to temperatures greater than 1200 °C (depending on the pressure) and the silicon atoms start to evaporate leaving behind the carbon atoms that subsequently rearrange themselves forming graphene sheets [30].

The graphene obtained by this procedure on the Si face of the SiC substrate can be of very good quality and, due to the fact that the graphene is growth directly on SiC substrate, for some applications, there is no need to transfer to other insulating substrate. Yet, the high cost of the SiC 4H and 6H substrates is a limiting factor for the industry. Also the transfer of the graphene to different substrates others than SiC is a challenge.

3.2.4 Chemical vapour deposition

In chemical vapour deposited (CVD) graphene the graphitic material is obtained by the decomposition of the hydrocarbons on the target surface following the chemical reaction (in the case of methane) $CH_4 \rightarrow C + 2H_2$. Nowadays the efforts are put mostly in the synthesis of graphene by the decomposition of hydrocarbons on metal surfaces. This is due to the well known capability of transition metals catalysing the hydrocarbon decomposition and graphitization processes[31]. More precisely, most of the groups working with CVD graphene are using copper due to the low solubility of carbon in this metal that allows a surface driven self controlled reaction that makes the growth of a new graphene layer more difficult once the metal surface has been covered [32].

With this method the produced single layer graphene is of good quality (mobility after transferring to insulated substrate is in the order of $\sim 10^3\,\mathrm{cm}^2/(\mathrm{Vs})$) and the process is scalable. The main problem with this technology is that, as the graphene is grown on a metal substrate, there is a need to transfer it form the metal substrate to the target insulating substrate. There are some groups trying to produce CVD graphene directly on insulating substrates [33]. However, the quality of the graphene-like film is still very poor compared to the graphene obtained using transition metals.

In this work, the graphene production will be based on CVD graphene grown on copper due to the fact that this technique is scalable, cost effective, reproducible and the quality of the graphene is good enough for use as TCF.

3.3 Transfer of graphene

To transfer the graphene to the target substrate there are several options to consider.

3.3.1 Wet etching and wet transfer

In this process the transition metal with graphene on top is first covered by a backbone polymer support (usually PDMS[1] or PMMA[2]). Then the metal is etched away with an etchant solution (usually $FeCl_3$ or HCl based solutions), cleaned in deionized water (DI), and finally the floating graphene with the polymer support is deposited (stamped) on top of the target substrate. Once the substrate is dry the polymer is removed (in case

[1] Poly-dimethyl siloxane
[2] Poly-methyl methacrylate

of PMMA or PDMS by using acetone). This process can also be performed without the use of a polymer support, in that case at the end no polymer needs to be removed. The process steps are illustrated in fig. 3.4 for the case of graphene grown on $Ni/SiO_2/Si$ substrate.

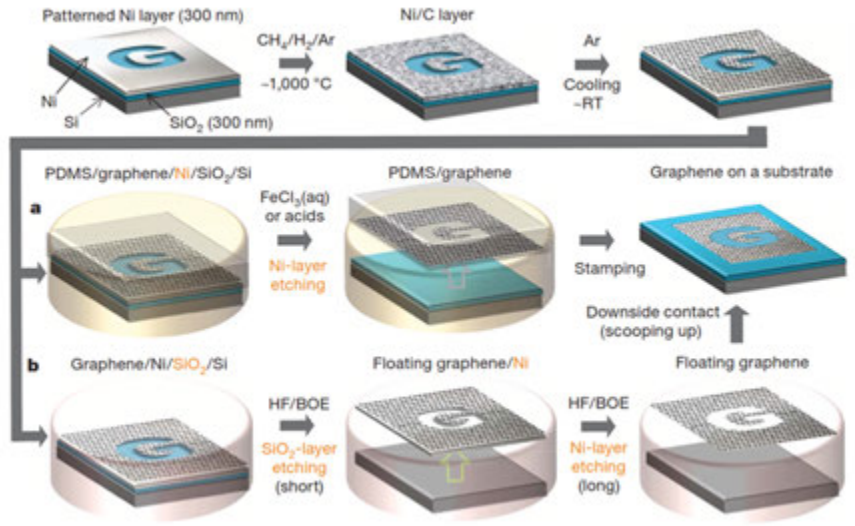

Figure 3.4: Transfer from $Ni/SiO_2/Si$ substrate to SiO_2 substrate using (a) PDMS as stamping material or (b) without any stamping material [34].

There are several problems with this technique. First, wrinkles and holes in the graphene sheet can easily be introduced. Secondly, the graphene is expose to an etchant solution that can further dope the graphene or introduce defects. Also the stamping step (the deposition on the substrate) is not trivial due to the fact that the stamping material can not be manipulated easily. For this reason in order to succeed in the transfer an skilled person is needed, reducing the scalability of the process.

3.3.2 Wet etching and dry transfer

This process also involve the etching of the metal used to grow the graphene by an etchant solution. The difference is mainly in the way the graphene is transferred from the polymer support to the target substrate. In this process, once the polymer support with the graphene is cleaned and dried the graphene is deposited onto the target substrate by pressing the polymer with graphene against the substrate. Once the graphene is

transferred the polymer will be released and there is not need for the removal of the polymer using organic solvents or any other wet chemicals.

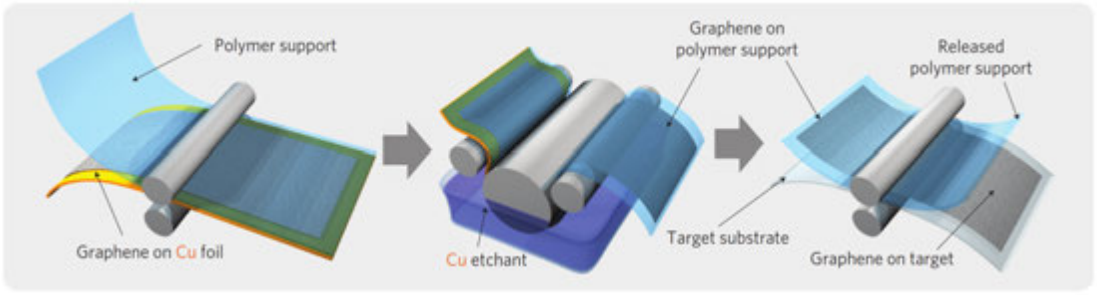

Figure 3.5: Schematic of the wet etching and dry transfer of the graphene [35].

It is clear that graphene is also exposed to the etchant solution. Moreover, keeping the pressure constant over the whole surface during the transfer from the polymer to the substrate is not trivial.

3.3.3 H_2 bubbling separation and wet transfer

This is a relatively new technique introduced by the end of 2011. The main idea behind the bubbling transfer is to separate the graphene and the polymer support from the metal by producing hydrogen bubbles between the catalytic metal and the graphene in a water electrolysis reaction. Thus, even if for some electrolytes the metal will be partially etched, it will not be consumed at the same extend as in the wet etching technique and could be reused to grow more graphene. Other advantages of this approach are that the graphene is not exposed to a strong etchant solution and that the time to separate the graphene from the metal by bubbling is much shorter than the time needed to etch away the metal completely. Once the graphene with the metal support has been separated the transfer to the substrate is similar to the wet transfer described in section 3.3.1.

The hydrogen production is a result of the water reduction in the cathode of an electrolytic cell when a current is applied. The half equations of the reactions in the cathode (eq. 3.3) and anode (eq. 3.4) of the cell are:

$$4H_2O_{(l)} + 4e^- \longrightarrow 2H_{2_{(g)}} + 4OH^-_{(aq)} \tag{3.3}$$

$$2H_2O_{(l)} - 4e^- \longrightarrow O_{2_{(g)}} + 4H^+_{(aq)} \tag{3.4}$$

From the equations it can be seen that the copper substrate with graphene should be use as a cathode and not as an anode in order to avoid the oxidation of graphene.

There are mainly two groups using electrolysis and bubbling to separate graphene from the metal used for the synthesis. The first group, coordinated by Yu Wang from the National University of Singapore [36], is using electrochemical de-lamination in an eletrolyte solution of diluted potassium peroxy-disulfite (K_2SO_8). Thus, the reaction will be a combination of electrochemical de-lamination of the graphene and metal etching. The etching will be driven mainly by the reaction:

$$Cu_{(s)} + S_2O^{2-}_{8(aq)} \longrightarrow Cu^{2+} + 2SO^{2-}_{4(aq)} \tag{3.5}$$

The Cu^{2+} will then precipitate as Cu_2O and CuO due to the hydroxyl ions produced during water electrolysis.

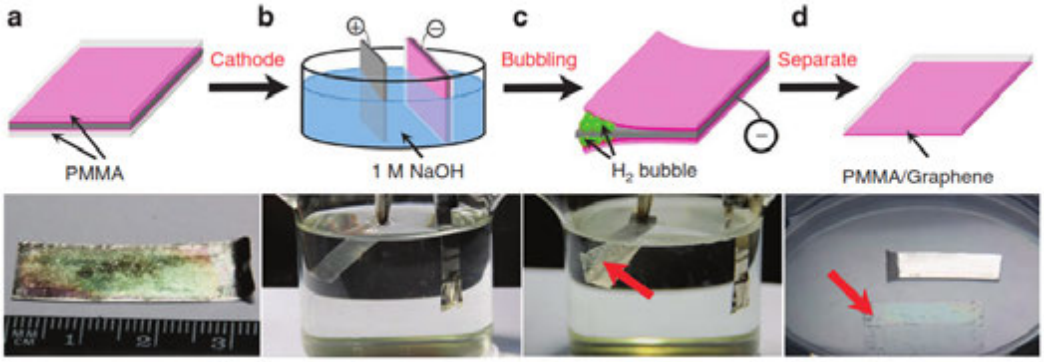

Figure 3.6: (a) Pt foil with graphene and PMMA. (b) The PMMA/graphene/Pt used as a cathode of an electrolytic cell. (c) PMMA/graphene gradually separated from Pt by H_2 bubbles (d) PMMA/graphene without the Pt substrate [37].

The second group, led by Libo Gao from the Institute of Metal Research (Chinese Academy of Science) [37], introduced in 2012 a method where there is no need for an etchant, only the bubbling is the responsible for the de-lamination. In this case the only reaction going on is the electrolysis of water described by equations 3.3 and 3.4. The electrolyte is only used to enhance the conductivity of water. In that particular research they where using sodium hydroxide (NaOH). This method results to be faster and more effective than the partial etching bubbling. Also the transition metal is almost not consumed at all. Due to the fact that there is no need to etch the transition metal, inert metals like platinum (Pt) can now also be used for the synthesis of graphene. A

sequence of the steps used in this process can be seen in fig. 3.6. In this work this method is developed further.

3.4 Graphene as TCF

Taking into consideration all the previously described characteristics of graphene as its high transparency (97.7%) and high mobility of the carriers (higher than 2,000 $cm^2/(Vs)$) it can be seen that graphene is an interesting alternative to ITO as TCF. A comparison of graphene versus other alternatives can be seen in fig. 3.7.

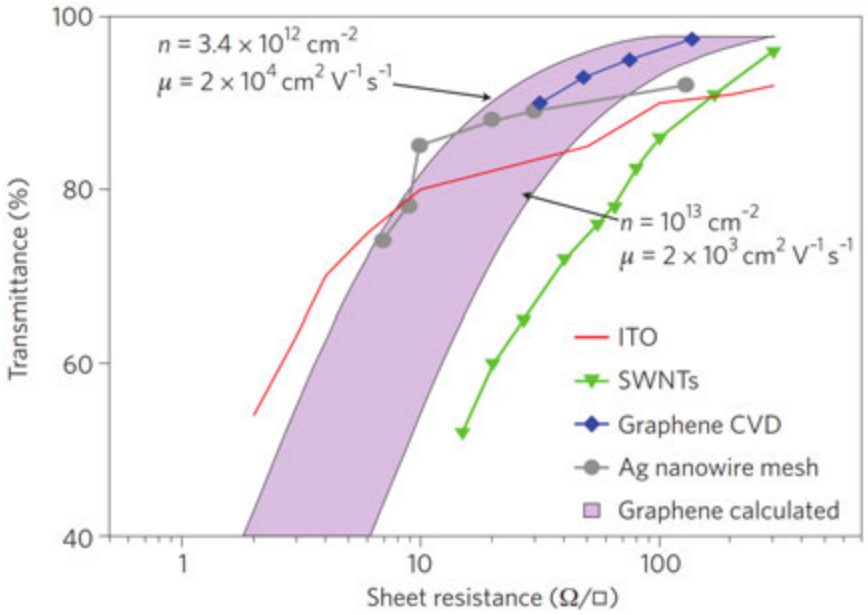

Figure 3.7: Comparison of graphene conductive films versus some other alternatives [23]. It is worth to notice that in this graph the ITO thickness is 550 nm.

It has been demonstrated that graphene p-doped with nitric acid can achieve sheet resistance of $\sim 125\,\Omega/\square$ while maintaining a transmittance of 97.4% [35]. Also, the current density that can be handled by graphene nano ribbons (GNR) is in the order of $10^8 A/cm^2$ [38]. However, the best reported contact resistance between graphene and p-GaN is only in the order of $\sim 0.5\,\Omega\,cm^2$ [39]. Thus if we compare this properties to the ones in table 2.1 for ITO it is clear that there are some problems. First the absorption of graphene is 2.1% higher than that of ITO and secondly the contact resistivity is one order of magnitude higher.

The higher absorption might not be such a big issue since the thickness of graphene is about 0.35 nm and the thickness of ITO is 50 nm. Thus if the film is placed in a node of the standing wave the effective absorption might be comparable to that of the 50nm ITO. On the other hand, the problem of the high contact resistivity and sheet resistance is more severe and need do be evaluated.

Yet, the industrial production of devices using graphene TCF also requires a production, doping and deposition of graphene on the p-GaN substrate technique that are reproducible. Thus it is important to consider not only the feasibility but also the reproducibility of the techniques used.

3.5 Summary

Graphene is a 2D material formed by a honeycomb lattice of sp^2 hybridized carbon atoms. This lattice arrangement of carbon atoms give rise to an unconventional energy dispersion of electrons where the conduction band touch the valence band in 6 points (Dirac Point) making graphene a zero bandgap semi-metal. Near the Dirac points the energy dispersion is linear and similar to the Dirac-Weyl equation for relativistic particles. Due to this unconventional energy dispersion the mobility of carriers of graphene can reach values higher than $\sim$200,000 $cm^2/(Vs)$ for suspended graphene and in the order of $10^3 cm^2/(Vs)$ for graphene on substrates. Also, graphene even at zero carrier concentration has conductivity in the order of e^2/h (experimental).

There are several techniques for the production of graphene, among the most relevant are exfoliated graphene, chemically exfoliated, SiC decomposition and chemical vapour deposited graphene. This work is focused on CVD graphene due to its scalability, reproducibility, and good quality (Mobilities in the order of $10^3 cm^2/(Vs)$)of the synthesized graphene with relatively large domains (millimetre size domains [37]) and cost effective production. Furthermore, the transition metal used for the the catalysis of the synthesis will be copper due to its surface-driven catalytic reaction that allows the control of single layer synthesis.

The transfer of the graphene from the Cu to the target substrate can be done by mean of wet etching of the metal and wet transfer, wet etching and dry pressurized transfer and H_2 bubbling separation of the polymer/graphene complex from the catalytic metal and further wet transfer. The selected method in this research will be based

on a variation of the the H_2 bubbling transfer due to the fact that it is faster, more reproducible and that the metal does not need to be etched away.

Several groups have demonstrated good sheet resistances in graphene ($\sim 125\,\Omega/\square$ [35]) and also good current densities in graphene nanoribbons have been measured ($10^8 \mathrm{A/cm^2}$ [38]). However the contact resistivity with p-GaN is still to high ($\sim\ 0.5\,\Omega\,\mathrm{cm}^2$ [39]) and the reproducibility and scalability of the process still need to be evaluated.

The graphene absorption is $\sim 2\%$ higher than in 50 nm ITO but due to its thickness (0.35 nm) the effective absorption of graphene, if it is positioned in a node of the standing wave in the laser cavity, will be similar to that of the ITO.

Thus, the main points that needs to be evaluated in order to demonstrated the feasibility of replacing ITO with graphene films are:

1. Synthesis of large scale graphene with enough quality for TCF.
2. Efficiency of the transfer to the target substrate.
3. Improvement of electrical properties (sheet resistance, contact resistivity, and current density) and assessment of optical properties.
4. Enhancement of the overall reproducibility of the process.

Chapter 4

Experiments, results and discussions

To investigate the possibility of replacing ITO with a graphene TCF different set of experiment were done. First, the synthesis of graphene was done using different surfaces for the catalysis. This was followed by experiments on the transfer of graphene to the target substrate. Finally, the optical properties were assessed and the electrical properties were improved and characterized fabricating devices for resistance measurements. Through all the experiments the reducibility of the technique used was taken into consideration. The details of the process, results and discussions are presented in the rest of this chapter.

4.1 Graphene synthesis

The process can be resumed to the following steps[1]:

1. Catalytic substrate cleaning in acetic acid, acetone and IPA[2] to romove any unwanted oxides or organic residues. This step is important to avoid any uncontrolled source of carbon.
2. Graphene synthesis on the catalytic substrate surface inside a cold-wall low-pressure CVD reactor specially designed for carbon deposition[3]. First the low-mass joule heater with the substrate on top is heated to 1,000 °C with a heating

[1]For the recipe of the process please refer to section A.1 of the Appendix A
[2]Isopropyl alcohol ($CH_3CHOHCH_3$)
[3]Black Magic, AIXTRON Nanoinstruments Ltd.

rate of 300 °C /min. and annealed during 5 minutes. During the annealing a flow of 20 sccm of H_2 and 1000 sccm of Ar is used. After annealing a 30 sccm flow of CH_4(5%):Ar(95%) is introduced to the reaction chamber to start the graphitization. The flow of the three gases is conserved during 5 minutes at a total pressure of 6.35 mbar. Then all the gasses flows are turned off and the system is evacuated to < 0.1 mbar. Finally, the samples are cooled at 300 °C /min. to room temperature[1] under 20 sccm of H_2 and 1000 sccm of Ar. This process is described in fig. 4.1.

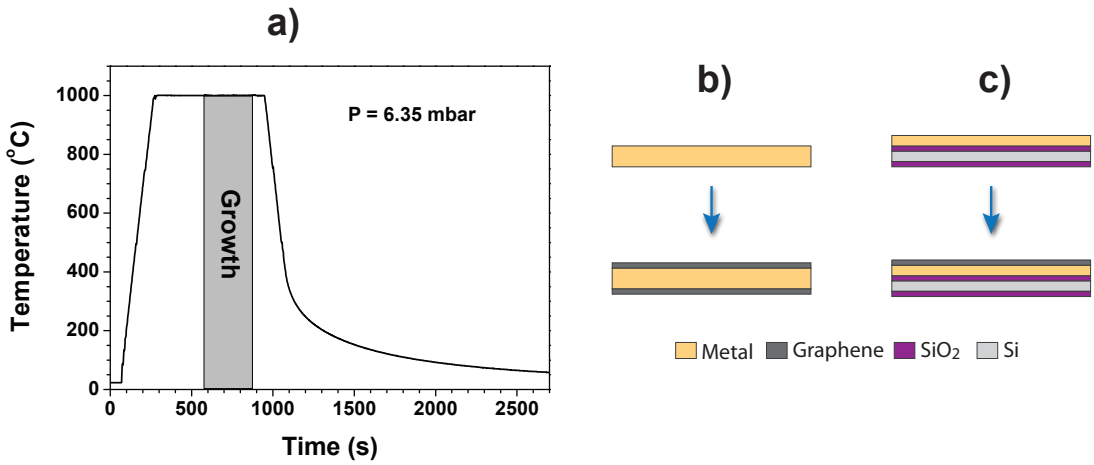

Figure 4.1: a) Temperature vs. time during the synthesis process [40]. b)Process flow using a metal substrate for catalysis. c)Process flow using evaporated metallic thin film on SiO_2/Si/SiO_2 substrate for catalysis.

Three different substrates were investigated for the graphitization process: Evaporated Cu thin film on SiO_2/Si/SiO_2 substrate, Cu foil, and Pt foil.

4.1.1 Raman spectrum of graphene

In order to characterize the quality of the graphene Raman spectroscopy with a 514.5 nm wavelength laser was used[2]. The Raman spectrum for carbon material has tree characteristic peaks; the D peak (around 1360 cm^{-1}), the G peak (around 1580 cm^{-1}) and the 2D peak (around 2700 cm^{-1}). The D peak, generated by zone-boundary phonons, gives information about the amount of defects and impurities in graphene. The G peak

[1] Below 300 °C the cooling rate can not be controlled.
[2] If a brief explanation of the technique is required please refer to the Appendix C section C.1

is a signature of graphitic material and is due to the degenerate E_{2g} mode[41, 42]. The 2D peak is the trademark for graphene. The characteristics of the 2D peak and further comparison with the G peak will be the key point for the identification and quality assessment of graphene.

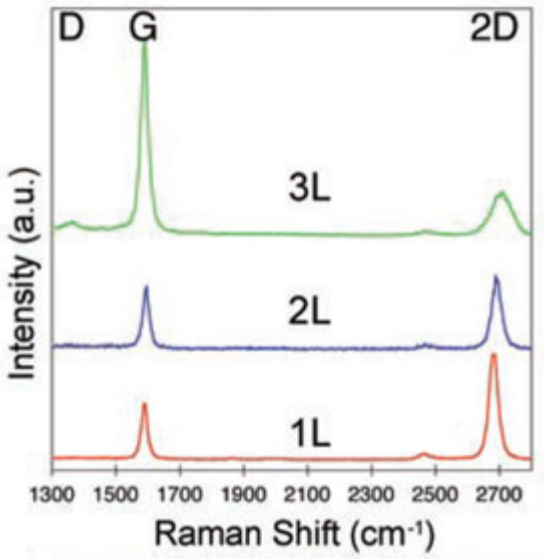

Figure 4.2: Raman spectra of 1, 2 and 3 layers graphene films [43].

As it can be seen in fig. 4.2 the 2D peak to G peak intensity ratio decrease drastically with the increase in the amount of layers. Thus, if the ratio of the 2D peak to the G peak (2D/G) ratio is less than 1 the synthesised film is considered to be multilayer graphene, if it is ~ 1 the film is bi-layer graphene, and if it is > 1.4 it can be considered a single layer graphene. Even higher 2D/G ratio implicate single layers of higher quality [43]. Also, For single layer, the 2D peak should be symmetric and the full width at half maximum (FWHM) of the this peak should be between $25\,\mathrm{cm}^{-1}$ and $40\,\mathrm{cm}^{-1}$. The D peak is not present in high quality graphene.

4.1.2 Synthesis on evaporated copper thin film

A Cu film with a thickness of 600 nm was deposited on top of a SiO_2/Si/SiO_2 substrate (thickness of SiO_2 was 300 nm) using an e-beam evaporation PVD[1] reactor. Raman measurement was performed on top of the Cu film and also after transferring the graphene

[1]Physical Vapour Deposition. More information about PVD in section C.3 in the Apendix C.

to a $SiO_2/Si/SiO_2$ substrate. It is important to notice that due to time constrains and availability of the Raman spectrometer the transferred graphene was not exactly the same as the measured on Cu foil. Both of them were produced together but one of them was transferred and the other remained in the Cu foil.

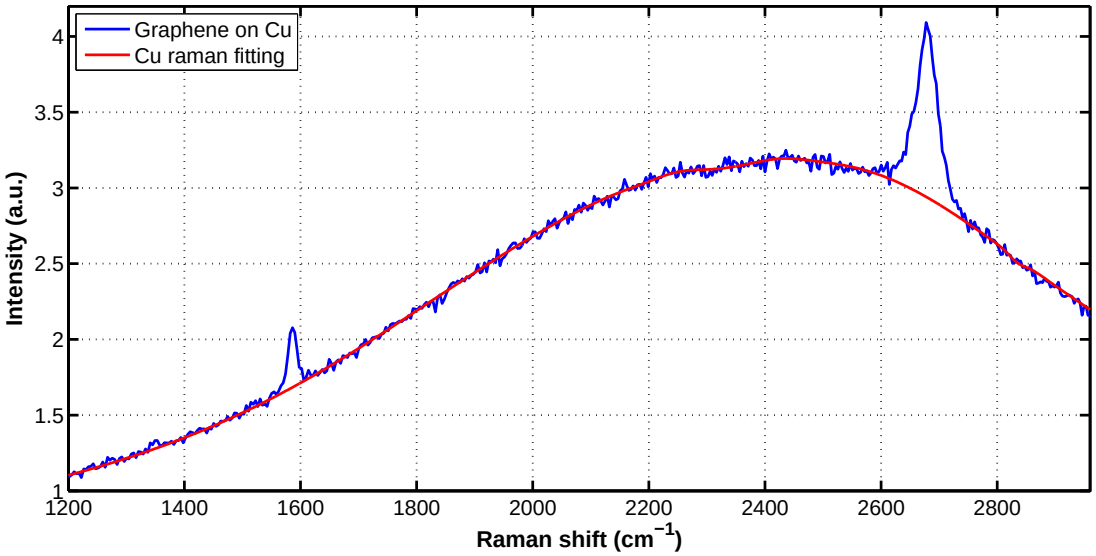

Figure 4.3: Raman data (blue) and Cu Raman fitting model data (red) for the analysis of graphene grown on thin film.

In order to avoid the deformation of the graphene Raman spectra due to the Cu film, the Raman on Cu foil was filtered by fitting a model for the Cu Raman (see fig. 4.3) and differentiating the Raman raw data with the Cu Raman model.

Figure 4.4 shows the resulting Raman spectrum for graphene on top of the Cu thin film. The 2D/G peak ratio of 2.921 and the FWHM of 37.7 cm^{-1} clearly denote the existence of a single layer graphene film. Furthermore it is good noticing that the D peak (about 1360 cm^{-1}) is probably very week and can not be seen in the spectrum.

On the other hand, in the figure 4.5 it can be seen that the 2D/G ratio of 2.662 and the FWHM of 34 cm^{-1} confirm the presence of good quality graphene even after the transfer to the SiO_2 substrate[1]. Nevertheless, there is a clear D/G ratio of 0.218 indicating the existence of some impurities or imperfections.

When comparing the Raman spectrum of the graphene on Cu film and the graphene after transferred a blue shift of the G peak can be noticed. After measuring the Raman

[1]From now on $SiO_2/Si/SiO_2$ substrate will be referred to as SiO_2 substrate.

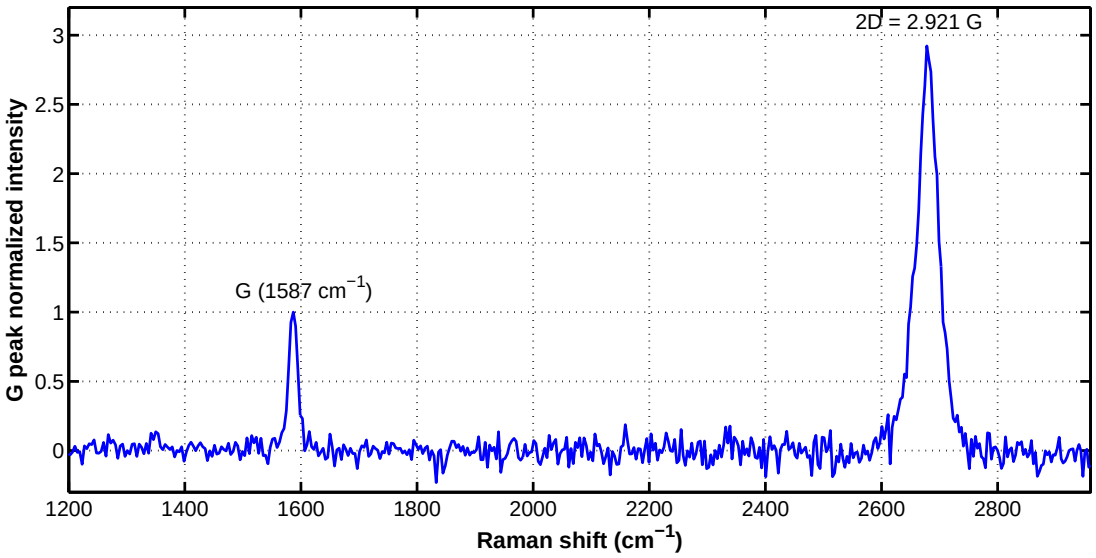

Figure 4.4: Raman of graphene film on Cu film after differentiating with the Cu Raman fitting model. The Cu thin film thickness was 600 nm and the FWHM of the 2D peak is 37.7 cm^{-1}.

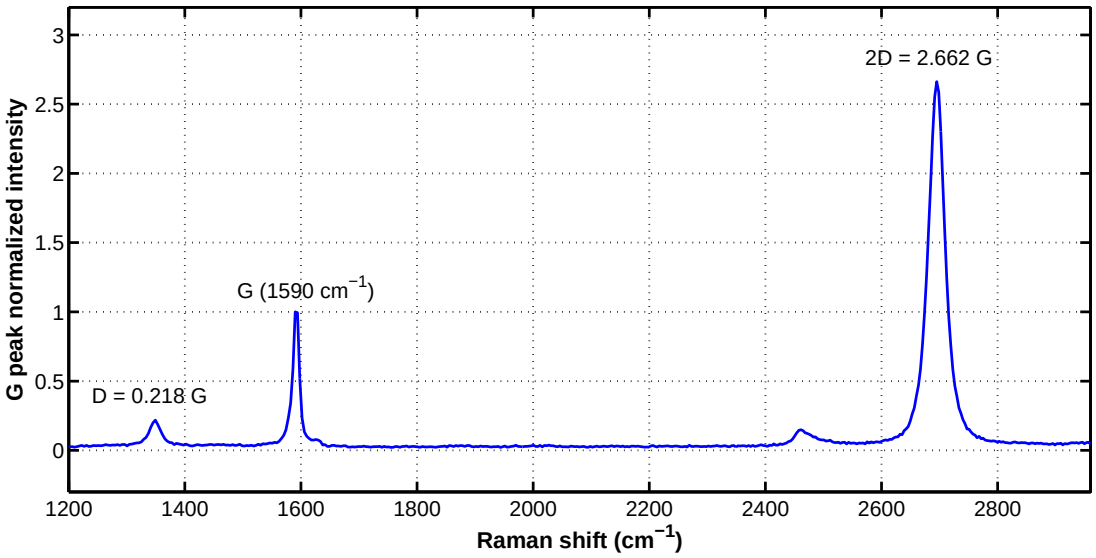

Figure 4.5: Raman of graphene film grown on Cu film after transferred to SiO_2/Si/SiO_2 substrate.The Cu thin film thickness was 600 nm and the FWHM of the 2D peak is 34 cm^{-1}.

the data set was aligned using as reference the well known silica peak (521 cm^{-1}) coming from the $SiO_2/Si/SiO_2$ substrate[1]. This blue shift after transferring could indicate a higher p-type carrier concentration[44].

Even if the quality of the Raman is relatively good the electrical performance of these films is relatively poor with measured mobilities in the order of 50 $cm^2/(Vs)$. This low performacne can be probably due to small domain sizes. These small domains would introduce a high amount of grain boundaries (see fig. 4.6) that deteriorate the electrical properties of the film. The reason why or how such small domain sizes could have been formed is not clearly understood at the moment and need further investigation.

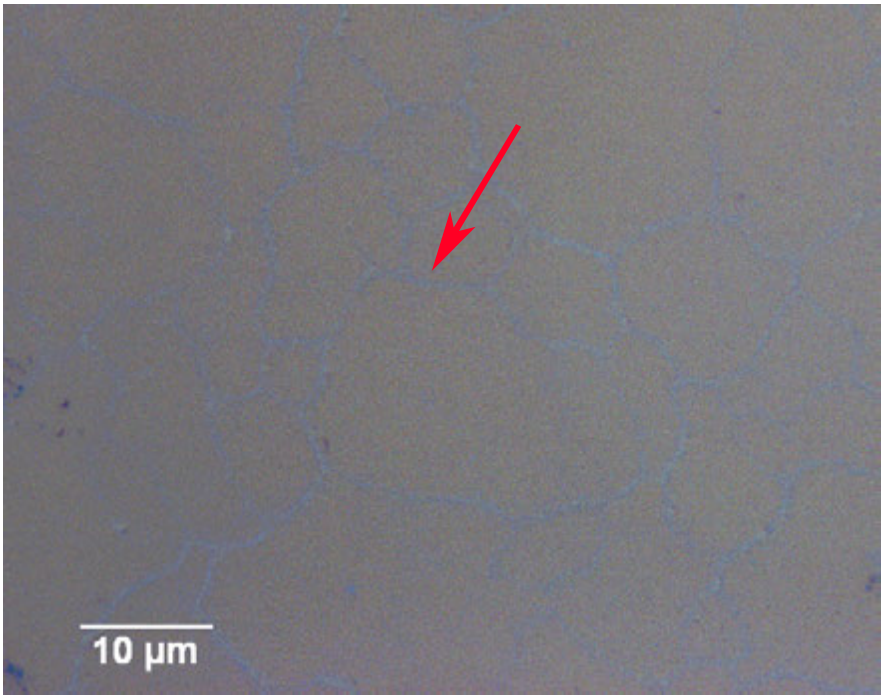

Figure 4.6: Optical image of graphene from Cu thin film after transferred to 300 nm SiO_2 surface. After contrast adjustment of the image it can be seen that there is a high amount of grain boundaries (red arrow) in the graphene film.

[1] As measurements were done during the same session it is expected that the calibration shift in the X axis with the SiO_2 data set can be use to calibrate the Cu film data set.

4.1.3 Synthesis on copper foil

Cu foil of 50 μm thickness and 99.995% was primarly used. Also some experiments were done on higher quality Cu film (99.9999%) but, due to the fact that the growth technique in that material is yet not perfectly tune for the instruments available in the research laboratory, the reproducibility is not that good and thus the research was focused on the 99.995% purity Cu foil.

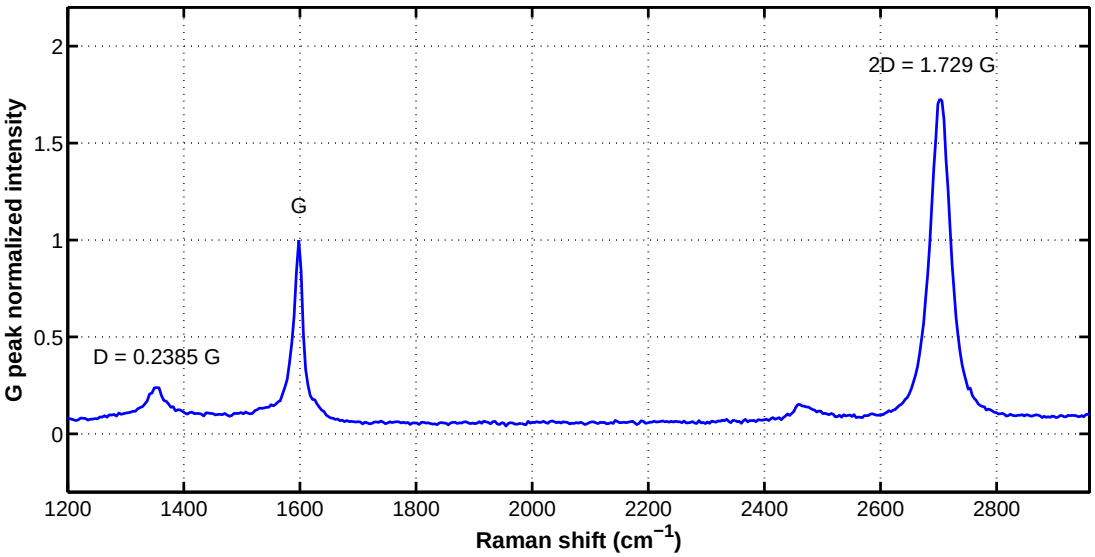

Figure 4.7: Raman spectrum of graphene from Cu foil on SiO_2 substrate. The thickness of the copper foils used for catalysis was 50 μm and the purity was 99.995%. The FWHM of the 2D peak is 37.7 cm^{-1}.

For the graphene Raman spectrum from Cu foil the majority of the samples had 2D/G ratios between 1.6 and 2 (there where few samples with higher ratios). Also, from figure 4.7, an increase of the D peak can be seen compared to the D peak of the Raman of graphene from thin film. The FWHM continues to be 37.7 cm^{-1}. The electrical properties of the graphene films from this Cu foil is also much better than for thin films (mobilities in the order of 10^3 cm^2/(Vs))[1].

With this 99.995% pure Cu foil the quality of the graphene (structural and electrical) is relatively good and, as the research group has a very good know-how, the synthesis process is very reproducible. Thus, during the rest of the experiments[2] the graphene

[1] The result of the of the electrical characterization will be introduced later in the section 4.3
[2] Excluding the e-beam fabricated devices.

used will be synthesized from 99.995% Cu foil.

4.1.4 Synthesis on Platinum

After the success of the group headed by Libo Gao in synthesising millimetre size graphene films with mobilities about 7,000 $cm^2/(Vs)$ [37] on platinum substrates the evaluation of using Pt for graphene catalysis in this project was decided. It is worth mentioning that as the dissociation energy of methane in Pt is smaller than in Cu (0.7 eV vs. 4.77eV [45]), the graphitization process in Pt will go faster than in Cu and it will be more difficult to control the number of layers.

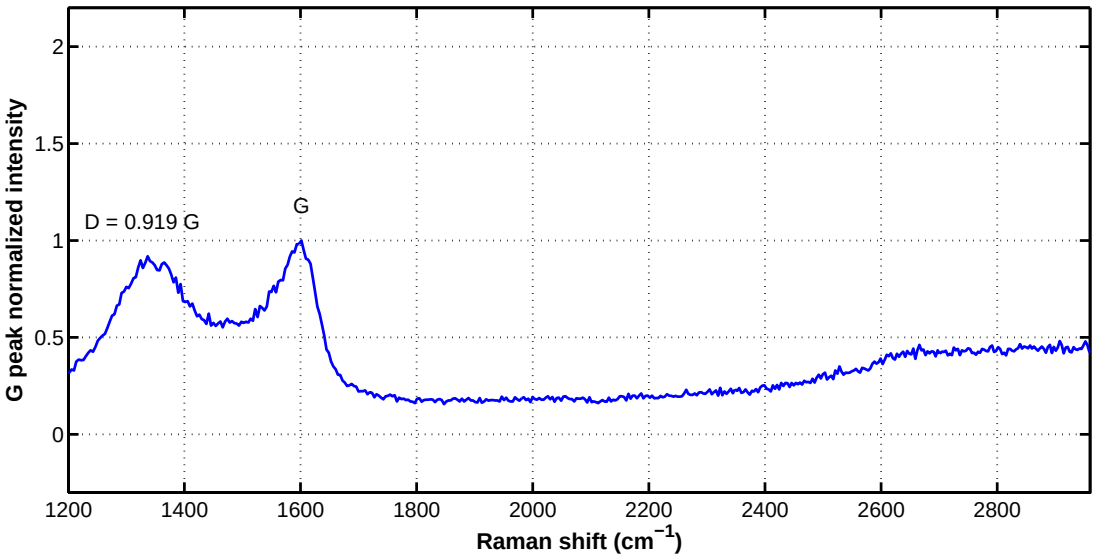

Figure 4.8: Raman spectrum of graphitic film from Pt substrate catalysis on SiO_2. The absence of the 2D peak and the high D/G ratio denote the lack of 2D order in the graphitic film eliminating the possibility of having single layer graphene.

The parameters of the graphitization process were changed in order to follow the guidelines of Gao's group. The annealing temperature was 930 °C during 10 minutes. The H_2 flow was 700 sccm and the flow of CH_4(5%):Ar(95%) was 80 sccm; the Ar flow remain the same (1,000 sccm). The graphitization time was 7 minutes. Although the recommendations from literature were followed, the results were not good and the presence of a graphitic film (not graphene) was observed as can be seen from the Raman spectra of the sample after transferred to a SiO_2 substrate in figure 4.8. Due to the bad quality of the film no further experiments were carried.

4.2 Graphene transfer from metallic surface onto target substrate

As described in section 3.3 there are several ways to transfer the graphene to the target substrate. In this particular work the focus will be on the wet etching – wet transfer (from now on referred only as "wet transfer") and the H_2 bubbling separation – wet transfer (from now on referred only as "bubbling transfer").

4.2.1 Wet transfer

Process description

The steps followed for the wet transfer can be summarized as[1]:

1. Spin coating of the Gr[2]/Cu-foil complex with PMMA and baking.
2. O_2 plasma removal of graphene on the backside of the PMMA/Gr/Cu foil.
3. Attachment of the PMMA/Gr/Cu-foil complex to the bottom of the etching acid container with an adhesive tape. This step was introduced to sustain the PMMA once the metal has been etched away preventing the PMMA to float freely in the acid and loose track of whether it is facing up or down (graphene will be on the bottom face).
4. Cu foil etching. For the etching of the Cu foil the PMMA/Gr/Cu-foil was submerged in a solution of HCl(37 wt%):H_2O = 1:7 with two drops of H_2O_2 and was left overnight. This process is not only slow but can also be detrimental to the quality of the graphene.
5. PMMA/Gr complex cleaning with DI water.
6. Deposition of the PMMA/Gr complex on top of the target substrate (SiO_2).
7. Drying of the PMMA/Gr/SiO_2 at room temperature and baking.
8. Removal of the PMMA by dipping in acetone
9. Cleaning of the Gr/SiO_2 substrate by dipping in IPA and blow dry with N_2.

[1] For more details recipe A.2 of Appendix A can be consulted.
[2] Gr will be used to denote graphene.

Characteristics of the transferred graphene

After deposited with this technique the graphene film shows to have a Raman spectrum with good 2D/G ratios and relatively small D peaks in small areas. The main problem is the amount of holes and wrinkles introduced due to the transfer. These imperfections induce less uniformity of the graphene along the whole surface and a less reproducible transfer process.

In order to have an idea of the distribution inside one sample, four Raman spectra were arbitrary obtained inside the sample 0010-SH-13 and the resulting 2D/G average was 1.449 with an standard deviation of 0.28. Only 50% of the points have 2D/G ratios higher than 1.4.

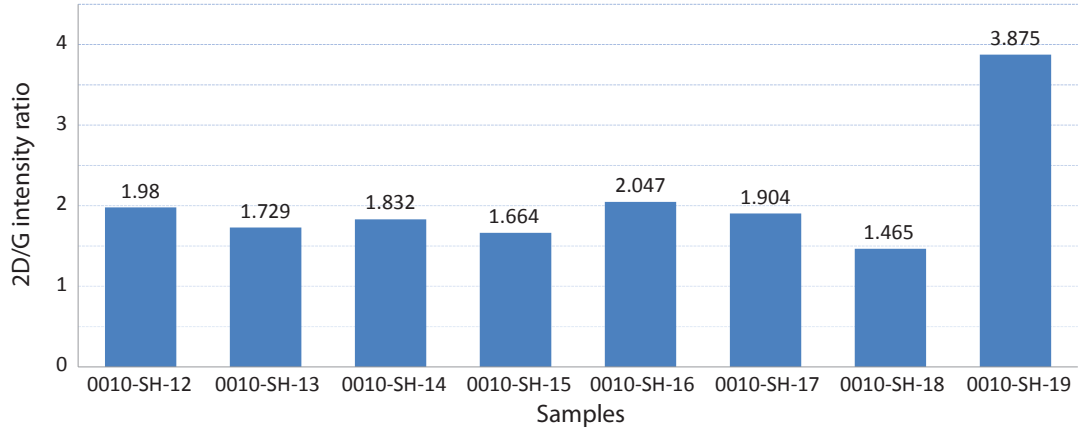

Figure 4.9: The average ratio was 2.062 with a standard deviation of 0.75.

Also, Raman spectra were mapped over 8 samples. The best 2D/G ratios in each sample was selected (see fig. 4.9). The average 2D/G ratio was 2.062 with a standard deviation of 0.75 and 100% of the samples had 2D/G ratios higher than 1.4. To compare with the next transfer technique 4 samples were selected arbitrary and one Raman measurements was aleatory perform in each the samples of the previous set of 8. The resulting average 2D/G ratio was of 1.611 with an standard deviation of 0.29.

4.2.2 Bubbling transfer

Process description

For the bubbling transfer a method similar to the one described in section 3.3.3 was used. The main difference being that a frame was used to support the PMMA/Gr complex in the edges after separation from the Cu foil (see fig. 4.10). The Frame/PMMA/Gr complex can be easily manipulated by tweezers for the cleaning and deposition on top of the target substrate as it is shown in fig. 4.10-b. As the PMMA/Gr is only being hold by the frame at the borders the central part of the PMMA/Gr is untouched. Once the PMMA/Gr has been deposited on the target substrate, the frame can be removed by cutting the PMMA/Gr complex in the inside borders of the frame.

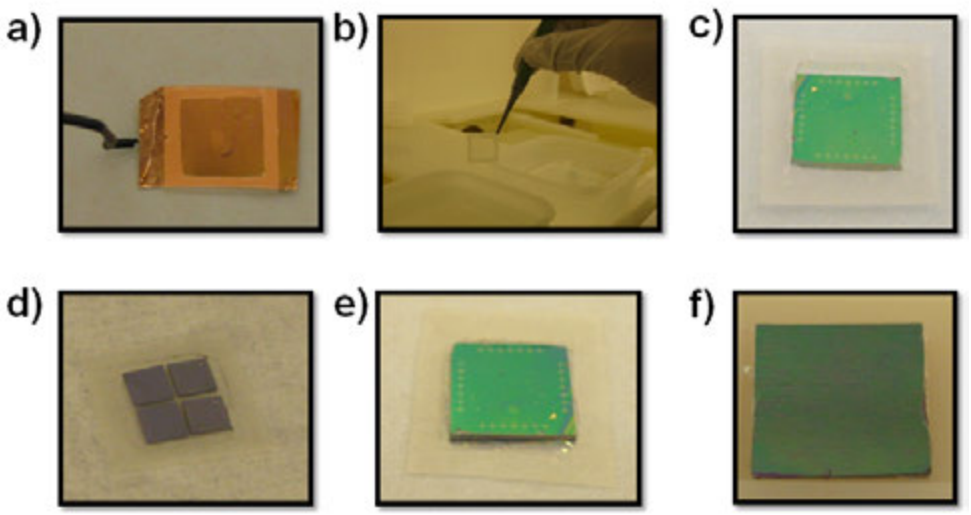

Figure 4.10: Pictures from bubbling transfer process. a) Frame on PMMA/G/Cu-foil. b) Frame/PMMA/Gr complex after separation form metal being cleaned while is held with tweezers. c) Frame/PMMA/Gr complex on target substrate. d) Demonstration of multiple samples transfer. e)Removal of the frame after dried. PMMA/Gr on target substrate after frame removal.

For these experiments thermal tape was used as the material for the frame. The thermal tape is flexible enough to support the deformation during the non uniform detachment from the Cu foil, yet rigid enough to facilitate the handling of the Frame/PMMA/Gr complex. Also, a more robust adhesive resistant to water and basic solutions was used based on neoprene rubber dissolved in a solution of 50% toluene and 10% butanone

commonly known as "contact cement". This adhesive was deposited on the frame side that will be in contact with the PMMA.

The main mechanism that drives the separation of the Frame/PMMA/Gr complex from the Cu foil is the production of hydrogen bubbles between the graphene and the Cu foil. For that reason the graphene is not being exposed to any etchant and, even more important, the separation takes place in seconds ($\sim$ 40 sec for 1.5cm^2 area). In order to increase the conductivity of water for the electrolysis process a solution of 0.25 M NaOH was used.

In general, as it is shown in fig. 4.11, the process steps for the bubbling transfer can be summarized as[1]:

1. Spin coating of the Gr/Cu-foil complex with PMMA and baking.
2. O_2 plasma removal of graphene on the backside of the PMMA/Gr/Cu foil.
3. Frame preparation and adhesion to the PMMA/Gr/Cu-foil complex.
4. Border scratch to enhance the permeation of the water during electrolysis.
5. Electrolysis separation of Cu foil in 0.25 M NaOH solution at 1 A during $\sim$40 sec.
6. Frame/PMMA/Gr cleaning in DI water, deposition on substrate and partial drying.
7. Frame removal.
8. PMMA/Gr/SiO_2 complex baking.
9. PMMA removal in acetone and cleaning of the Gr/SiO_2 complex.

It is interesting mentioning that with this method it was possible to transfer several layers of graphene by repeating the procedure several time on the same substrate. Also, the transfer of graphene films using this method was very reproducible and does not required any special "artisanal" skill as in the case of the wet transfer where expertise was required in order to deposit the PMMA/Gr complex on top of the substrate with few wrinkles and bubbles.

Characteristics of the transferred graphene

In general, the graphene from bubbling transfer is more uniform due to the fact that the films is not exposed to any etchant or kept in any chemical for prolonged time. Also

[1]For a more detailed description recipe A.4 can be consulted.

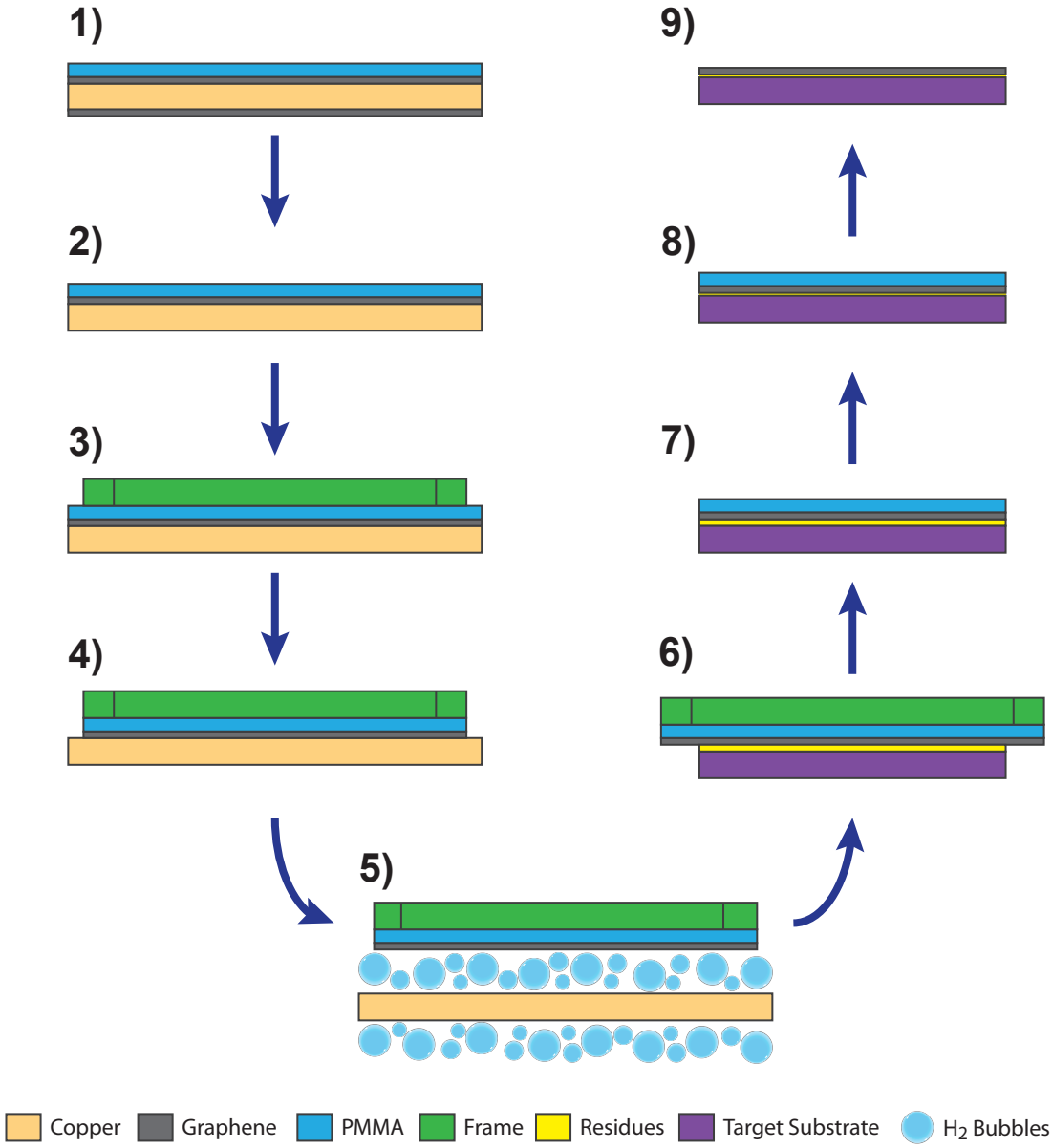

Figure 4.11: Schematic of the bubbling transfer process. Different steps of the bubbling transfer process schematically represented.

the amount of wrinkles and bubbles after deposition is reduced due to the rigidity of the frame.

In order to characterize the transferred graphene a Raman spectra mapping of a $11.8\,\mu\text{m} \times 22.1\,\mu\text{m}$ area was made thanks to the collaboration of Dr. Cole from the division of electrical engineering, Cambridge University.

The graphene was transferred to a glass substrate instead of the SiO_2 substrate used in the wet transfer technique because it was going to be use also for transmittance analysis. The ratio of the 2D/G peak of the Raman spectrum of each point is presented in fig. 4.12 The average value for the 2D/G ratio of the data set (180 points in the same sample) was about 1.566 with an standard deviation of 0.140 and 86.7% of the samples with ratios higher than 1.4. For the D/G ratio the average was 0.250 with a standard deviation of 0.046.

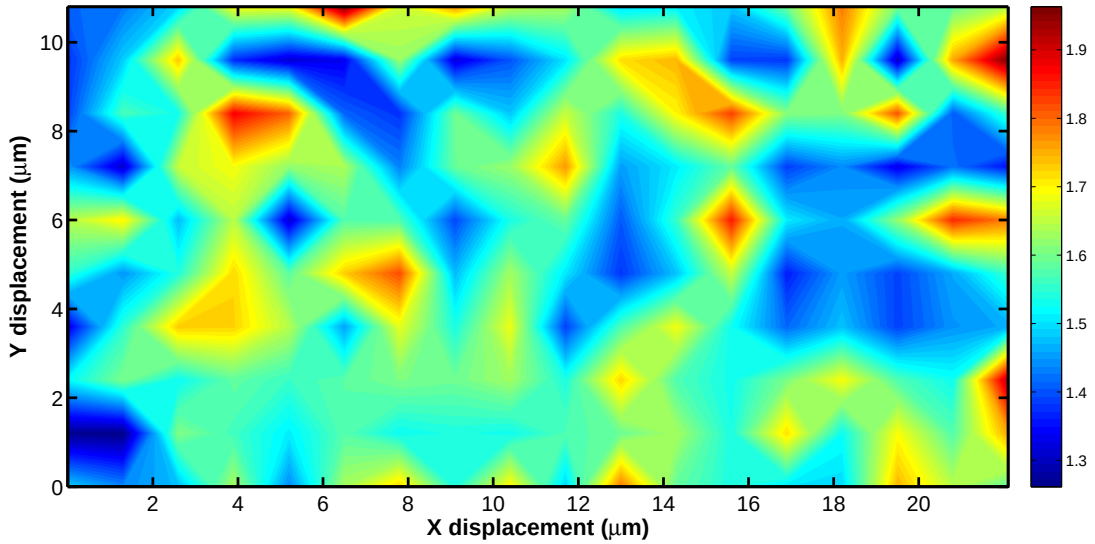

Figure 4.12: Mapping of the 2D/G Raman peaks ratio of a graphene film transferred to glass substrate using bubbling technique. The size of the mapped area is $11.8\,\mu\text{m}$ by $22.1\,\mu\text{m}$.

Using bubble transfer, graphene was also transferred to four different p-GaN substrate that were going to be used for device fabrication. The Raman spectrum was measured immediately after transfer before continuing with the device fabrication. The average intensity of the 2D/G ratio was 1.560 with a standard deviation of 0.263. It is remarkably that the average for different samples was so similar to the average inside

one sample (where the Raman mapping and transmittance analysis were done – 1.560 vs 1.566).

Before continuing, to be able to compare the wet and bubbling transfer the purity, uniformity and reproducibility were assessed. The 2D/G peak ratio average was taken as a quantitative measure of the purity, the standard deviation of the 2D/G peak inside one sample can be seen as a measure of the uniformity, and the standard deviation of the 2D/G ratio between measurements in different samples can be seen as an indicator of the reproducibility of the technique.

To compare with the wet transfer 4 points were arbitrary selected from the 180 points of the previous Raman map. This set of points inside the same sample gives an average 2D/G ratio of 1.574 with a standard deviation of 0.13. The resulting 2D/G ratio average and standard deviation from the 4 points (instead of 180) were quite similar to the ones from the whole population.

The purity of the graphene after transfer with both techniques is almost the same (slightly better for bubbling transfer) as can be seen from the 2D/G ratio average (1.574 vs 1.449). The uniformity, on the other hand, of the bubble transferred is more than two times better ($\sigma_{2D/G}$ is equal to 0.13 for bubbling vs 0.28 for wet transfer). The reproducibility was also better for the bubbling transfer process. This can be seen from the standard deviation of the 2D/G ratio between different samples (0.26 vs 0.29). The average of the 2D/G ratio (and thus the purity) among different samples is still similar for both transfer techniques (slightly better for wet transfer – 1.611 vs 1.506).

A Raman mapping was also done on a sample where two layers of graphene film were deposited one on top of the other. The resulting 2D/G ratios of the raman spectrum of each point are presented in fig. 4.13. Apparently the graphene layers are not interacting and the 2D/G average ratio was of 1.618 with an standard deviation of 0.130 and 95.56% of the samples had a 2D/G ratio above 1.4.

By studying the transferred graphene in an optical microscope, it can be seen that the bubbling transferred graphene is very uniform and has very low amounts of defects (fig. 4.14 a). It can also be seen that, even if it is possible to transfer a second layer of graphene, the amount of defects will increase (fig. 4.14 b). When comparing two devices fabricated from bubbling transferred graphene (fig. 4.14-c) and wet transferred graphene (fig. 4.14-d) it can be seen that the amount of defects introduced is higher for the wet transfer technique.

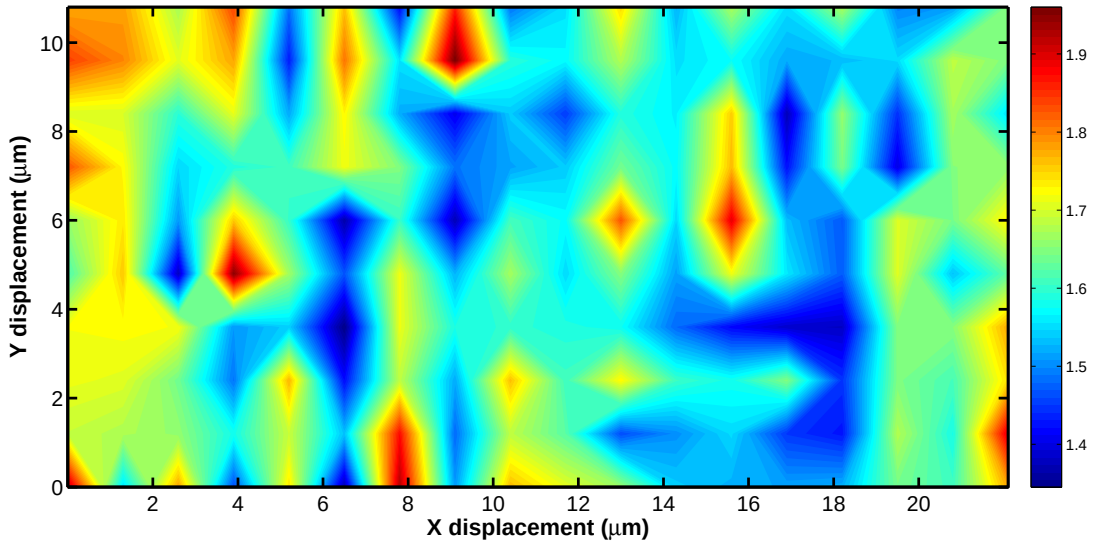

Figure 4.13: Mapping of the 2D/G Raman peaks ratio of two graphene films deposited one on top of the other using bubbling transfer technique. The size of the mapped area is 11.8 μm by 22.1 μm.

4.3 Sheet resistance improvement

To improve the sheet resistance of the graphene film (normally around 500 $\Omega/\square$ after deposited) five options were analysed: two graphene layers in parallel, doping with HNO_3, doping with $FeCl_3$, doping with S1813[1] and doping with poly-vinyl alcohol (PVA).

For the double layer film the motivation was that by having two layers of graphene in parallel the sheet resistance of the material should be reduced to half. However, the transmittance will increase to 95.4% (theoretically).

Doping in graphene can be achieved by substitution of the carbon atoms in the honeycomb lattice of graphene with other atoms with different number of valence electrons (substitutional doping) or by surface transfer of carriers from a dopant adsorbed on the surface (surface doping). Substitutional doping will disrupt the sp^2 hybridization of carbon atoms due to the incorporation of foreign atoms. Surface doping, on the other hand, does not disrupt the structure of carbon lattice. Therefore it was decide to focus on surface doping.

[1]Standard resist used in photolitography.

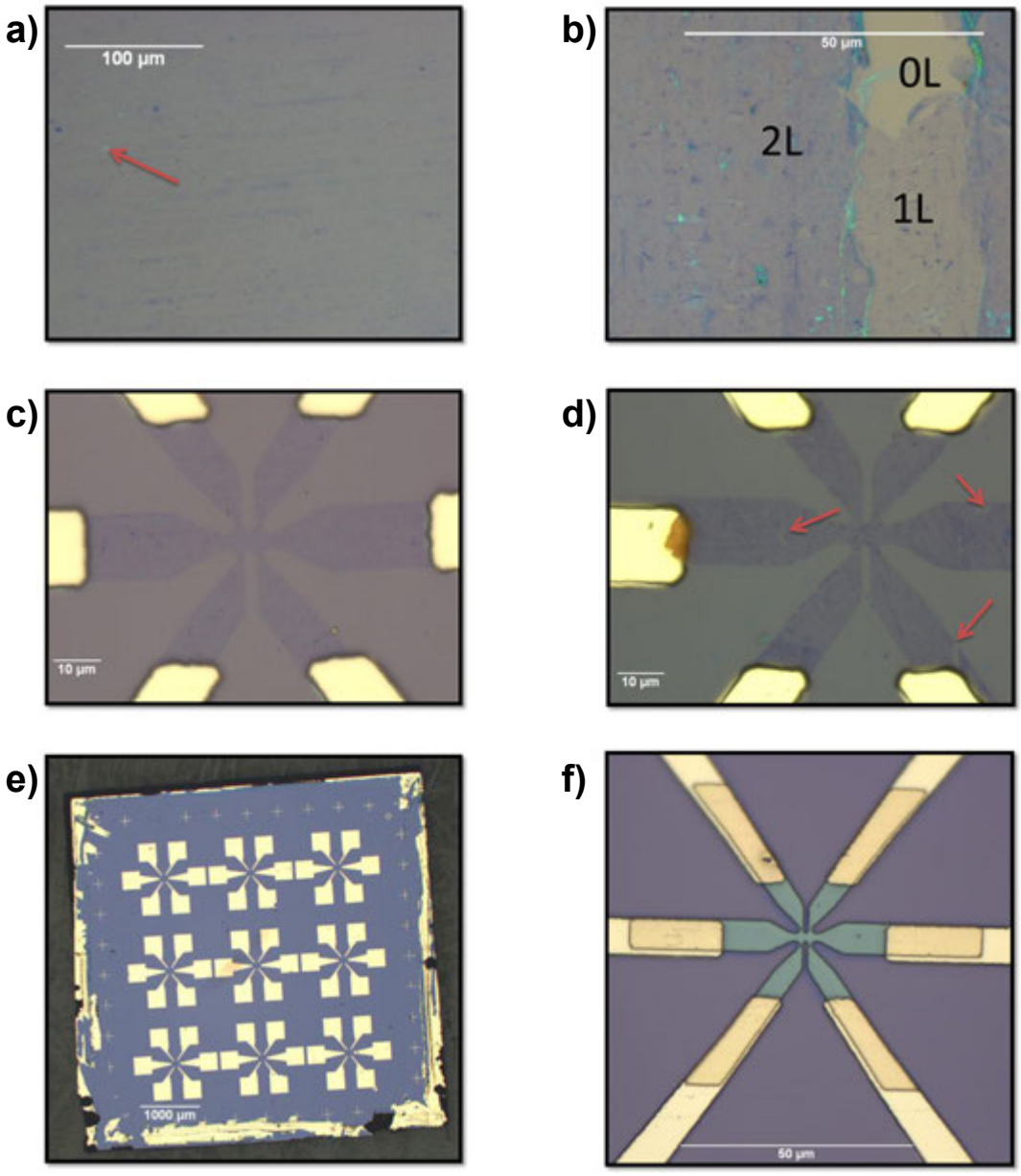

Figure 4.14: a) Single layer graphene (bubbling transfer). b) Two layers of graphene film (bubbling transfer). The 0, 1 and 2 layers areas can be identified by the contrast change. c) Device fabricated with graphene film from bubbling transfer. d) Device fabricated using wet transfer. Red arrows indicate defects. e) Chip with fabricated devices used for electrical characterization. f) Device with patterned S1813 resist on top.

The target substrate will be p-GaN, thus, the interest is to p-dope the graphene film. The p type dopants HNO_3 and $FeCl_3$ were selected due to the success demonstrated by several groups [35, 46]. During device fabrication it was seen that the devices fabricated using e-beam lithography were less doped that the ones fabricated by photolithography where S1813 resist is used for patterning[1]. Thus the possible doping of graphene by S1813 was also evaluated.

It was also decided to evaluate PVA, wich is a n-dopant to see if it was possible to induce, with either p or n-dopant, higher carrier concentration than the limits of 10^{14}cm^{-2} normally achieved in graphene doping from literature.

The mechanism of how the doping is occurring is not clearly understood at the moment. For that reason, detailed explanations related to the doping are avoided in this report. However, for the HNO_3, $FeCl_3$ apparently the driving mechanism is a charge transfer induced disproportionation reaction due to an initial (yet incomplete) charge transfer between the absorbed species and the graphene lattice that destabilize the chemical integrity of the parent compound [47]. For the S1813, probably the mechanism is related to the photo-chemical gating process as described in reference [48] for the doping of ZEP520A (common resist for e-beam lithography).

4.3.1 Doping process

In the fabrication of devices for electrical characterization, the dopant has to be protected from the processes and chemicals used in the fabrication. After evaluating several alternatives it was decided to trap the dopant between two layers of graphene. Also, by doing that, the resistance of the sample will benefit from the second layer. The general process steps were: First, doping of the graphene on the substrate by spin coating or dipping,and second, deposition of a second layer of graphene using bubbling transfer (see fig. 4.15-b). For the S1813 doping there was no second layer deposition due to the fact that the doping was done after device fabrication.

For HNO_3 the process was not successful. After the first layer of graphene was transferred, the substrate was dipped in a solution of HNO_3 69 wt% during 5 minutes following guidelines from literature with minor modifications [35]. However, almost immediately the graphene separate from the substrate and the sample was destroyed.

[1]For e-beam devices the resist used was the copolymer PMMA/MMA.

The reason is probably the existence of residues between the graphene and the substrate which are being etched away once submerged into the acid. Nevertheless, more experiments need to be done in order to draw a more firm conclusion.

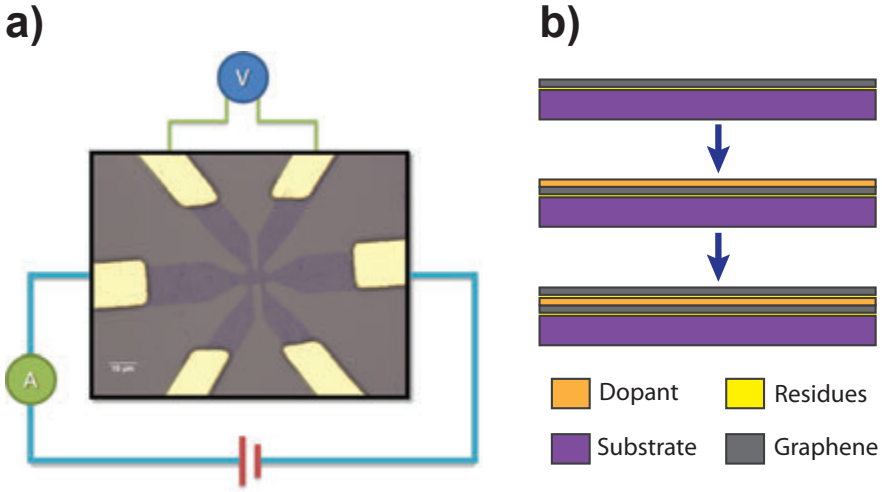

Figure 4.15: a) Schematic of the set up for electrical measurement. b) Schematic of the process used to enhanced the electrical properties. First the dopant is deposited and then other graphene film is deposited.

For the detailed recipes of the doping process for $FeCl_3$, PVA and S1813 sections A.5, A.8 and A.6 of Appendix A can be consulted.

4.3.2 Devices for electrical characterization

The device fabricated for the electrical characterization is shown in figure 4.15-a. This device has six contacts and is used to do a conventional 4 proves measurement (two contacts are redundant). The fabrication process was:

1. Lift-off process for the deposition of the gold contacts (see recipe A.9).
2. Graphene patterning by dry etching in oxigen plasma (see recipe A.10).

The two lateral contact are used to inject the current and the two upper contacts are used to measure de potential drop. The two bottom contacts are redundant contact in case the upper ones do not work. The region where the potential drop is measured was designed to have a longitude to width ratio of 1. This was done to measure sheet resistance directly from the resistance measurement ($R = R_s \frac{l}{w}$ thus if $\frac{l}{w} = 1$ then

	Sheet Resistance ($\Omega/\square$)	**Mobility** ($\mathbf{cm^2/(Vs)}$)	**Eff. Carriers** ($10^{13}\,\mathbf{cm^{-2}}$)	**Transmittance** (%)
Gr	452	1,186	1.1	97.6
Gr/Gr	204	1,268	2.3	95.0
Gr/$FeCl_3$/G	300	291	6.3	94.9*
Gr/PVA/Gr	591	1,776	0.6	94.3*
S1813/Gr	626	526	1.8	N/A

Table 4.1: Electrical and optical characteristics of the different assessed techniques.
*Indirect estimation from measurements on PVA/Gr and $FeCl_3$/Gr.

$R = R_s$). In reality the $\frac{l}{w}$ ratio after the device fabrication is not exactly 1 but 1.039. Thus in order to have the proper sheet resistance the measured values should be divide by 1.039.

The device was fabricated on a SiO_2 substrate. Hence, for the field effect measurement, the silicon between the two layer of SiO_2 was used for gating the device. In order to access the silicon the gold residues from the contact deposition left in the border of the chip (see fig. 4.14-e) was used. To measure the conductance dependence on the gating voltage a fixed current was driven trough the lateral contacts while measuring the potential drop through the upper contacts. Then the gate voltage was varied and the resistance variations were measured.

From this field effect resistance measurement the mobility and carrier concentration were obtained using a mobility model based in the Drude theory of metal[1]. Yet, the reliability of this model is not very good for samples where there is a pronounced valley in the conductance values (good mobility). For that reason in the relatively good samples from e-beam lithography fabrication, a more sophisticated model [49] was used in order to have a more reliable value.

4.3.3 Results from the electrical characterization

The results from all the measurements are summarized in table 4.1 and were performed at room temperature.

[1]For more details regarding this model sections C.2 can be consulted.

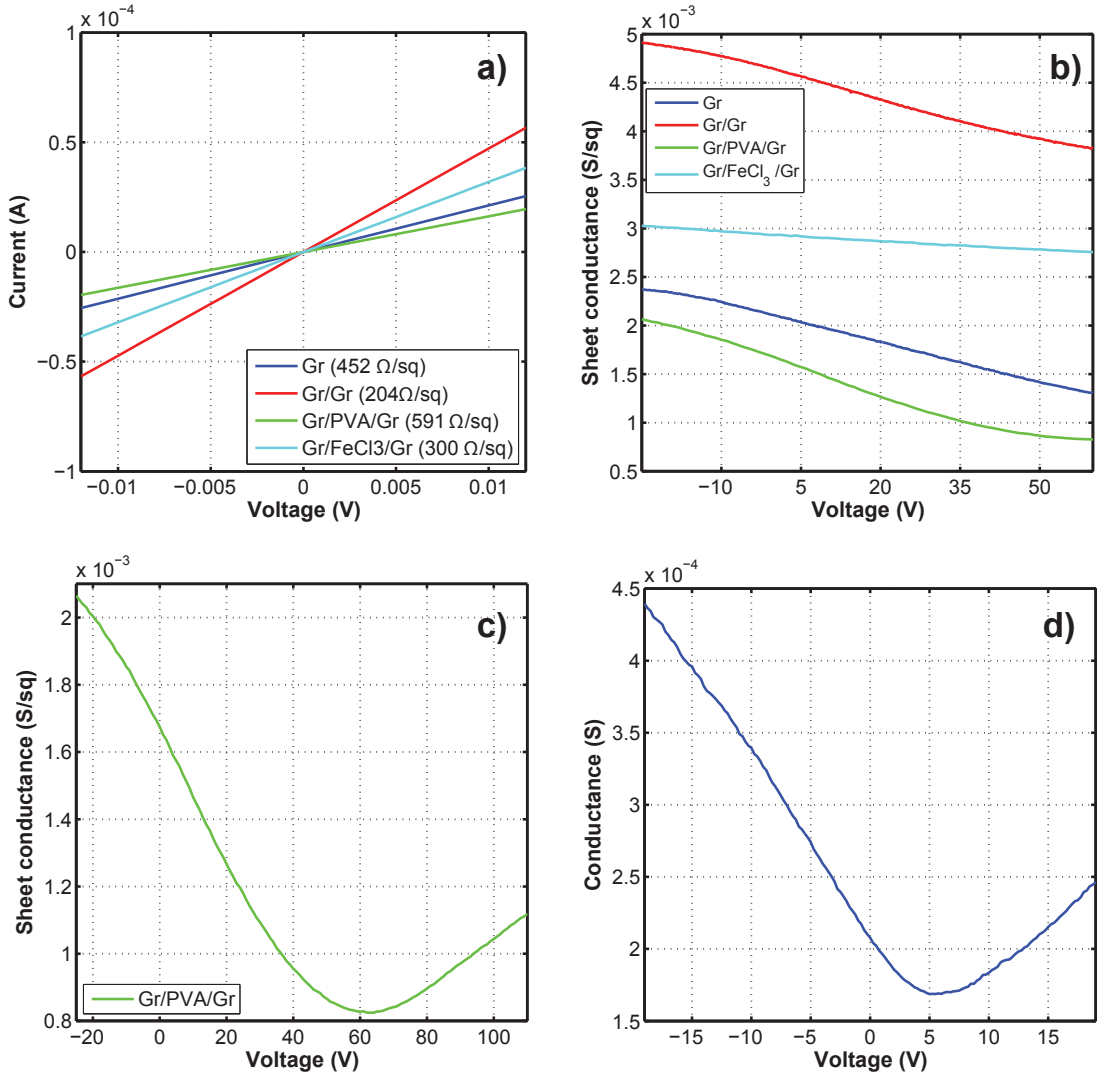

Figure 4.16: Electrical characteristics of 1-layer graphene, 2-layer graphene, PVA and $FeCl_3$. a) Current vs. voltage b) Sheet conductance vs. gating voltage. C) Sheet conductance vs. gating voltage for PVA. d)Conductance vs. gating voltage for an e-beam fabricated single layer graphene device from Cu foil with 99.9999% purity.

	Sheet Resistance ($\Omega/\square$)	**Mobility** ($\mathbf{cm^2/(Vs)}$)	**Carrier Concentration** ($10^{13}\,\mathbf{cm^{-2}}$)
G	452	1,186	1.1
S1813/G	672	544	1.6
S1813/G (Exposed)	626	526	1.8

Table 4.2: Electrical characteristics of the devices intentionally doped with S1813

Single layer graphene

The device with a single layer graphene had a sheet resistance of $452\,\Omega/\square$, as can be seen from figure 4.16. The mobility was of $1{,}185\,\mathrm{cm}^2/(\mathrm{Vs})$ and the effective carrier concentration was in the order of $1.1\times10^{13}\,\mathrm{cm}^{-2}$.

From this values it can be seen that the graphene is already doped. This doping probably originate from the interaction of graphene with the substrate or with residues of chemicals involved during device fabrication.

The maximum linear current density[1] that was reached in single layer graphene devices before destroying it was 4.30 A/cm.

S1813

To investigate the effect of S1813, a new layer of the resist was spin coated on top of the single layer graphene device. The sample was patterned by exposing to UV light during 5 seconds and then etching away the exposed part in MF-319 developer during 40 seconds (see fig. 4.14-f). After that, the sample was characterized and then flood exposed to ultra violet (UV) light during 1 min. and characterized again. The results are summarized in table 4.2.

It can be seen that S1813 is indeed doping the graphene but also deteriorating the mobility of the graphene and degrading overall the sheet resistance. Interesting to notice is that the carrier concentration is increase when S1813 is exposed to UV light, suggesting more strongly that the doping mechanism could be related to the phenomena of photochemical gating [48].

[1] As graphene is a 2D material the units will be A/cm instead of $\mathrm{A/cm}^2$.

Double layer graphene

A second layer of graphene was deposited using bubbling transfer on top of a Gr/SiO_2 substrate. Then the device was fabricated following the procedure described in section 4.3.2

The sheet resistance for double layer graphene was $204\,\Omega/\square$. The mobility was in the order of $1{,}268\,cm^2/(Vs)$ and the effective carrier concentration was about $2.3\times10^{13}\,cm^{-2}$. The sheet resistance is approximately half of that of a single layer, the carrier concentration almost double and the mobility is only slightly higher than for a single layer graphene, which indicates a reproducible growth and transfer process.

The slightly higher mobility might be due to one of the two layers having slightly higher mobility (growth induced) or the fact that the upper layer is not so heavily doped by the SiO_2 substrate.

The maximum linear current density that was reached in double layer graphene devices before destruction was 11.32 A/cm.

Intercalated $FeCl_3$ between two layers of graphene

$FeCl_3$ 45 wt% was spin coated at 2,000 rpm. during 1 minute on top of a single layer graphene. After dried, a second layer of graphene was deposited using bubbling transfer (for details see recipe A.5). Then the device was fabricated following the procedure described in section 4.3.2

For iron chloride the sheet resistance was $340\,\Omega/\square$, which is higher than that of dual layer graphene without any intentional doping despite of the high carrier concentration of $6.3\times10^{13}\,cm^{-2}$. This is due to the deteriorated mobility of $291\,cm^2/(Vs)$. Thus, even if $FeCl_3$ can effectively dope the graphene, it is not a good option to reduce the sheet resistance since the induced detriment of the mobility takes away the advantages of the doping.

Intercalated PVA between two layers of graphene

PVA 4 wt% was spin coated at 2,000 rpm. during 1 minute on top of a single layer graphene. After dried, a second layer of graphene was deposited using bubbling transfer (for details see recipe A.8). Then the device was fabricated following the procedure described in section 4.3.2

In the PVA doped sample, the measured sheet resistance was 591 $\Omega/\square$, the mobility was 1776 $cm^2/(Vs)$ and the effective carrier concentration was 0.6×10^{13} cm^{-2}. Therefore it can be inferred that the effective injection of n-carriers from the PVA doping was also in the order of 10^{13} cm^{-2} from comparing either to the single layer graphene or the dual layer graphene films. The reduction of the carrier concentration increased the mobility of the sample and allows the manifestation of a valley in the conductance vs. gate voltage curve (see fig. 4.16-c) that indicate the change from p-carriers dominating transport to n-carriers. Nevertheless it was not possible to induce a doping higher than the maximum values reported in literature (about 8.9×10^{14} cm^{-2} for $FeCl_3$)[50].

4.3.4 Devices fabricated with e-beam lithography

With the collaboration of Lic. Lindvall from the Quantum Device Physics Laboratory at Chalmers University of Technology devices were fabricated using e-beam lithography instead of photolithography. By doing so it was possible to use PMMA/MMA instead of S1813 during the patterning process. Devices were fabricated on graphene grown on Cu thin films and on Cu foil with 99.9999% purity. For the thin films, the mobilities were in the order of 50 $cm^2/(Vs)$ while the the mobility for graphene grown on Cu foil was in the order of 2,000 $cm^2/(Vs)$ (see fig. 4.16-d).

The graphene from 99.9999% Cu foil showed very good mobilities but due to the problem of reproducibility during the growth discussed previously it is not suitable yet for industrial applications.

4.4 Transmittance of the different treated samples

For the transmittance measurement, graphene was transferred to four optical microscope sample glass using the bubbling transfer technique. The samples were a single layer graphene film, a dual layer graphene film, a single layer graphene spin coated with PVA and the fourth was a single layer graphene spin coated with $FeCl_3$[1]. The samples where then sent to Dr. Cole in the department of Electrical Engineering at the University of Cambridge to realize the transmittance measurements.

The 97.6% transmittance of the single layer graphene is only 0.1% different to the values reported in literature (97.7%) and the double layer graphene had almost exactly,

[1]For more details please refer to recipes A.11, A.12, A.13, A.14 respectively.

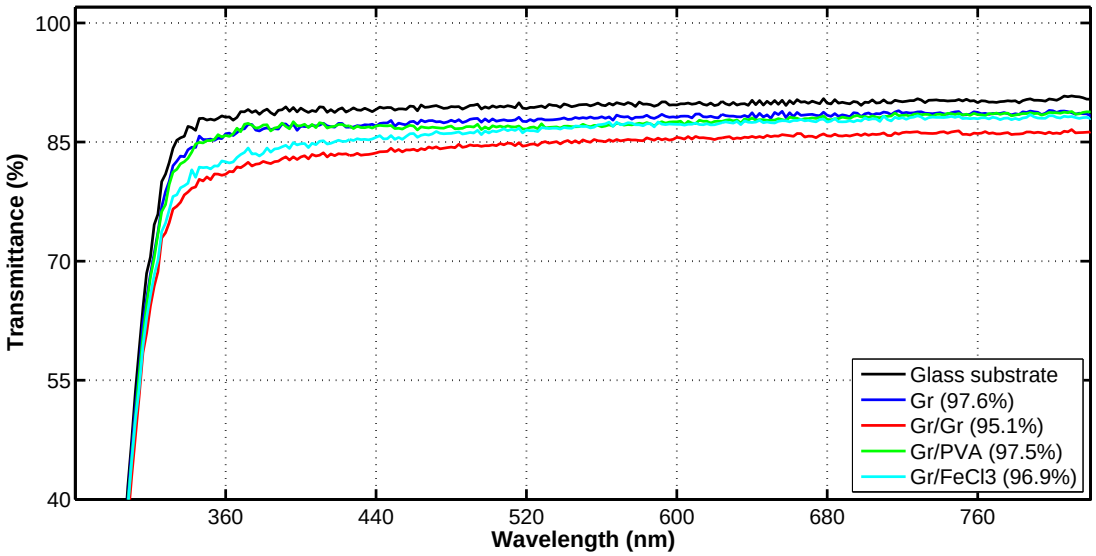

Figure 4.17: Transmittance of the differently treated graphene films.

twice absorption as the single layer following the expectations from the observation presented in section 3.1.2. The PVA film deposited had much lower absorption (only 0.1%) compared to the dual layer graphene as also did the $FeCl_3$ film (0.7%). The results are summarized in fig. 4.17.

4.5 GaN-based light emitting diode (LED)

To see how graphene perform on GaN-based devices, test structures as well as LEDs were fabricated, with the collaboration of Lic. Stattin at the Photonic Laboratory at Chalmers University of Technology. A schematic view of processed devices as well as optical pictures can be seen in figure 4.18.

Graphene can not be seen optically on GaN. Thus, after depositing the graphene on the untreated surface of the LED structure using bubbling transfer, the Raman spectrum was measured to confirm the existence of graphene. The measurement was done in the graphene that was on top of the gold n-contacts to avoid the unintentional optical pumping of the quantum wells in the active region of GaN with the Raman laser (514.5 nm) that would saturate the Raman spectrometer with the spontaneously emitted light. After the data was processed a procedure similar to the one done to eliminate the contribution of copper in section 4.1.2 was done to eliminate the contribution of the

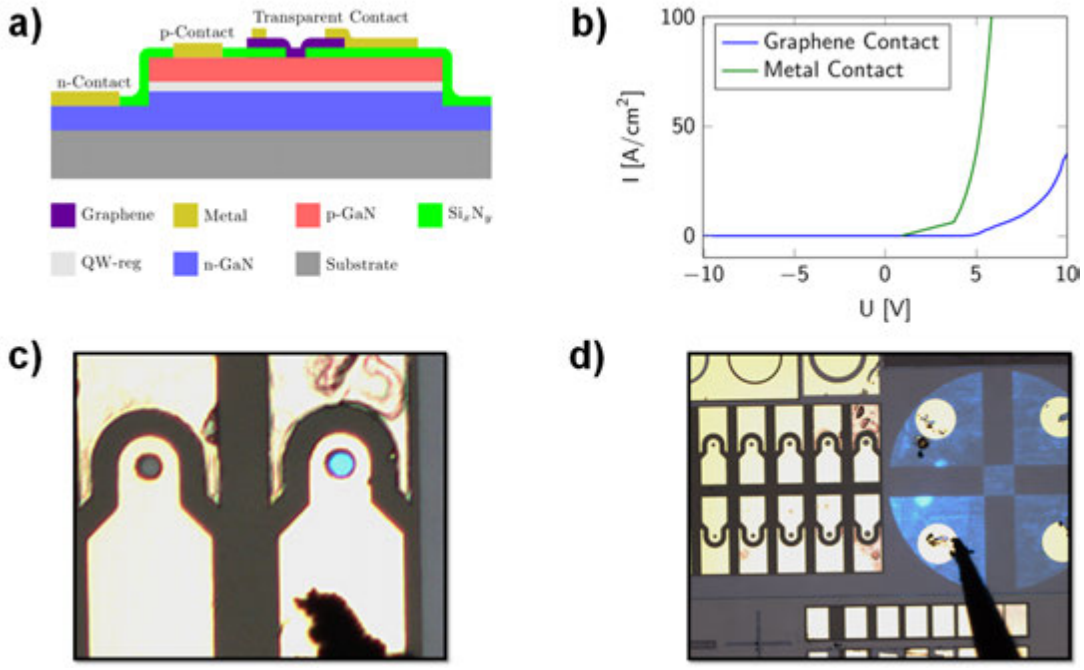

Figure 4.18: GaN-based LED with graphene TCF. a) Schematic of the fabricated LED. b) Current density vs. voltage curve of the LED with graphene and using the *p*-metal contact. c) Image of the 12 μm LED with uniform light intensity across the TCF. d) Current spreading in the whole Hall structure through the graphene TCF.

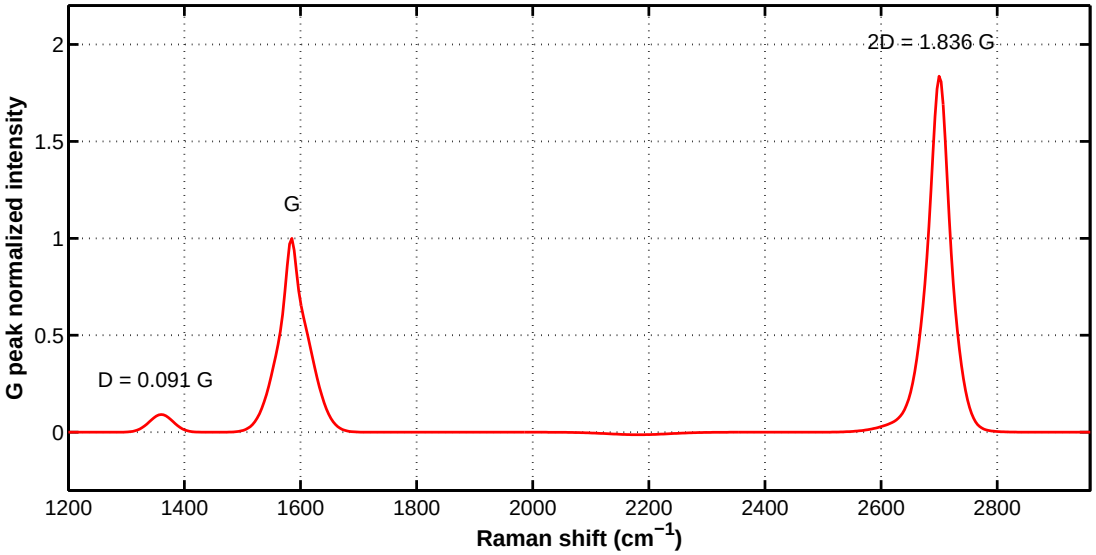

Figure 4.19: Raman spectrum of graphene after deposited on top of the GaN LED structure. The 2D/G ratio of 1.836 and the 2D peak FWHM of 37.7 cm^{-1} clearly identify a single layer graphene film.

	Bubbling transfer	Wet transfer	Better if:
<2D/G> (same)	1.574	1.449	High
<2D/G> (diff.)	1.506	1.611	High
$\sigma_{2D/G}$ **(same)**	0.13	0.28	Low
$\sigma_{2D/G}$ **(diff.)**	0.26	0.29	Low

Table 4.3: Quality, uniformity and reproducibility of the different transfer techniques. 2D/G average was linked to the quality, $\sigma_{2D/G}$ inside the same sample was linked to the uniformity and $\sigma_{2D/G}$ between different samples was linked to the reproducibility

gold spectrum to the graphene spectrum. The resulting spectrum is shown in fig. 4.19. The presence of a single layer film is clearly identified by the 2D/G ratio of 1.836 and the 2D peak FWHM of 37.7 cm^{-1}. Furthermore it is worth noticing the low D/G ratio.

The graphene TCF on p-GaN, after device fabrication, showed to have a sheet resistances in the order of 550 $\Omega/\square$, a mobility of 654 $\mathrm{cm}^2/(\mathrm{Vs})$ from Hall measurements and a carrier concentration of $1.7\times 10^{13}\,\mathrm{cm}^{-2}$. The measured specific contact resistivity of graphene/p-GaN from differential resistance measurements was estimated to be lower than $0.4\Omega\,\mathrm{cm}^2$, and the maximum current density[1] before failure was about 50 A/cm^2.

4.6 Summary

The graphene growth on Cu thin films (600 nm) demonstrate good quality (2D/G: 2.662, D/G: 0.218, 2D FWHM: 34 cm^{-1}) but, probably due to the small domain and the high amount of grain boundaries, the overall electrical properties are not good ($\mu \sim 50\,\mathrm{cm}^2/(\mathrm{Vs})$).

Graphene synthesised from Cu foil 99.995% have good quality, good electrical properties ($\mu \sim 1000\,\mathrm{cm}^2/(\mathrm{Vs})$), and larger domain sizes. The growth recipe for this type of Cu foil is well tuned allowing good reproducibility of the graphene synthesis. For these reasons this Cu foil was selected for the device fabrication in this work.

For transferring the graphene to a target substrate two techniques were assessed: wet transfer and bubbling transfer. In order to evaluate the purity, uniformity and reproducibility of the graphene film deposited with each technique the purity was linked

[1]Here the measured current density is the total current going through the film divided by the contact area of the p-GaN in contact with the graphene (the area emitting light).

to the average of the 2D/G ratio, the uniformity to the standard deviation of the 2D/G ratio inside one sample and the reproducibility to the standard deviation of measurements in different samples. It is good noticing that for the standard deviation the lower the better and for the 2D/G ratio average the higher the better. The results are summarized in table 4.3.

The bubbling transfer is more uniform and reproducible than the wet transfer technique. The purity of the graphene after transfer is almost the same for both techniques. It is worth noticing that the tranferred graphene is being unintentionally p-doped, probably by the transfer process, the interaction with the substrate or both.

The results of the electrical and optical characterization of different techniques used to improve the performance of the TCF are summarized in table 4.1. The most favourable option is to use double graphene layers without doping. This option also offer higher reproducibility and uniformity due to the fact that it only relies on the bubbling transfer and graphene synthesis.

As proof of concept a LED device was fabricated depositing one layer of graphene as TCF. As graphene on GaN substrate can not be seen, the success of the transfer was tested by Raman measurement after depositing. The summary of the electrical properties of the graphene TCF on the p-GaN can be seen in the table 4.4.

Parameter	**Value**
Sheet Resistance	$550\,\Omega/\square$
Mobility	$654\,\mathrm{cm}^2/(\mathrm{Vs})$
Carrier concentration	$1.7\times 10^{13}\,\mathrm{cm}^{-2}$
Contact Resistance	$0.4\,\Omega\,\mathrm{cm}^2$
Max. Current Density	$50\,\mathrm{A}/\mathrm{cm}^2$

Table 4.4: Characteristic of graphene TCF (1 layer) on p-GaN.

Chapter 5

Conclusions

Synthesis of graphene

Large domain of single layer graphene films were synthesized using a cold-wall low-pressure reactor. After evaluating platinum and copper recipes for graphene synthesis it was concluded that the quality of the film was optimal for Cu catalysed growth due to the surface driven catalysis of Cu. Furthermore, Cu foil of 50 μm and 99.995% purity was identified as the most effective substrate among the candidates[1] for the grahene synthesis due to the large domain obtained and because of the reproducibility of the process with the equipments and current know-how available in this research group. Clear indicators of the existence of single layer graphene are the 2D/G ratios in the Raman spectrum higher than 1.4 for more than 86.7% of the samples, in addition to a D/G ratio lower than 0.3 and a FWHM of the 2D peak smaller than 40 cm^{-1} (see fig. 4.7).

Transfer technique

For transferring graphene two technique were evaluated, wet transfer (section 4.2.1) and bubbling transfer (see 4.2.2). The quality from the film transferred with the bubbling transfer techniques resulted to be more uniform and the process was more reproducible. This conclusion arise from the analysis of the Raman spectra of samples transferred from each technique. The results demonstrate that both the standard deviation of

[1] 600 nm Cu thin film and Cu foil 99.9999% were also evaluated.

the measurements in the same sample and the standard deviation of measurements among different samples were lower for samples from bubbling transfer (see table 4.3). Moreover, Using the bubbling transfer technique it was possible to transfer multiple layer of graphene by repeating the process.

Improvement of electrical properties and assessment of optical properties

From the assessed techniques the most promising is the deposition of two layer of graphene without any intentional doping. From table 4.1 it can be seen that the increase in the carrier concentrations by the methods evaluated was followed by a disproportionally large reduction of the mobility and thus increasing the overall sheet resistance. It was not possible[1] to produce higher carrier (either n or p type) concentrations than $\sim 10^{13}\,\mathrm{cm}^{-2}$.

The optical absorption for the double layer graphene TCF was about 5%, slightly different to the values previously reported in literature. The difference form the expected value (4.6%) could be related to the presence of a residual layer between the substrate and the deposited graphene film.

The contact sheet resistivity of the graphene/p-GaN interface was determined to be in the order of $0.4\,\Omega\,\mathrm{cm}^2$ or less. The current density that the devices was able to handle before irreversible damage was $50\,\mathrm{A/cm}^2$.

Comparison with ITO solutions

Taking into consideration all the resulting information, the proposed TCF would have two layers of graphene synthesized on Cu foil 99.995% and transferred one by one using the bubbling technique to the p-GaN. The best predicted values from the data form the experiments are presented in table 5.1.

With the properties that the Gr/Gr TCF has right know, the Gr/Gr TCF can not replace the ITO solutions mainly due to the low maximum current density that it can withstand. This low maximum current density is most likely due to the high contact resistivity between the graphene and the p-GaN.

[1] With the evaluated techniques.

However, the graphene TCF has shown to effectively spread the current on the GaN-based LED structure demonstrate in fig. 4.18.

Parameter	**ITO**	**Graphene TCF (2L)**
Sheet Resistance ($\Omega/\square$)	283.8	204
Contact Resistance ($\Omega\,cm^2$)	0.0541	$\sim$0.4
Absorption(%)	$<$0.5	5
Thickness(nm)	30	0.35*
Max. Current Density (A/cm^2)	12,400	50 (1 layer)

Table 5.1: Characteristic of ITO vs. graphene TCF
*This is a theoretical value and has not been assessed in this work.

Chapter 6

Future outlook

As a continuation of this research several factors needed to be tackled:

1. The source of the high contact resistivity and the low maximum current density should be assessed. Theses values can be possibly explained by a residual layer between the graphene and the *p*-GaN, that has to be removed.

2. The improvement of contact resistivity and maximum current density by thermal annealing should also be considered.

3. The thickness of the Gr/Gr TCF should be assessed in order to ensure the lower absorption once placed in a optical node of the longitudinal wave inside the resonant cavity.

4. The use of NHO_3 at lower concentrations and before transferred to the substrate should be evaluated. In the literature researchers has reported values 4 times betters than the values presented in this investigation [35]. Thus is worth to continue trying.

5. The graphene growth on the Cu foil of 99.9999% purity shows good mobilities when characterized by fabricating devices with e-beam lithography. It would be useful to asses whether or not the process can be as reproducible as it is now with the Cu foil of 99.995%.

6. Finally, it is necessary to realize more experiments with the transfer to *p*-GaN in order to ensure reproducibility.

Appendix A

Recipes

A.1 Graphene synthesis with Cu in CVD hot plate reactor

Catalytic substrate is required.

1. Catalytic substrate cleaning
   (a) Dipping in acetic acid (CH_3COOH) during 5 min. at room temperature.
   (b) Dipping in acetone (CH_3COCH_3) during 5 min. at room temperature.
   (c) IPA dipping and blow drying with N_2.
2. Graphene synthesis on top of catalytic substrate inside CVD reactor.
   (a) Heating to 1,000 °C at 300 °C /min.
   (b) Annealing during 5 min. with a maintained flow of 20 sccm of H_2 and 1000 sccm of Ar.
   (c) CH_4(5%):Ar(95%) 30 sccm flow during 5 min at 6.35 mbar.
   (d) Stop gas flow and evacuation of the reacting chamber to <0.1 mbar
   (e) Cooling to room temperature at 300 °C /min. under 20 sccm of H_2 and 1000 sccm of Ar.

A.2 Wet etching – wet transfer

1. Spin coating of PMMA on top of the Gr/Cu-foil complex during 1 minute at 1,000 rpm and baking during 5 minutes at 160 °C .

2. O_2 plasma graphene dry etching on the backside of the PMMA/Gr/Cu-foil during 40 sec. with an O_2 flow of 10 sccm at 50 W.
3. Cu foil etching overnight in acidic solution of HCl(37 wt%):H_2O = 1:7 with two drops of H_2O_2.
4. PMMA/graphene complex cleaning with DI water.
5. Deposition of the PMMA/Gr complex on top o the target substrate (SiO_2).
6. Partial drying of the PMMA/Gr/SiO_2 at room temperature and posterior baking during 5 minutes at 160 °C .
7. Removal of the PMMA by dipping in acetone during 5 minutes at room temperature and 2 minutes at $\sim$ 60 °C .
8. Cleaning of the graphene/SiO_2 substrate by dipping in IPA and blow drying with N_2.

A.3 0.25 M NaOH solution preparation

1. Add 10 gr of NaOH to 990 ml of water while steering.
2. Keep steering until the NaOH pellet are completely dissolved.

A.4 H_2 Bubbling separation – wet transfer

0.25 M NaOH solution (recipe A.3) and a Cu foil with graphene (recipe A.1) are required.

1. Spin coating of PMMA on top of the Gr/Cu-foil complex during 1 minute at 2,000 rpm and baking during 5 minutes at 160 °C .
2. O_2 plasma graphene dry etching on the backside of the PMMA/Gr/Cu-foil during 40 sec. with an O_2 flow of 10 sccm at 50 W.
3. Frame preparation and adhesion to the PMMA/Gr/Cu-foil complex.
   (a) Cutting of the frame.
   (b) Deposition of adhesive in the more sticky part of the frame.
   (c) Deposition of the frame on the PMMA/Gr/Cu-foil complex (the part with adhesive toward PMMA/Gr/Cu-foil).
4. Border scratch to enhance the permeation of the water during electrolysis.
5. Electrolysis separation of Cu foil in 0.25 M NaOH solution at 1 A during $\sim$40 sec.

6. Frame/PMMA/Gr cleaning in DI water, deposition on target substrate and room temperature drying.
7. Frame removal.
8. PMMA/Gr/SiO_2 complex baking during 5 minutes at 160 °C .
9. PMMA removal and cleaning.
   (a) Removal of the PMMA by dipping in acetone during 5 minutes at room temperature and 2 minutes at $\sim$ 60 °C .
   (b) Cleaning of the graphene/SiO_2 substrate by dipping in IPA and blow drying with N_2.

A.5 $FeCl_3$ doping

A substrate with one layer of graphene (recipe A.4) and $FeCl_3$ 45 wt% are required as starting point.

1. Spin coating of $FeCl_3$ 45 wt% during 1 min. at 2,000 rpm.
2. Baking of the $FeCl_3$/Gr/Substrate during 2 minute at 70 °C
3. Deposition of a second layer of graphene using bubbling transfer.

A.6 S1813 doping process

A substrate with fabricated device is required.

1. Spin coating of the S1813 resist during 1 min. at 8,000 rpm.
2. Baking during 1 min. at 100 °C
3. Photolitography to pattern the resist only on top of the graphene.
   (a) Mask alignment.
   (b) Exposure during 5 sec.
   (c) Develop using MF-319 during 40 sec.
   (d) Cleaning by dipping in DI water and blow drying with N_2.
4. First set of measurements.
5. Flat exposure in UV light during 1 min.
6. Second set of measurements.

A.7 Poly-vinyl alcohol (PVA) 4 wt% preparation

The PVA used for this application was:

Product name: Poly(vinyl alcohol)
Properties: M_w 89,000-98,000 – 99+% hydrolyzed.
Product number: 341584
Product brand: Aldrich
CAS number: 9002-89-5

Process steps:

1. Add 2 g. of PVA to 48 ml of DI water while stirring at room temperature.
2. Once the PVA is disperse start increasing the temperature until reaching 80 °C .
3. Keep stirring at 80 °C until the PVA is completely dissolved.
4. Cool down the solution below 35 °C .

A.8 PVA doping

A substrate with one layer of graphene (recipe A.4) and a PVA 4 wt% (recipe A.7) solution is required as starting point.

1. Spin coating of the PVA on top of the Gr/Substrate during 1 min. at 2,000 rpm.
2. Baking during 1 min. at 100 °C .
3. Transfer of the second layer of graphene using bubbling method.

A.9 Lift-off process for the formation of the gold contacts.

It is very important to keep in mind that this process should be done before patterning of graphene.

1. S1813 Spin coating of the sample during 1 min. at 3,000 rpm.
2. Baking during 1 min. at 100 °C .
3. Photolitography to pattern the resist.
   (a) Mask alignment.
   (b) Exposure during 10 sec.

   (c) Surface treatment of the exposed resist in C_7H_8 (toluene) during 2 min.
   (d) Develop using MF-319 during 60 sec.
   (e) Cleaning by dipping in DI water and blow drying with N_2.
4. Deposition of a 100 nm of Au using an electron gun physical vapour deposition (PVD) reactor.
5. Dipping in acetone during 5 min. at room temperature.
6. Dipping in acetone during 2 min. at $\sim 60\,^{\circ}\mathrm{C}$.
7. Splash acetone from the acetone dispenser carefully to help the removal of the non desired Au.
8. Cleaning by IPA dipping and blow drying with N_2.

A.10 Graphene patterning

This process should be done after the metal contact deposition.

1. S1813 Spin coating of the sample during 1 min. at 8,000 rpm.
2. Baking during 1 min. at $100\,^{\circ}\mathrm{C}$.
3. Photolitography to pattern the resist.
   (a) Mask alignment (alignment done with the markers from the gold deposition).
   (b) Exposure during 5 sec.
   (c) Develop using MF-319 during 40 sec.
   (d) Cleaning by dipping in DI water and blow drying with N_2.
4. O_2 plasma to remove the graphene not protected by the resist.
5. removal of the resist by dipping in acetone during 4 min. at room temperature.
6. Cleaning by IPA dipping and blow drying with N_2.

A.11 Single layer graphene (Gr) sample preparation for transmittance

An optical microscope sample glass and a Cu foil with graphene (recipe A.1) are required.

1. Cleaning of the glass substrate

(a) Ultrasonic bath in acetone during 2 min. at room temperature and maximum power.

(b) IPA dipping and N_2 blow dying.

(c) O_2 plasma during 1 min. with O_2 flow of 80 sccm at 250 W.

2. Deposition of 1 layer of graphene using bubbling transfer (recipe A.4)

A.12 Gr/Gr sample preparation for transmittance

Departing from 1 sample prepared using recipe A.11. Cu foil with graphene is required.

1. Deposition of 1 layer of graphene using bubbling transfer (recipe A.4)

A.13 PVA/Gr sample preparation for transmittance

Departing from 1 sample prepared using recipe A.11. Cu foil with graphene (recipe A.1) and PVA 4 wt% (A.7)solution are required.

1. Spin coating of the PVA on top of the Gr/Substrate during 1 min. at 2,000 rpm.
2. Baking during 1 min. at 100 °C .

A.14 $FeCl_3$/Gr sample preparation for transmittance

Departing from 1 sample prepared using recipe A.11. Cu foil with graphene (recipe A.1) and $FeCl_3$ 45 wt% solution are required.

1. Spin coating of the $FeCl_3$ 45 wt% on top of the G/Substrate during 1 min. at 2,000 rpm.
2. Baking during 2 min. at 70 °C .

Appendix B

SEM images: a closer look to the graphene film.

B.1 SEM of the transferred graphene film

Using a scanning electron microscope (SEM) high magnification optical images of the graphene film were obtained. The graphene was synthesised on 99.995% purity Cu foil with a thickness of 50 μm in a cold-wall low-pressure CVD reactor following recipe A.1. After, it was transferred to a $SiO_2/Si/SiO_2$ substrate using the bubbling transfer technique following recipe A.4.

The SEM images of the grahene film surface reveal the existence of dark dots as can be seen in fig. B.1. In a higher magnification SEM image (fig. B.2) part of the film was folded thus creating a bi-layer graphene. The difference in the contrast of the single layer film, the bi-layer part and the substrate can be identified. It is clear that the colour of the dots is similar to that of bi-layer graphene. A possible explanation for this dots is that something (possible the metal impurities) in the Cu-foil is absorbing carbon during the hight temperature graphitization process and then this carbon precipitated toward the surface once the sample is cooled down. Also it can be that a second graphene layer is started during the graphitization process.

However, as the amount of dots is less for graphene from higher purity cu-foils or e-beam evaporated Cu thin film, it is possible that this dots are related to the impurities in the Cu foil.

B. SEM IMAGES: A CLOSER LOOK TO THE GRAPHENE FILM.

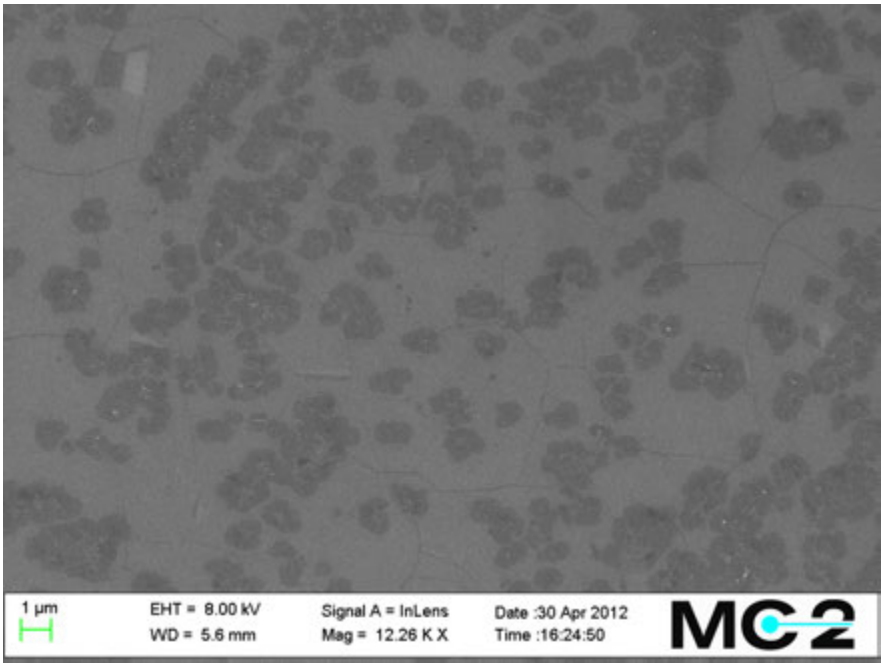

Figure B.1: SEM image of the tansferred graphene film. The film was synthesized on 99.995% Cu foil and transferred to $SiO_2/Si/SiO_2$ substrate

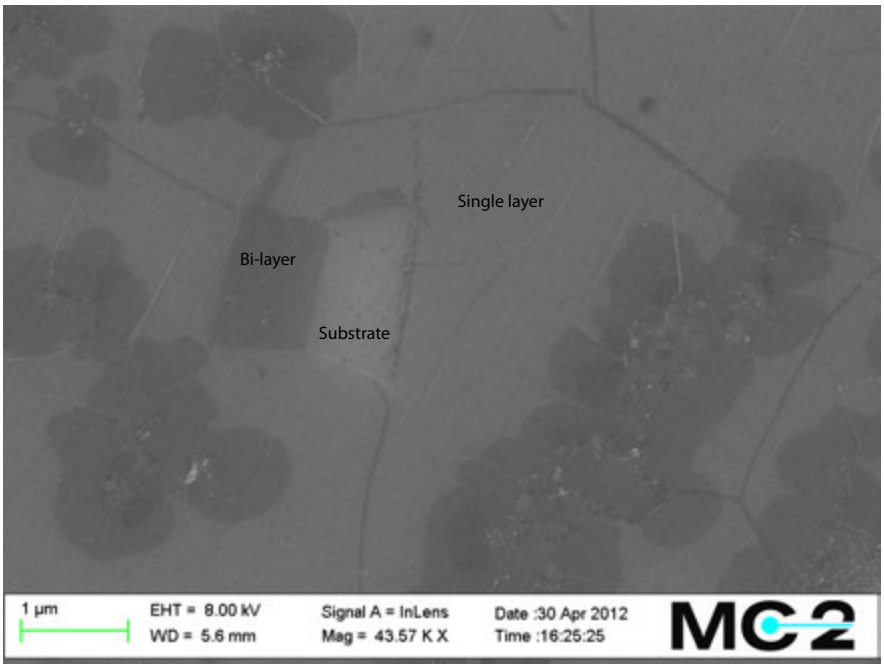

Figure B.2: 43.57 K X magnified SEM image of graphene film. The substrate, single layer and bi-layer graphene can be identified by the contrast difference.

B.2 Why 0.25 M NaOH solution for the bubbling transfer?

During the water electrolysis process for the H_2 bubbling transfer described in section 4.2.2 an electrolyte is required in order to enhance the conductivity of the water. Different concentrations of NaOH were tried (4 M, 1 M, 0.5 M) before choosing to work with 0.25 M.

With higher concentration the current spreading in the water is more uniform and less potential is required to achieve the target current, thus consuming less power. Also the H_2 bubbles on the surface of the Cu foil are more uniform. However, when using solutions with concentrations of 4 M and 1 M some "crystal-like" formations where identified on top of the graphne film even after cleaning by dipping in DI water (see fig. B.3 and B.4).

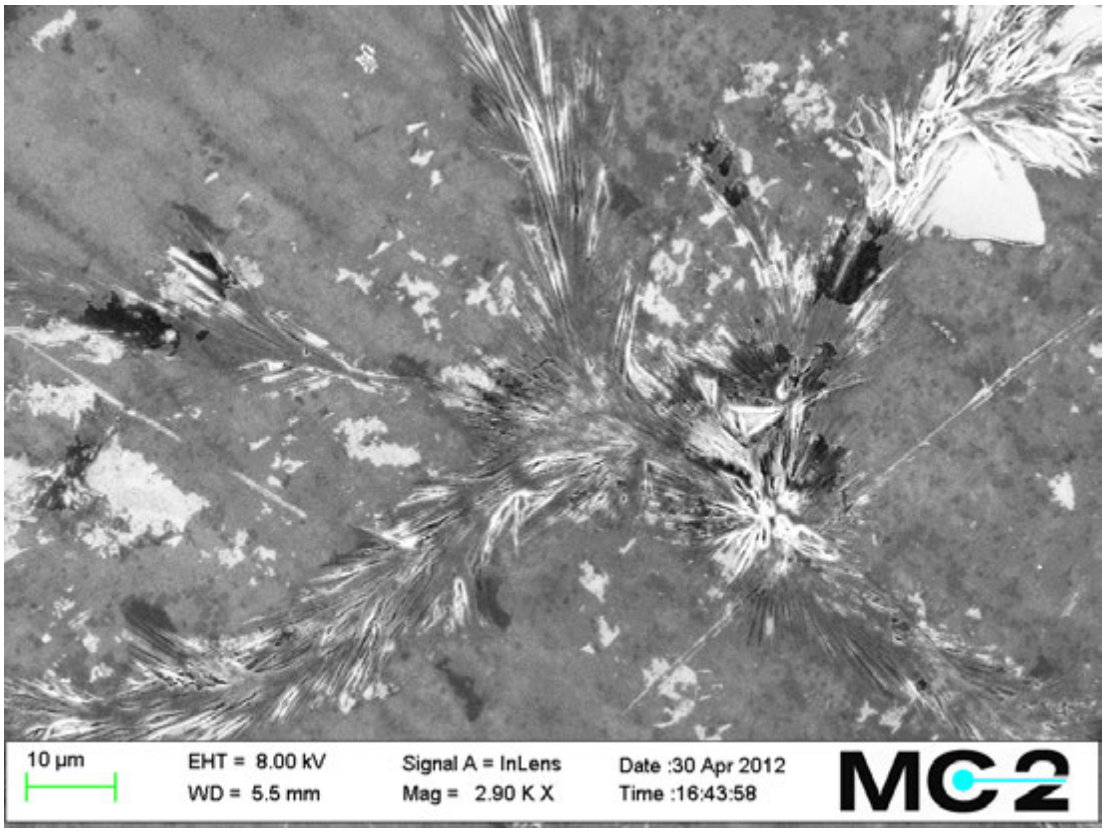

Figure B.3: Residues on top of graphene film after transferred. 4 M NaOH solution was used to transfer the graphene to the target substrate using bubbling transfer.

The origin of this residues is not well understood and could be possible due to

solidification of NaOH or the formation of water insoluble metal-hydroxides from the impurities on the Cu foil. However, this residues are greatly reduced by decreasing the concentration of NaOH in the solution. After several tries it was concluded the best transfer was obtained for concentrations of 0.25 M NaOH.

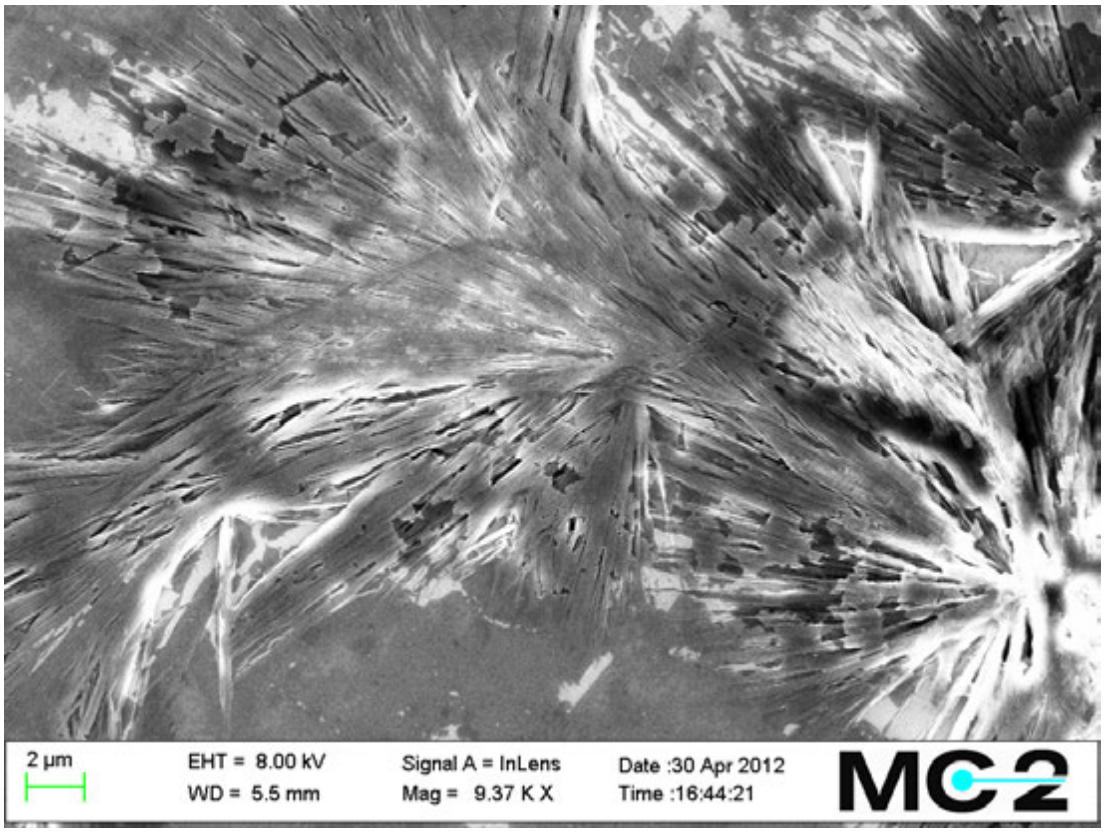

Figure B.4: Magnified SEM image of the residues.

Appendix C

Supplementary information

C.1 Raman spectroscopy

This is a non-destructive spectroscopy technique based on inelastic scattering of monochromatic light after interacting with the atoms and molecules of the surface being analysed. When the light reach the surface being analysed, the photons of the monochromatic light are absorbed and then re-emitted by the sample. Normally, the energy of the re-emitted photon is the same as the incident photon energy. This type of elastic scattering of photons is known as Rayleigh Scattering. Now, when the energy of the re-emitted photon is different than the incident photon the phenomena is known as Raman scattering.

This Raman effect has its roots on the deformation of the molecules of the sample when exposed to an electric field. This deformation is caused by the dipole moment $P = \alpha E$ induced by the electrical field E (α is the polarizability of the molecule). Yet, as the electric field is varying in time, the deformation will also change in time making the molecules vibrate at certain frequency ν_m. In summary, the electric field will exited the molecules and turn them into oscillating dipoles.

If the molecule have no Raman active mode, the molecule will absorb the photon with frequency ν_p and then, once the excited molecules returns to its basic vibrational state will release a photon of frequency ν_p.

On the other hand, if the molecule has an active Raman mode, once the photon is absorbed energy will be transferred to the Raman mode and the re-emitted photon will have a frequency ν_p - ν_m giving rise to what is known as "Stoke" scattering.

Similarly, if at the moment of interaction, the molecule with active Raman mode is already excited, the released photon will have an energy of $\nu_p + \nu_m$ and an "Anti-Stoke" scattering takes place.

By analysing the active vibrational Raman modes in a sample this can be characterized and then the spectra can be used as a signature of the material.

C.2 Mobility calculation model from Drude theory

Before starting analysing the model it is worth mentioning that, as the present model will be applied to a 2D material some considerations should be taken into account. First, the sheet conductance in the 2D material will be equal to the conductivity due to the fact that there is no thickness. Secondly, the carrier density in the 2D material will have units of cm^{-2} instead of the normal cm^{-3} in 3D materials.

From the Drude model of electrical conduction we have that the mobility can be defined as:

$$\mu = \frac{\sigma}{qn} \tag{C.1}$$

If we consider that σ and n are both depending on a gating potential the previous equation should be rewritten as:

$$\mu_{(vg)} = \left(\frac{d\sigma_{(vg)}}{qdV_g}\right)\left(\frac{dV_g}{dn_{(vg)}}\right) \tag{C.2}$$

Now lets describe the device used for electrical characterization. The sheet conductance of the graphene layer on top of the SiO_2 is being measured while varying the gating potential through the Si underneath the SiO_2. Thus, we are having a capacitor with the SiO_2 as the dielectric. Recalling from electrostatic capacitance theory that:

$$C_g = \frac{\epsilon_r \epsilon_0 S}{t_h} \tag{C.3}$$

$$V_g = \frac{qn_{(vg)}S}{Cg} + constant = \frac{qn_{(vg)}t_h}{\epsilon_r\epsilon_0} + constant \tag{C.4}$$

$$\frac{dVg}{dn_{(vg)}} = \frac{qt_h}{\epsilon_r\epsilon_0} \tag{C.5}$$

Where C_g is the capacitance of the device being used that is described by the device geometry (S is the area and t_h is the thickness of the dielectric). If we know substitute C.4 in C.2 we obtain:

$$\mu_{(vg)} = \frac{d\sigma_{(vg)}}{qdV_g} \times \frac{qt_h}{\epsilon_r \epsilon_0} = K\frac{d\sigma_{(vg)}}{dV_g} \tag{C.6}$$

$$K = \frac{t_h}{\epsilon_r \epsilon_0} \tag{C.7}$$

Thus, the value of the mobility can be obtained by differentiating the measured values of sheet conductance[1] as a function of the applied gate voltage (Vg).

For the proportionality constant K the thickness of the SiO_2 (t_h) is 300 nm and the relative permittivity (ϵ_r) is 3.9. The other parameters are the electron charge (q) and the vacuum permittivity (ϵ_0).

C.3 Fabrication techniques

Micro fabrication techniques are well explained in a vast amount of books. Thus, in this section only a brief description of the techniques used for fabrication will be presented.

Spin coating

Spin coating is a process where an uniform thin film is applied to a flat substrate by means of the centrifugal effect once it is rotated at a certain angular speed. The thickness of the film will depend on both, the angular speed and the viscosity of the deposited material.

Etching

This process is used to remove unwanted material during the fabrication procedure. The removal of the material can be done in two ways: wet etching and dry etching.

In the wet etching the material is removed by the use of wet chemicals that attack the target material. The removal of the metal by using HCl based solutions can be taken as an example. Normally wet etching techniques are isotropic. Thus it is difficult to control the directional etching of a material by using wet etching.

The removal of material by dry etching techniques is achieved by bombarding the target material by ions (usually a plasma of reactive gases) directed toward the material

[1] It is worth remembering that as it is a 2D material $G_s = \sigma$

by means of electromagnetic forces. Once the ion from the plasma reach the target it remove portion of the material from the surface. This kind of etching can be anisotropic and the directionality of the etching can be controlled.

Photolithography

Photolitography is a process where, through the light exposition in selective areas of a sensitive resist, areas of a surface can be patterned for posterior selective removal or deposition of material on the surface of the patterned sample. The photolithography process normally follow these steps:

1. Deposition of a light sensitive resist on top of the target sample.
2. Alignment of the target sample with the mask that has the pattern that needs to be engrave in the surface of the sample.
3. Exposure of light sensitive resist to UV light through the patterned mask.
4. Developing of the light sensitive resist.

The used resist can be either positive or negative depending whether it is needed to remove the exposed part of the resist or the unexposed part.

The developing of the resist is done by using a chemical that will only develop the exposed (or unexposed in case of negative resist) areas due to the difference in the molecular weight (the polymerization degree is being altered by the light).

E-beam lithography

In e-beam lithography the feature is engraved in the resist by a beam of electrons directed toward the sample. The shape of the feature is achieved by deflecting the electron beam. This technique has as principal benefice that can defeat the diffraction limit in photolithography, allowing smaller features sizes. However, the principal disadvantage is the small throughput due to its "serial" nature.

The e-beam process also allows he use of PMMA/MMA as resist. As this resist does not dope the graphene, with this technique the graphene can be patterned without damaging to much the mobility of the sample.

Chemical vapour deposition (CVD)

This technique allow the deposition of material on top of a surface by exposing it to one or more precursors that will react insider the reaction chamber compensating on top of the surface of the target sample. There are several CVD reactors types, the most relevant for this work being the low pressure cold wall CVD reactor. This reactor is heat the sample by means of joule heating of a hot plate, avoiding this way the heating of the walls of the reaction chamber and reducing the deposition of materials in the walls. Also, the due to the low pressure that can be achieved during deposition the technique allows de deposition of layers of remarkable uniformity and material characteristic with very good step coverage. Yet, the drawback is the high temperature required (higher than $600\,^{\circ}\mathrm{C}$) and the slow deposition rate. Nevertheless, none of this are a problem for the application used in this research.

Physical vapour deposition

In this research the metal was deposited in a physical vapour deposition reactor with an electron beam evaporator. In PVD (evaporation) reactors the samples ar positioned in a chamber with high vacuum in line of sight with the material that is going to be deposited. Then the material to be deposited is either heated by jule heating the crucible that contains it or by locally directing an electron beam until it evaporates. Once evaporated the material moves freely in the vacuum chamber and condensate on top of the substrate where it needs to be deposited. In this kind of reactor the step coverage is not as good as in the CVD process.

Lift-off

Lift-off is a process where a sacrificial material (a resist) is used to protect the area where a material (normally a metal) that will be deposited is not wanted.

The process steps are:

1. The resist is deposited on the substrate.
2. The resist is exposed to light through a mask with the pattern.
3. The surface of the resist is hardened.
4. The resist is developed.

5. The metal is deposited.
6. The sacrificial layer with the unwanted metal is removed.

This method is used to avoid depositing the metal film in the whole surface and then patterning and etching. If we do so, a material underneath (in our case graphene) can be damage. Also this technique is used with materials that are more inert and can not be etched easily (as gold).

It is important to realize that there is a need to have and undercut in the resist to allow the penetration of the solvent easily when removing the sacrificial layer.

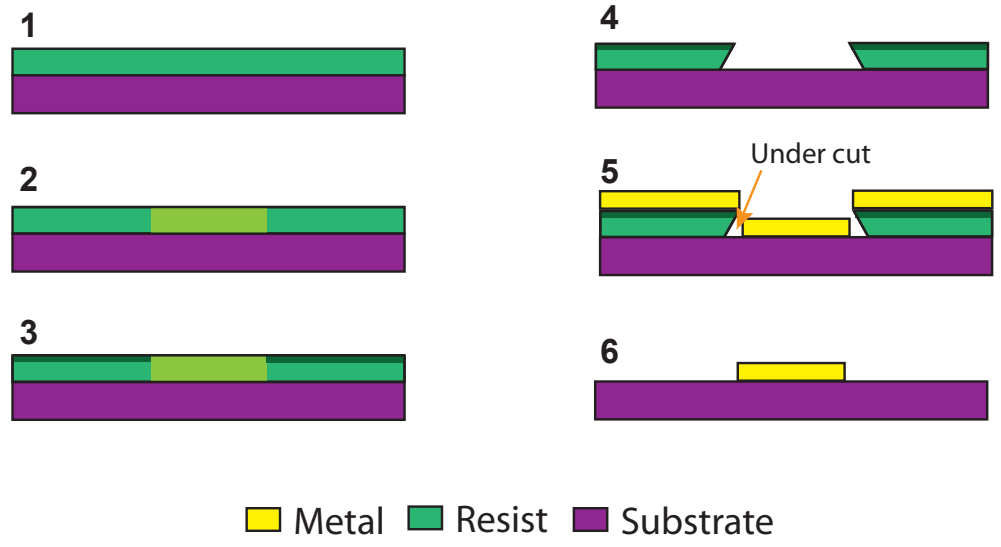

Figure C.1: 1-Deposition of the sacrificial resist. 2-engraving of the pattern. 3-Hardening of the resist surface. 4-Developing of the resist. 5-Deposition of the metal. 6-Removal of the sacrificial layer.

Appendix D

Journal manuscript

Frame assisted H_2O electrolysis induced H_2 bubbling transfer of large area graphene grown by chemical vapour deposition on Cu

César J. Lockhart de la Rosa, Jie Sun, Niclas Lindvall, Matthew T. Cole, Kenneth B. K. Teo, and August Yurgens

Applied Physics Letters

Frame assisted H_2O electrolysis induced H_2 bubbling transfer of large area graphene grown by chemical vapor deposition on Cu

César J. Lockhart de la Rosa,[1,2] Jie Sun,[1,a)] Niclas Lindvall,[1] Matthew T. Cole,[3] Kenneth B. K. Teo,[4] and August Yurgens[1]

[1)] *Department of Microtechnology and Nanoscience, Quantum Device Physics Laboratory, Chalmers University of Technology, SE-41296 Gothenburg, Sweden*

[2)] *Department of Microtechnology and Nanoscience, Photonics Laboratory, Chalmers University of Technology, SE-41296 Gothenburg, Sweden*

[3)] *Department of Engineering, Electrical Engineering Division, University of Cambridge, 9 JJ Thomson Avenue, CB3 0FA Cambridge, United Kingdom*

[4)] *AIXTRON Nanoinstruments Ltd., Swavesey, CB24 4FQ Cambridge, United Kingdom*

(Dated: 6 August 2012)

An improved technique for transferring large area graphene grown by chemical vapor deposition on copper is presented. It is based on mechanical separation of the graphene/copper by H_2 bubbles during H_2O electrolysis, which only takes a few tens of seconds while leaving the copper cathode intact. A semi-rigid plastic frame in combination with thin PMMA layer span on graphene gives a convenient way of handling- and avoiding wrinkles and holes in graphene. Optical and electrical characterization proves the graphene quality is better than that obtained by traditional wet etching transfer. This technique appears to be highly reproducible and cost efficient.

Graphene, a two-dimensional material formed from a hexagonal lattice of sp^2 carbon atoms, has been identified as a promising candidate in several applications ranging from beyond-CMOS technology[1] to DNA sequencing.[2] This is due to its impressive properties, such as extremely high intrinsic mobility for both electrons and holes,[3,4] high transparency,[5] high thermal conductivity,[6] large tensile strength,[7] etc. For some time, however, problems in scaling, reproducibility and uniformity of the techniques used for graphene production and subsequent transfer to various target substrates have limited its use in industry. Chemical vapor deposition (CVD) is the most promising methods for graphene synthesis. It is feasible for large scale production of uniform graphene in an industrial-friendly fashion.[8–15] Also, it has been demonstrated that the quality of CVD graphene grown on catalytic metals is good enough to be used in optoelectronics where transparency and conductivity are equally important.[16]

A bottleneck of the CVD technique, however, is the graphene transfer from metals to foreign substrates; a direct growth of graphene on insulators is not yet mature.[17,18] Commonly, graphene is supported by a polymeric film while the metal is removed.[8–15] The resultant polymer/graphene complex is then placed on the target after which the polymer is removed by a solvent. In this process, the graphene is exposed to metal etchant for a great many hours, which may induce defects and/or excess doping. Also, the handling and cleaning of the fragile material once metal is etched away is not easy; folding or rapture of graphene is often seen. The so-called roll-to-roll printing process alleviates the problem and gains more reproducibility.[9] Still, the pressure homogeneity and therefore the graphene adhesion to substrate is hard to maintain uniform over large areas during stamping. Most importantly, however, the expensive high purity metal catalysts are etched away, increasing cost of the graphene industrial production.

Very recently, Cheng et al.[19] have suggested a transfer technique based on the mechanical separation of graphene from Pt foils by H_2 bubble formation at the cathode of an electrolytic cell. The catalyst is not consumed and can be used repeatedly. To date, however, there are no detailed reports on the generalized transfer technology for the most common catalyst in CVD graphene: copper, despite a combined effort of wet etching and electrochemical separation.[20] In this letter, we present an electrolysis bubbling-assisted transfer of graphene grown by CVD on Cu. The metal is not consumed, proving the method to be cost-efficient for real applications. Furthermore, we ease manipulation of graphene by using a plastic frame attached to the polymer/graphene prior to separation from copper. The frame also alleviates the effect of turbulence during the bubbling. Altogether, this results in much fewer wrinkles and holes in the transferred graphene. The process is accomplished in a few tens of seconds, producing material comparable or better than the graphene transferred by wet etching of Cu,[15] as characterized by optical and electrical means.

For the graphene synthesis, 50 μm thick 99.99% pure Cu foils and a cold-wall low-pressure CVD reactor (Black Magic, AIXTRON) are used. After standard cleaning, the Cu foil is heated to $\sim$ 1,000 °C and annealed for 5 min with a flow of 20 sccm H_2 and 1,000 sccm Ar. Then, 30 sccm prediluted CH_4 (5% in Ar) is used during another 5 min as the carbon source. After the growth, the system is evacuated to < 0.1 mbar and cooled. The process is reported in greater detail in our previous publication.[15]

[a)] Electronic mail: jiesu@chalmers.se.

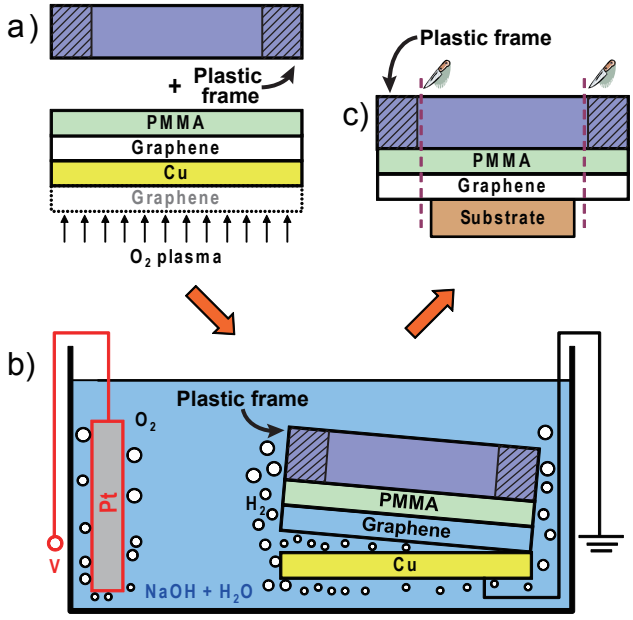

FIG. 1. Schematic illustration of the frame assisted H_2 bubbling transfer. a) Deposition of the PET frame on top of the sample and etching of the graphene at the unprotected side of Cu with O_2 plasma. b) H_2 bubbling separation of the frame/PMMA/graphene from the Cu foil induced by H_2O electrolysis. c) Frame removal after transfer.

A schematic representation of the graphene transfer process can be seen in Fig. 1. In this work, spin coated PMMA (2,000 rpm, 5 min cure at 160 °C) is used as the supporting polymer thin film. The graphene on the bottom face of the foil is dry etched by O_2 plasma (graphene is usually formed on both sides of the metal foil). For simplicity, we remove the bottom graphene in this letter. However, we can simultaneously isolate two graphene films from both sides of Cu as well, doubling the yield, which is impossible to achieve in the wet etching based technology. For the supporting frame, we opted to use 100-200 μm thick PET (see Fig. 2(a)), even though any semi-rigid plastics that are inert during the electrolysis would be suitable. Many glues (e.g. epoxy) that remain sticky in wet environments could be used to attach the frame to the PMMA/graphene/Cu-sandwich. However, we found that PMMA itself (drop coated onto the frame that was going to be in contact with the PMMA/graphene/Cu complex, 160 °C cure) was the cleanest and most efficient choice. The gluing was carried out also at 160 °C on a hot plate, well above the glass transition temperature of PMMA ($T_g \approx 105$ °C).

The frame/PMMA/graphene/Cu-bundle is then used as the cathode of an electrolytic cell with 0.25 M NaOH aqueous solution electrolyte. For the anode, a platinum electrode is used (see Fig. 1(b)). To start the process, the current is ramped to ∼1 A and maintained at that level until the graphene is completely separated from the Cu foil by the H_2 bubbling. The typical time required for separation is ∼30 s. Subsequently, the frame/PMMA/graphene-bundle is picked up and rinsed in several DI water baths (Fig. 2(b)). It is then placed on the target substrates (e.g. Si with 300 nm SiO_2) and left at room temperature until it gets dry. It is remarkable to notice that the graphene film can be transferred to several substrates at once (Fig. 2(c)). The frame is easily removed simply by cutting through the PMMA at the inside borders (Fig. 1(c)); it can be reused many times. Afterwards, the samples are baked at 160 °C for 5 minutes to remove water residue and improve adhesion before the PMMA is dissolved by acetone. By repeating the procedure, multiple layers of graphene can also be deposited, as discussed in more detail in the supplementary material.[21]

Gas bubbles are known to be very effective in separating solid layers uniformly. For example, in commercial silicon on insulator (SOI) technology, hydrogen bubbles are used to separate ultra-thin silicon film (commonly known as "smart cut") for the transfer to a handle wafer. Here, we use H_2 bubbling to isolate graphene because other common gases such as O_2 and Cl_2 (anode products) may oxidize graphene. Furthermore, if Cu is used as the anode, it may be electrochemically oxidized and etched. The half equations of the reactions at our cathode (Eq. 1) and anode (Eq. 2) of the cell are

$$4H_2O_{(l)} + 4e^- \longrightarrow 2H_{2_{(g)}} + 4OH^-_{(aq)} \quad (1)$$

$$2H_2O_{(l)} - 4e^- \longrightarrow O_{2_{(g)}} + 4H^+_{(aq)}, \quad (2)$$

respectively. Obviously, the NaOH electrolyte is only used to enhance the electrical conductivity of water. The absence of Na^+ in the essential reaction is ensured by its very negative standard electrode potential of E^0=−2.71 V. Note that many electrolyte solution can be used for bubbling transfer of graphene, such as Na_2SO_4, etc. We have also found that a lower concentration of NaOH leads to a cleaner graphene surface; ∼0.25 M NaOH is identified as providing the best balance between graphene quality and effective bubble production. More details can be seen in the supplementary material.[21]

In our experiments, we have found that the H_2 bubbles can detach most foreign materials (including graphene, PMMA, etc.) that are loosely bound to the metal surface. This might cause some difficulties when transferring graphene grown on evaporated Cu thin films on SiO_2/Si. Due to the weak bonding to the substrate, the Cu thin film becomes separate both from the graphene and the underlying SiO_2/Si, making the thin-film recycling difficult unless an appropriate adhesion metal layer is used when depositing the copper thin film. We also notice that tightly bonded materials (e.g. native oxide of Cu) are usually difficult to detach. Finally, we stress that the plastic frame is important to preserve a smooth graphene surface. Intensive H_2 bubbles create considerable turbulence, often resulting in broken or severely corrugated graphene if not using the frame.

The inset of Fig. 4 demonstrates an electron diffraction pattern of the as-grown graphene obtained in transmission electron microscope (TEM). The diffraction dots with six-fold symmetry and their equal intensity clearly indicate high quality monolayer graphene. Fig. 2(d) shows a typical optical image of the graphene electrochemically transferred to SiO_2/Si wafer. The graphene is seen to be very uniform and smooth. Fig. 3(a) shows the Raman spectrum measured after the transfer. The 2D/G peak ratio is as high as ∼2.3. The full width half maximum (FWHM) of the 2D peak is 32.4 cm^{-1}. This confirms the existence of single layer graphene.[8–15] A very small D/G peak ratio of 0.13 indicates that the amount of defects introduced by the transfer technique is negligible. For optical transparency analysis, the graphene is transferred to microscope glass slide. The transmittance for the single layer and artificial bilayer graphene (two step transfer) are shown in Fig. 3(b). By subtracting the effect from the glass substrate, single and double layer graphene films show transmittance of 97.6% and 95.1%, respectively, in good agreement with the expected values.[5]

Transistor devices are fabricated by a two-step electron beam patterning (in the channels and Ti/Au electrodes, respectively) of the graphene transferred on Si wafers with 300 nm thermal oxide. The resistance of the graphene device is measured at ambient conditions

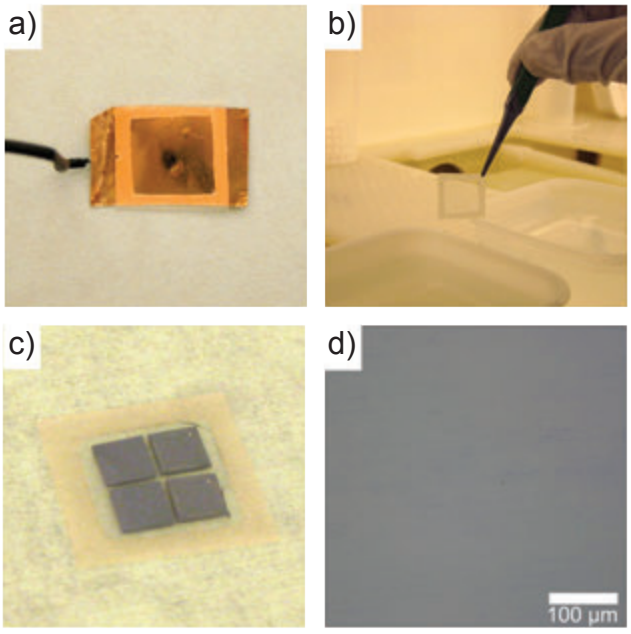

FIG. 2. Images of different stages in the graphene transfer technique. a) Frame on the PMMA/graphene/Cu complex. b) Detached frame/PMMA/graphene dipping into water for cleaning. c) Simultaneous transfer to 4 target substrates ($6 \times 6\,mm^2$). d) Optical microscope image of the transferred graphene film on 300 nm SiO_2/Si. Video of the bubbling transfer is available online.[21]

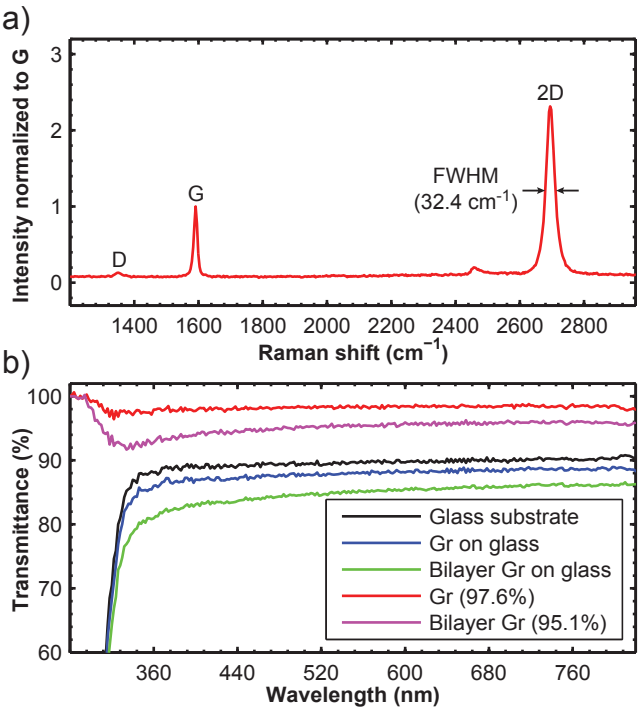

FIG. 3. Optical characteristics of the as-transferred graphene. a) Raman spectrum (514.5 nm) of the graphene transferred to SiO_2/Si. b) Optical transmittance of a single layer and a bilayer graphene film transferred to glass substrates. The transmittance for monolayer and bilayer graphene are extracted from the measured values by subtracting the substrate absorption. Gr denotes graphene.

as a function of the back gate voltage, V_G, which is applied to the conducting Si substrate (see Fig. 4). Following the model previously reported in literature,[22] the field-effect carrier mobility is estimated to be about 2,000 $cm^2V^{-1}s^{-1}$. It is worth noting that no special treatments (vacuum or current annealing, etc.) have been carried out before the electrical characterization. The results are comparable or better than those achieved in the traditional wet-etching graphene transfer.[15,21]

In summary, an electrochemical technique to transfer graphene grown on Cu has been proposed. Using Cu as the cathode, the graphene can be readily detached from the metal by H_2 bubbling resulting from H_2O electrolysis. The catalyst remains unconsumed (except for the native oxide removal prior to CVD) and can be reused many times, thereby drastically reducing the material cost of graphene synthesis. Another innovative aspect is the use of a semi-rigid frame, supporting the polymer/graphene bundle all the time, reducing the amount of wrinkles/holes and making the technique reproducible and robust. Optical and electrical characterization suggests that the quality of graphene is similar or better than that attained by traditional etching-based transfer methods, but at a much higher efficiency and lower cost.

César J. Lockhart de la Rosa is grateful to Åsa Haglund

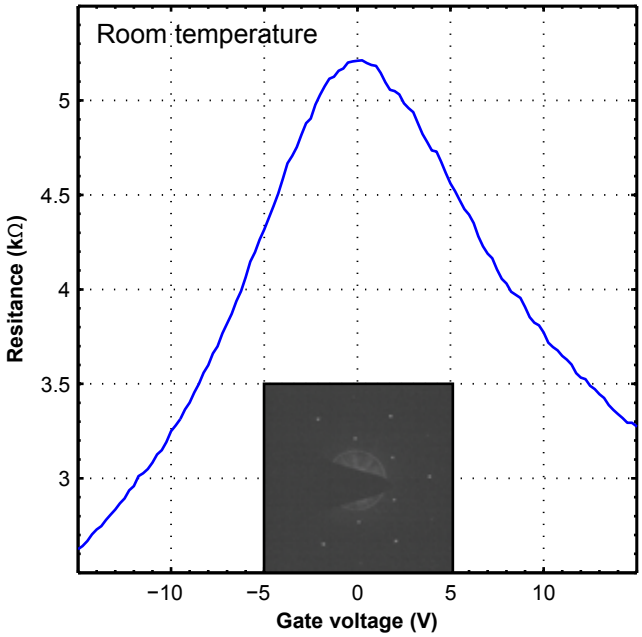

FIG. 4. Device resistance as a function of the gate voltage V_G for field effect mobility measurement. In the inset, an electron diffraction pattern of the monolayer graphene film is shown.

and Marc Heyns for their guidance. Matthew T. Cole thanks the Isaac Newton Trust, Trinity College, Cambridge University for generous financial support. Kenneth B. K. Teo acknowledges the support of the EU project GRAFOL. We thank Olof Bäcke and Eva Olsson for the assistance in TEM. The authors thank the Swedish Research Council and the Swedish Foundation for Strategic Research for financial support. CVD and other clean-room processing were performed in the Nanofabrication Laboratory on equipment sponsored by the Knut and Alice Wallenberg Foundation.

[1]S. K. Banerjee, L. F. Register, E. Tutuc, D. Basu, S. Kim, D. Reddy, and A. H. MacDonald, Proc. IEEE **98**, 2032 (2010).
[2]S. K. Min, W. Y. Kim, Y. Cho and K. S. Kim, Nature Nanotechnol. **6**, 162 (2011).
[3]K. S. Novoselov, A. K. Geim, S. V. Morozov, D. Jiang, Y. Zhang, S. V. Dubonos, I. V. Grigorieva, and A. A. Firsov, Science **306**, 666 (2004).
[4]K. I. Bolotin, K. J. Sikes, Z. Jiang, M. Klima, G. Fudenberg, J. Hones, P. Kim, and H. L. Stormer, Solid State Commun. **146**, 351 (2008).
[5]R. R. Nair, P. Blake, A. N. Grigorenko, K. S. Novoselov, T. J. Booth, T. Stauber, N. M. R. Peres, and A. K. Geim, Science **320**, 1308 (2008).
[6]A. A. Balandin, S. Ghosh, W. Bao, I. Calizo, D. Teweldebrhan, F. Miao, and C. N. Lau, Nano Lett. **8**, 902 (2008).
[7]C. Lee, X. Wei, J. W. Kysar, and J. Hone, Science **321**, 385 (2008).
[8]K. S. Kim, Y. Zhao, H. Jang, S. Y. Lee, J. M. Kim, K. S. Kim, J.-H. Ahn, P. Kim J.-Y. Choi, and B. H. Hong, Nature **457**, 706 (2009).
[9]S. Bae, H. Kim, Y. Lee, X. Xu, J.-S. Park, Y. Zheng, J. Balakrishnan, T. Lei, H. R. Kim, Y. I. Song, Y.-J. Kim, K. S. Kim, B. Özyilmaz, J.-H. Ahn, B. H. Hong, and S. Iijima, Nature Nanotechnol. **5**, 574 (2010).
[10]L. Gomez De Arco, Y. Zhang, A. Kumar, and C. Zhou, IEEE Trans. Nanotechnol. **8**, 135 (2009).
[11]X. Li, W. Cai, J. An, S. Kim, J. Nah, D. Yang, R. Piner, A. Velamakanni, I. Jung, E. Tutuc, S. K. Banerjee, L. Colombo, and R. S. Ruoff, Science **324**, 1312 (2009).
[12]M. P. Levendorf, C. S. Ruiz-Vargas, S. Garg, and J. Park, Nano Lett. **9**, 4479 (2009).
[13]S. Bhaviripudi, X. Jia, M. S. Dresselhaus, and J. Kong, Nano Lett. **10**, 4128 (2010).
[14]T. Shen, W. Wu, Q. Yu, C. A. Richter, R. Elmquist, D. Newell, and Y. P. Chen, Appl. Phys. Lett. **99**, 232110 (2011).
[15]J. Sun, N. Lindvall, M. T. Cole, K. T. T. Angel, T. Wang, K. B. K. Teo, D. H. C. Chua, J. Liu, and A. Yurgens, IEEE Trans. Nanotechnol. **11**, 255 (2012).
[16]F. Bonaccorso, Z. Sun, T. Hasan, and A. C. Ferrari, Nature Photon. **4**, 611 (2010).
[17]J. Sun, N. Lindvall, M. T. Cole, K. B. K. Teo, and A. Yurgens, Appl. Phys. Lett. **98**, 252107 (2011).
[18]J. Sun, M. T. Cole, N. Lindvall, K. B. K. Teo, and A. Yurgens, Appl. Phys. Lett. **100**, 022102 (2012).
[19]L. Gao, W. Ren, H. Xu, L. Jin, Z. Wang, T. Ma, L.-P. Ma, Z. Zhang, Q. Fu, L.-M. Peng, X. Bao, and H.-M. Cheng, Nature Commun. **3**, 699 (2012).
[20]Y. Wang, Y. Zheng, X. Xu, E. Dubuisson, Q. Bao, J. Lu, and K. P. Loh, ACS Nano **5**, 9927 (2011).
[21]See supplementary material at http://dx.doi.org/10.1063/1.3675632 for more information about the graphene bubbling transfer.
[22]S. Kim, J. Nah, I. Jo, D. Shahrjerdi, L. Colombo, Z. Yao, E. Tutuc, and S. K. Banerjee, Appl. Phys. Lett. **94**, 062107 (2009).

Supplementary material

Applied Physics Letters

2012

Frame assisted H_2O electrolysis induced H_2 bubbling transfer of large area graphene grown by chemical vapor deposition on Cu

César J. Lockhart de la Rosa,[1), 2)] Jie Sun (孙捷),[1), a)] Niclas Lindvall,[1)] Matthew T. Cole,[3)] Kenneth B. K. Teo (张谋瑾),[4)] and August Yurgens[1)]

[1)] *Department of Microtechnology and Nanoscience, Quantum Device Physics Laboratory, Chalmers University of Technology, SE-41296 Gothenburg, Sweden*
[2)] *Department of Microtechnology and Nanoscience, Photonic Laboratory, Chalmers University of Technology, SE -41296 Gothenburg, Sweden*
[3)] *Department of Engineering, Electrical Engineering Division, University of Cambridge, 9 JJ Thomson Avenue, CB3 0FA Cambridge, United Kingdom*
[4)] *AIXTRON Nanoinstruments Ltd., Swavesey, CB24 4FQ Cambridge, United Kingdom*

A video of the frame assisted bubbling transfer procedure can be found at http://dx.doi.org/10.1063/1.3675632.

NaOH, widely used in the semiconductor industry, is known to have some cleaning function (similar to the role of $NH_3 \cdot H_2O$ in SC-1 solution in RCA clean). Nevertheless, we found that if the concentration was too high, some contamination could be discovered on the graphene. For example, in Fig. S1, a scanning electron microscope (SEM) image, tree-like materials were found in several places on the graphene transferred to SiO_2/Si using 4 M NaOH solution. It is clear that this is a crystal-like structure. At this stage, the exact origin of these residues is not completely clear. As they can not be removed by water rinsing, it is reasonable to assume they are related to small amounts of metal hydroxides in the system, formed by reaction with sodium hydroxide. The amount of these contaminants, however, can be heavily reduced by decreasing the concentration of NaOH, as evidenced in Fig. S2, which shows an SEM image of a sample transferred using 2 M NaOH aqueous solution.

In Fig. S3 (a) a picture of an artificially created (sequential transfer to 300 nm SiO_2/Si) 2-layer graphene film is presented. Fig. S3 (b) shows a picture at one corner of the sample that was intentionally scratched to generate a contrast in appearance to discriminate between the graphene single and bilayer films and the substrate. Multi terminal electronic devices were fabricated by conventional photolithography. In Fig. S4, the device fabricated from (a) single and (b) dual layer film can be seen. The configuration of optical microscope (white balance, gain, contrast, and brightness) was kept identical while taking both pictures. It can be clearly seen that the graphene in (b) is darker than (a). By four probe measurements, the sheet resistances for the single and dual layer graphene were found to be 452 Ω/□ and 204 Ω/□, respectively. Obviously, the graphene sheets involved are very similar to each other, confirming that the frame assisted bubbling transfer technique is indeed rather reproducible.

[a)] Author to whom correspondence should be addressed. Electronic mail: jiesu@chalmers.se.

Fig. S5 shows an optical comparison of the devices fabricated in graphene films transferred to 300 nm SiO_2/Si using (a) frame assisted bubbling and (b) wet etching transfer. It can be seen that the amount of defects induced by the transfer are greatly reduced with frame assisted bubbling technology. The standard deviation σ_u of 2D/G ratio in the Raman spectra measured at different points within a certain sample was taken as a quantitative measure of the uniformity of the transferred graphene. The standard deviation of the 2D/G ratios were 0.13 and 0.28 for the bubbling and wet etching transfers, respectively. Clearly, the frame assisted bubbling method led to a much higher uniformity in the graphene thin film. Finally, the standard deviation σ_r of the 2D/G ratio recorded from samples transferred in different runs was taken as a quantitative measure of the process reproducibility. Again, the bubbling transfer is superior to the wet etching transfer, as evidenced by the difference in σ_r value: 0.26 vs. 0.29, which are calculated from a set of four samples for each technique.

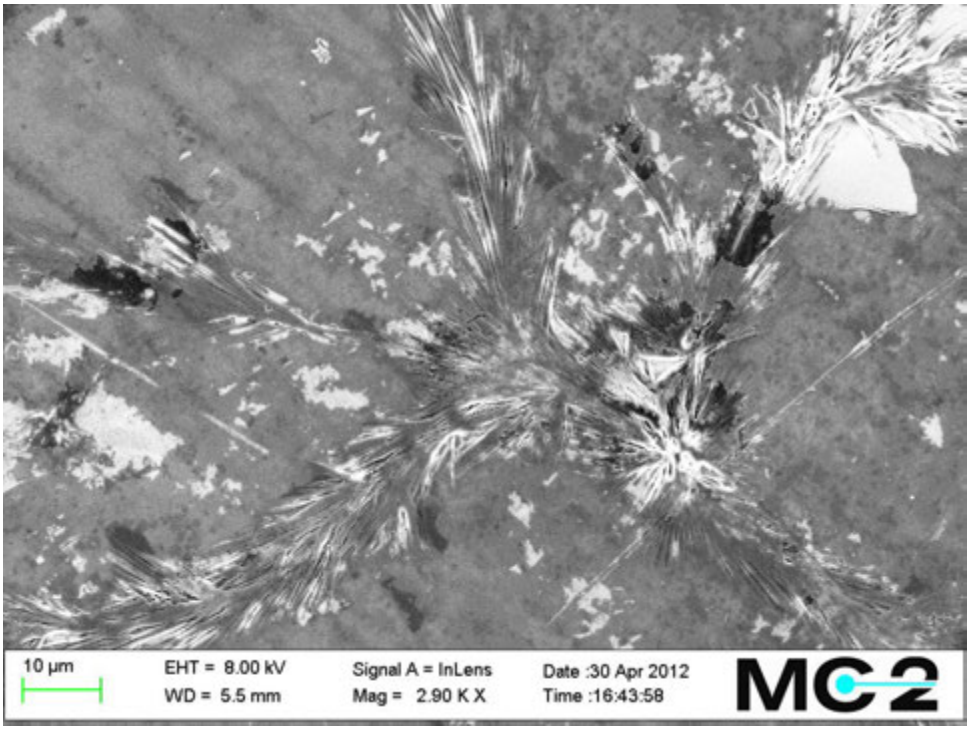

Figure S1: An SEM image of an anomalous contaminant on a graphene film transferred using 4 M NaOH solution.

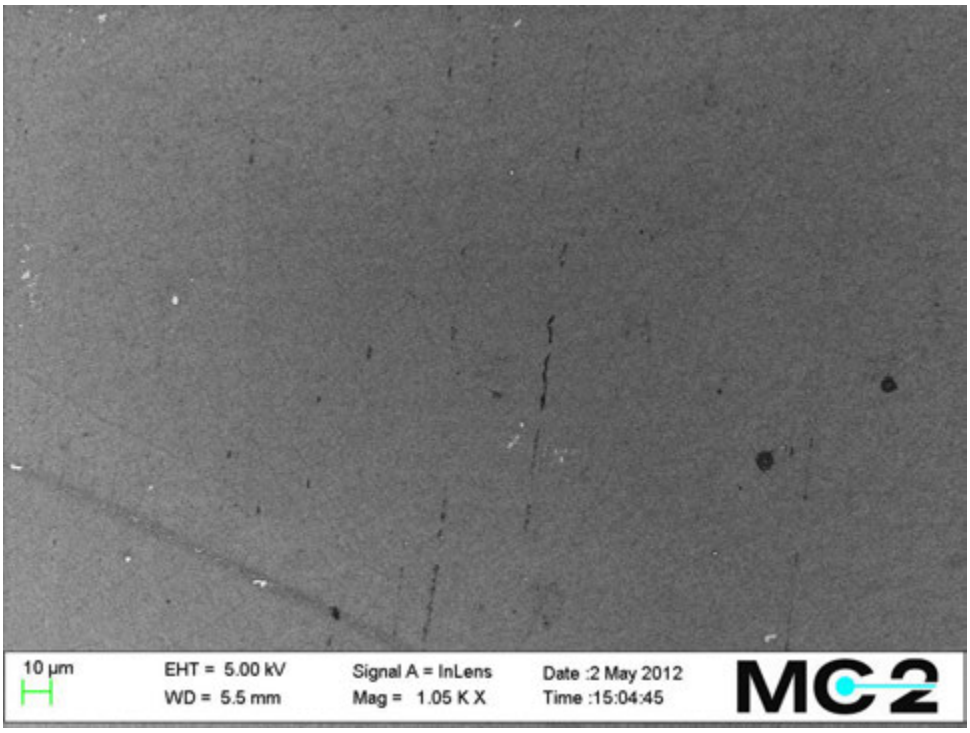

Figure S2: SEM image of a graphene film transferred using 2 M NaOH solution.

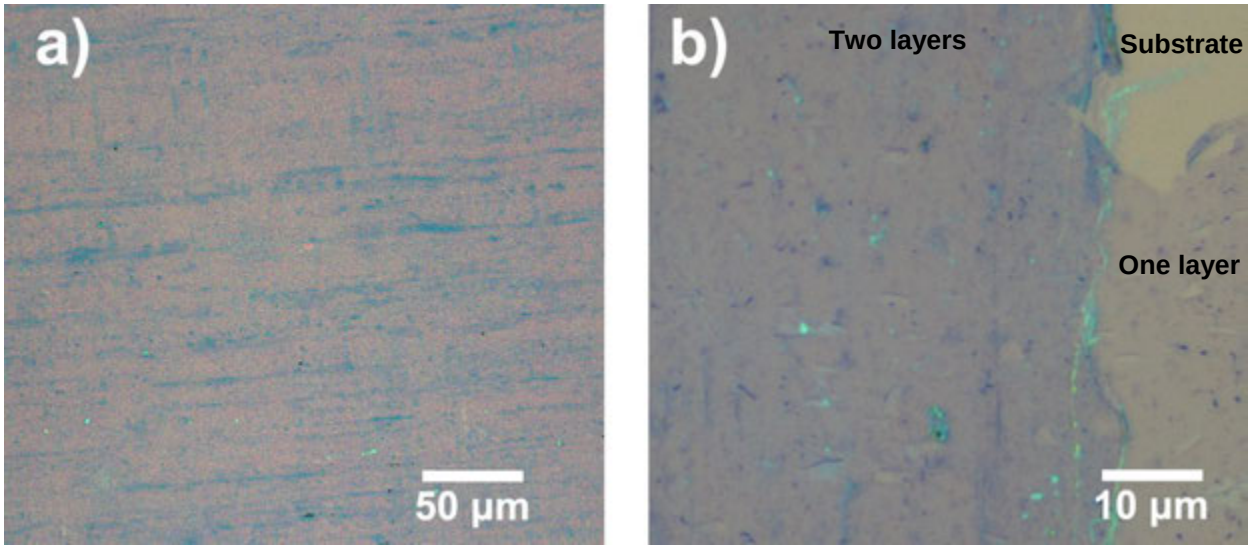

Figure S3: Double layer graphene thin films artificially created on 300 nm SiO_2/Si. a) As-transferred. b) Intentionally scratched to generate some optical contrast.

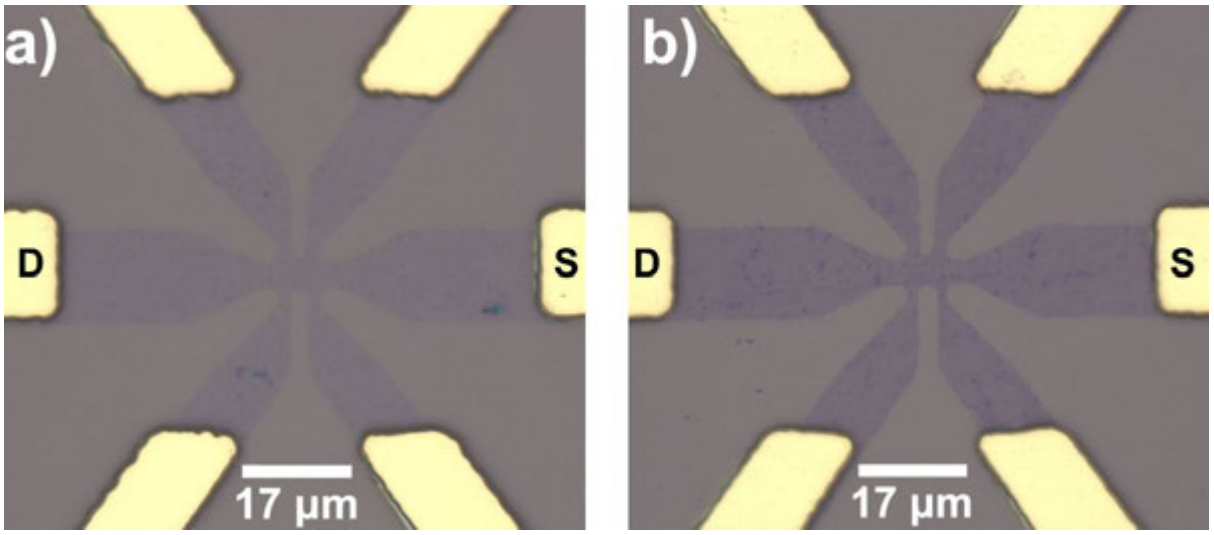

Figure S4: Optical images of devices fabricated using a) monolayer and b) artificially created dual layer graphene.

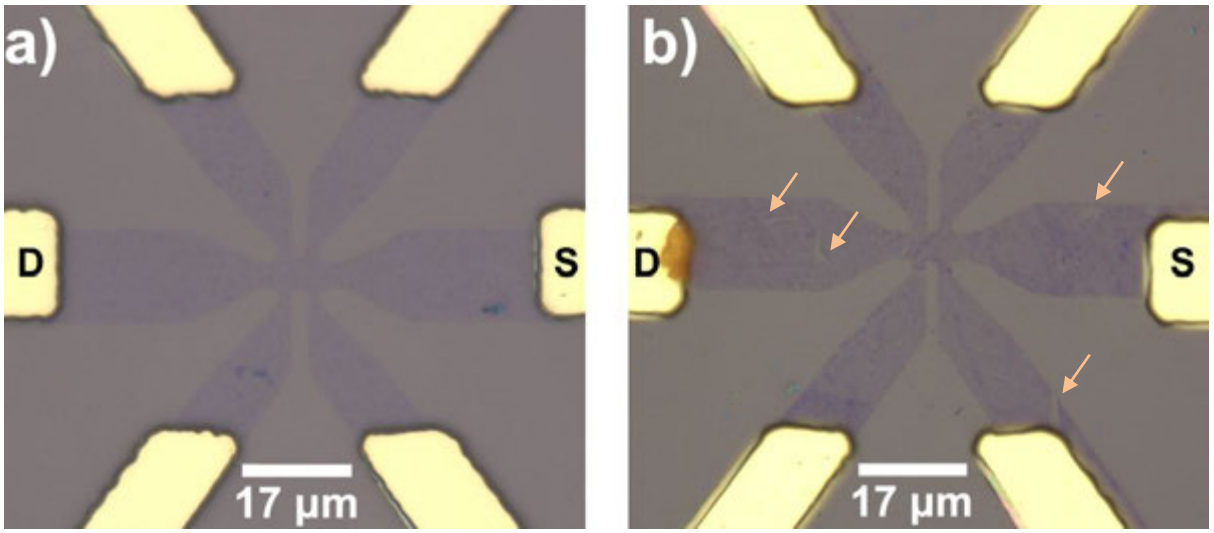

Figure S5: Optical images of monolayer graphene devices fabricated from materials transferred by (a) frame assisted bubbling and b) wet etching. Arrows are signaling some of the holey defects.

References

[1] Arpad A. Bergh. **Blue laser diode (LD) and light emitting diode (LED) applications**. *Physisca Status Solidi (a)*, **201**:2740–2754, 2004.

[2] Yu Higuchi, Kunimichi Omae, Hiroaki Matsumura, and Takashi Mukai. **Room-temperature CW lasing of a GaN-based vertical cavity surface emitting laser by current injection**. *Applied Physics Express*, **1**:121102(1–3), 2008.

[3] Tien-Chang Lu, Shih-Wei Chen, Tzeng-Tsong Wu, Po-Min Tu, Chien-Kang Chen, Cheng-Hung Chen, Zhen-Yu Li, Hao-Chung Kuo, and Shing-Chung Wang. **Continuous wave operation of current injecterd GaN vertical cavity surface emitting lasers at room temperature**. *Applied Physics Letters*, **97**:071114(1–3), 2010.

[4] Petter Westbergh. *High speed vertical cavity surface emitting lasers for short reach communication. MC2-190.* PhD thesis, Chalmers Tekniska Högskola, 2011.

[5] Martin Stattin. **Towards novel AlGaN-based light emitters. Lic. Thesis**. Technical report, Chalmers Tekniska Högskola, 2011.

[6] Daiji Kasahara, Daisuke Morita, Takao Kosugi, Kyosuke Nakagawa, Jun Kawamata, Yu Higuchi, Hiroaki Matsumura, and Takashi Mukai. **Demonstration of blue and green GaN-based vertical-cavity surface-emitting lasers by current injection at room temperature**. *Applied Physics Express*, **4**:072103(1–3), 2011.

[7] J. K. Sheu, Y. K. Su, G. C. Chi, P. L. Koh, M. J. Jou, C. M. Chang, C. C. Liu, and W. C. Hung. **High-transparency Ni/Au ohmic contact to p-type GaN**. *Applied Physics Letters*, **74**:2340–2342, 1999.

[8] D. F. Feezell, R. M. Farrell, M. C. Schmidt, H. Yamada, M. Ishida, S. P. DenBaars, D. A. Cohen, and S. Nakamura. **Thin metal intracavity contact and lateral current-distributin scheme for GaN-based vertical-cavity lasers**. *Applied Physics Letters*, **90**:181128(1–3), 2007.

[9] Tadatsugu Minami. **Transparent conducting oxide semiconductors for transparent elctrodes**. *Semiconductor Science and Technology*, **20**:S35–S44, 2005.

[10] Tzeng-Tsong Wu, Chien-Chung Lin, Yun-Lin Wu, Chien-Kang Chen, Tien-Chang Lu, Hao-Chung Kuo, and Shing-Chung Wang. **Enhaced output power of GaN-based resonance cavity light-emitting diodes with optimized ITO design**. *Journal of Lightwave Technology*, **29**:3757–3763, 2011.

[11] Amy C. Tolcin. **Indium**. Technical report, U.S. Geological Survey, 2012.

[12] K. S. Novoselov, A. K. Geim, S. V. Morosov, D. Jiang, Y. Zhang, S. V. Dubonos, I. V. Grigorieva, and A. A. Firsov. **Electric field effect in atomically thin carbon films**. *Science*, **306**:666–669, 2004.

[13] Mikhail I. Katsnelson. **Graphene: carbon in two dimensions**. *Materials Today*, **10**:20–27, 2007.

[14] A. H. Castro Neto, F. Guinea, N. M. R. Peres, K. S. Novoselov, and A. K. Geim. **The electronic properties of graphene**. *Reviews of Mothern Physics*, **81**:109–162, 2009.

[15] P. R. Wallace. **The band theory of graphite**. *Physical Review*, **71**:622–634, 1947.

[16] Xuebin Li. *Epitaxial graphene films on SiC: growth, characterization, and devices.* PhD thesis, Shool of Physics, Georgia Institute of Technology, 2008.

[17] Yuanbo Zhang, Yan-Wen Tan, Horst L. Stormer, and Philip Kim. **Experimental observation of the quantum hall effect and Berry's phase in graphene**. *Nature*, **438**:201–204, 2005.

[18] Y.-W. Tan, Y. Zhang, K. Bolotin, Y. Zhao, S. Adam, E. H. Hwang, S. Das Sarma, H. L. Stormer, and P. Kim. **Measurement of scattering rate and minimum conductivity in graphene**. *Physical Review Letters*, **99**:246803(1–4), 2007.

[19] K. I. Bolotin, K. J. Sikes, Z. Jiang, M. Klima, G. Fudenberg, J. Hone, P. Kim, and H. L. Stormer. **Ultrahigh electron mobility in suspended graphene.** *Solid State Communications*, **146**:351–355, 2008.

[20] A. K. Geim and K. S. Novoselov. **The rise of graphene**. *Nature Materials*, **6**:183–191, 2007.

[21] P. M. Ostrovsky, I. V. Gornyi, and A. D. Mirlin. **Quantum criticality and minimal conductivity in graphene with long-range disorder**. *Physical Review Letters*, **98**:256801(1–4), 2007.

[22] Caterina Soldano, Ather Mahmod, and Erik Dujardin. **Production, properties and potential of graphene**. *Carbon*, **48**:2127–2150, 2010.

[23] F. Bonaccorso, Z. Sun, T. Hasan, and A. C. Ferrari. **Graphene photonics and optoelectronics**. *Nature Photonics*, **4**:611–622, 2010.

[24] P. Blake, E. W. Hill, A. H. Castro Neto, K. S. Novoselov, D. Jiang, R. Yang, T. J. Booth, and A. K. Geim. **Making graphene visible**. *Applied Physics Letters*, **91**:063124(1–3), 2007.

[25] Changgu Lee, Xiaoding Wei, Jeffrey W. Kysar, and James Hone. **Measurement of the elastic properties and intrinsic strength of monolayer graphene**. *Science*, **321**:385–388, 2008.

[26] Alexander A. Balandin, Suchismita Ghosh, Wenzhong Bao, Irene Calizo, Desalegne Teweldebrhan, Feng Miao, and Chun Ning Lau. **Superior thermal conductivity of single-layer graphene**. *Nano Letters*, **8**:902–907, 2008.

[27] K. S. Novoselov, D. Jiang, F. Scheidin, T. J. Booth, V. V. Khotkevich, S. V. Morozov, and A. K. Geim. **Two-dimensional atomic crystals.** *PNAS*, **102**:10451–10453, 2005.

[28] William S. Jr. Hummers and Richard E. Offeman. **Preparation of graphitic oxide**. *Journal of American Chemical Society*, **80**:1339–1339, 1958.

[29] Daniela C. Marcano, Dmitry V. Kosynkin, Jacob M. Berlin, Alexander Sinitskii, Sun Zhengzhong, Alexander Slesarev, Lawrence B. Alemany, Wei Lu, and James M. Tour. **Improved synthesis of graphene oxide**. *ACS Nano*, **4**:4806–4814, 2010.

[30] J. Hass, W. A. de Heer, and E. H. Conrad. **The growth and morphology of epitaxial multilayer graphene**. *Journal of Physics: Condensed Matter*, **20**:323202(1–27), 2008.

[31] A. Ōya and H. Marsh. **Review phenomena of catalytic graphitization**. *Journal of Material Science*, **17**:309–322, 1982.

[32] Cecilia Mattevi, Hokwon Kim, and Manish Chhowalla. **A review of chemical vapour deposition of graphene on copper**. *Journal of Materials Chemestry*, **21**:3324–3334, 2011.

[33] Jie Sun, Niclas Lindvall, Mathew T. Cole, Keneth B. K. Teo, and August Yurgens. **Large-area uniform graphene-like films grown by chemical vapour deposition on silicon nitride**. *Applied Physics Letters*, **98**:252107(1–3, 2011.

[34] keun Soo Kim, Yue Zhao, Houk Jang, Sang Yoon Lee, Jong Min Kim, Kwang S. Kim, Jong-Hyun Ahn, Philip Kim, Jae-Young Choi, and Byung Hee Hong. **Large-scale pattern growth of graphene films for stretchable transparent electrodes**. *Nature*, **457**:706–710, 2009.

[35] Sukang Bae, Hyeongkeun Kim, Youngbin Lee, Xiangfan Xu, Jae-Sung Park, Yi Zheng, Jayakumar Balakrishnan, Tian Lei, Hye Ri Kim, Young Il Song, Young-Jin Kim, Kuang S. Kim, Barbaros ʕOzyilmaz,

Jong-Hyun Ahn, Byung Hee Hong, and Sumio Lijima. **Roll-to-roll production of 30-inch grpahene films for transparent electrodes**. *Nature Nanotechnology*, **5**:574–578, 2010.

[36] Yu Wang, Yi Zheng, Xiangfan Xu, Emilie Dubuisson, Qiaoliang Bao, Jiong Lu, and Kian Ping Loh. **Electrochemical delamination of CVD-grown graphene film: toward the recyclable use of copper catalyst.** *ACS Nano*, **5**:9927–9933, 2011.

[37] Libo Gao, Wencai Ren, Huilong Xu, Li Jin, Zhenxing Wang, Teng Ma, Lai-Peng Ma, Zhiyong Zhang, Quiang Fu, Lian-Mao Peng, Xinhe Bao, and Hui-Ming Cheng. **Repeated growth and bubbling transfer of graphene with millimetre-size single-crystal grains using platinum**. *Nature Communications*, **3**:699(1–7), 2012.

[38] Raghunath Murali, Yinxiao Yang, Kevin Brenner, Thomas Beck, and James D. Meindl. **Breakdown current density of graphene nanoribbons**. *Applied Physics Letters*, **94**:243114(1–3), 2009.

[39] Yiyun Zhang, Liancheng Wang, Xiao Li, Xiaoyan Yi, Ning Zhang, Jing Li, Hongwei Zhu, and Guohong Wang. **Annealed InGaN green light-emitting diodes with graphene transparent conductive electrodes**. *Journal of Applied Physics*, **111**:14501(1–5), 2012.

[40] Jie Sun, Niclas Lindvall, Mathew T. Cole, Koh T. T. Angel, Teng Wang, Kenneth B. K. Teo, Daniel H. C. Chua, Johan Liu, and August Yurgens. **Low partial pressure chemical vapor deposition of graphene on copper**. *IEEE Transaction son Nanotechnology*, **11**:255–260, 2012.

[41] F. Tuinstra and J. L. Koenig. **Raman spectrum of graphite**. *The Journa of Chemical Physics*, **53**:1126–1130, 1970.

[42] Stephany Reich and Christian Thomsen. **Raman spectroscopy of graphite**. *Philosofical Transactions of the Royal Society (a)*, **362**:2271–2288, 2004.

[43] Xuesong Li, Weiwei Cai, Jinho An, Seyoung Kim, Junghyo Nah, Dongxing Yang, Richard Piner, Aruna Velamakanni, Inhwa Jung, Emanuel

Tutuc, Sanjay K. Banerjee, Luigi Colombo, and Rodney S. Ruoff. **Large-area synthesis of high quality and uniform graphene films on copper foils**. *Science*, **324**:1312–1314, 2009.

[44] Fethullah G"unes, Hyeon-Jin Shin, Chandan Biswas, Gang gee Han, Eun Sung Kim, Seung Jun Chae, Jae Young Choi, and Young Hee Lee. **Layer-by-layer doping of few-layer graphene film**. *ACS Nano*, **4**:4595–4600, 2010.

[45] Meng-Sheng Liao, Chak-Tong Au, and Ching-Fai Ng. **Methane dissociation on Ni, Pd, Pt and Cu metal (111) surfaces – a theoretical comparative study**. *Chemical Physics Letters*, **272**:445–452, 1997.

[46] Weilie Zhao, Ping Heng Tan, Jian Liu, and Andrea C. Ferrari. **Intercalation of few-layer graphite flakes with $FeCl_3$: Raman determination of Fermi level, layer by layer decoupling, and stability**. *Journal of the American Chemical Society*, **133**:5941–5946, 2010.

[47] Razvan A. Nistor, Dennis M. Newns, and Glenn J. Martyna. **The role of chemestry in graphene doping for carbon-based electronics**. *ACS Nano*, **5**:3096–3103, 2011.

[48] Samuel Alejandro Lara-Avila. *Magnetotransport characterization of epitaxial graphene on SiC. MC2-224*. PhD thesis, Chalmers Tekniska Högskola, 2012.

[49] Seyoung Kim, Junghyo Nah, Insun Jo, Davood Shahrjerdi, Luigi Colombo, Zhen Yao, Emanuel Tutuc, and Sanjay K. Banerjee. **Realization of a high mobility dual-gated graphene field effect transistor with Al_2O_3 dielectric**. *Applied Physics Letters*, **94**:062107(1–3), 2009.

[50] Ivan Khrapach, Freddie Withers, Thomas H. Bointon, Dmitry K. Polyushkin, William L. Barnes, Saverio Russo, and Monica F. Craciun. **Novel highly conductive and transparent graphene-based conductors**. *Advanced Materials*, **24**:2844–2849, 2012.

Declaration

I herewith declare that I have produced this paper without the prohibited assistance of third parties and without making use of aids other than those specified; notions taken over directly or indirectly from other sources have been identified as such. This report has not previously been presented in identical or similar form to any other examination board.

The thesis work was conducted from the 16^{th} of January, 2012 to the 1^{st} of June, 2012 under the coordination of Ass. Prof. Åsa Haglund, Ass. Prof. Jie Sun, and Prof. Marc Heyns at the departments of Photonics Laboratory and Quantum Device Physics at MC2 Microtechnology and Nanoscience, Chalmers Tekniska Högskola.

Göteborg, 2012